SANDIA REPORT

SAND2012-9951
Unlimited Release
Printed December 2012

Elpasolite Scintillators

F. Patrick Doty, Xiaowang Zhou, Pin Yang, and Mark A. Rodriguez

Prepared by
Sandia National Laboratories
Albuquerque, New Mexico 87185 and Livermore, California 94550

Sandia National Laboratories is a multi-program laboratory managed and operated by Sandia Corporation, a wholly owned subsidiary of Lockheed Martin Corporation, for the U.S. Department of Energy's National Nuclear Security Administration under contract DE-AC04-94AL85000.

Issued by Sandia National Laboratories, operated for the United States Department of Energy by Sandia Corporation.

Available to DOE and DOE contractors from
U.S. Department of Energy
Office of Scientific and Technical Information
P.O. Box 62
Oak Ridge, TN 37831
Telephone: (865) 576-8401
Facsimile: (865) 576-5728
E-Mail: reports@adonis.osti.gov
Online ordering: http://www.osti.gov/bridge

Available to the public from
U.S. Department of Commerce
National Technical Information Service
5285 Port Royal Rd.
Springfield, VA 22161
Telephone: (800) 553-6847
Facsimile: (703) 605-6900
E-Mail: orders@ntis.fedworld.gov
Online order: http://www.ntis.gov/help/ordermethods.asp?loc=7-4-0#online

SAND2012-9951
Unlimited Release
Printed December 2012

ELPASOLITE SCINTILLATORS

F. Patrick Doty, Xiaowang Zhou, Pin Yang, and Mark A. Rodriguez
Rad/Nuc Detection Materials & Analysis

Sandia National Laboratories
P.O. Box 969
Livermore, CA. 94551-0969

ABSTRACT

This work was funded by the U.S. Department of Energy Office of Nonproliferation Research to develop elpasolite materials, with an emphasis on high-atomic-number rare-earth elpasolites for gamma-ray spectrometer applications. Low-cost, high-performance gamma-ray spectrometers are needed for detection of nuclear proliferation. Cubic materials, such as some members of the elpasolite family (A_2BLnX_6; Ln-lanthanide and X-halogen), hold promise due to their high light output, proportionality, and potential for scale-up. Using both computational and experimental studies, a systematic investigation of the composition–structure–property relationships of these high-atomic-number elpasolite halides was performed. The results reduce the barrier to commercialization of large single crystals or transparent ceramics, and will facilitate economical scale-up of elpasolites for high-sensitivity gamma-ray spectroscopy.

ACKNOWLEDGEMENT

The authors would like to thank Tom Chavez and Clay S. Newton for their assistance in thermal analysis and the hot forging experiment. The financial support from DoE NA-22 Advanced Material Portfolio is also greatly appreciated.

This project is supported by DOE/NNSA Office of Nonproliferation Research and Development, Proliferation Detection Program, Advanced Materials Portfolio. Sandia National Laboratories is a multi-program laboratory managed and operated by Sandia Corporation, a wholly owned subsidiary of Lockheed Martin Corporation, for the U.S. Department of Energy's National Nuclear Security Administration under contract DE-AC04-94AL85000.

CONTENTS

1. Introduction 9
1.1 Background and Approach 10
2. Theoretical Investigation of Elpasolites Structure 13
2.1 Background on Ionic Structure Prediction 13
2.2 Interatomic Potential 14
2.2.1 Background 14
2.2.2 Embedded-Ion Method Potential Model 15
2.2.3 Function Forms 17
2.3 Monovalent Binary Systems 20
2.3.1 Calibrated EIM Parameters 20
2.3.2 Characteristics of Calibrated Parameters 23
2.3.3 Molecular Dynamics Study of Crystal Stability 27
2.4 Quaternary Elpasolite Systems 32
2.4.1 Development of the EIM Database 32
2.4.2 Characteristics of the EIM Database 33
3. Experimental Investigation of Elpasolite Structure: Synthesis And Characterization 41
3.1 Background and Introduction 41
3.2 Experimental Procedure 42
3.2.1 Compound Formation and Synthesis 42
3.2.2 Single Crystal Growth 43
3.2.3 Hot Pressing 44
3.2.4 Thermal Analysis and Structural Refinement 44
3.2.5 Photoluminescence and Radioluminescence 45
3.3 Results and Discussion 45
3.3.1 Synthesis, Crystal Growth, and Thermal Measurements 45
3.3.2 Structural Refinement 50
3.3.3 Hot Pressing 64
3.3.4 Photoluminescence and Radioluminescence 66
Appendix A: Effect of Variable Charge Models 73
Appendix B: EIM Database 75
Appendix C: Structural Factors for all 640 Compounds 87

FIGURES

Figure 1. Effects of parameters on pair energy function $\phi(r)$. 19
Figure 2. Magnitude of charge as a function of electronegativity difference. 24
Figure 3. Parameter r_e and calculated crystal bond length as a function of experimental crystal bond length for cation–anion pairs. 25
Figure 4. Calculated and experimental cohesive energies for the 20 binary compounds and the nine elements. 26
Figure 5. Various energy components as a function of hydrostatic strain for LiF. 27
Figure 6. Change of a metastable B2 crystal of NaCl after the simulated-annealing. 28
Figure 7. Crystal phase diagrams obtained at different pressures using the calibrated parameters. 29
Figure 8. Structure vs. bond length map obtained from unmodified and perturbed NaCl parameters. 30
Figure 9. Crystal phase diagrams obtained at zero pressure using all calibrated and perturbed parameters. 31
Figure 10. Comparison of calculated and experimental lattice constants and cohesive energies. 35
Figure 11. Schematic of perovskite structure. 36
Figure 12. Two different tilts of halogen octahedrons. 37
Figure 13. $BaBiO_3$-structure and hexagonal orientation of $a^0a^0a^0$ structure. 37
Figure 14. EIM distortion metric η as a function of rank number sorted with this metric. 40
Figure 15. The differential scanning calorimetric data during the solidification cycles for the Cs_2NaLaI_6. Data were collected at 3 °C/min under a flowing argon condition. 46
Figure 16. X-ray diffraction data illustrate compositional variations for a single crystal $Cs_2LiLaBr_6:Ce^{3+}$ grown by a Bridgman technique. Crushed powder of these sections was collected from the top (milky), middle (mid, transparent) and bottom (milky) of the crystal for the x-ray diffraction study. 47
Figure 17. Single crystals of elpasolite halides grown to different sizes: (a) 0.75 in. dia. Cs_2LiYCl_6 (CLYC) and 1 in. dia. $Cs_2LiLaBr_6$ (CLLB), both shown under black light excitation; (b) two 0.75 in. dia., 0.5 in. thick $Cs_2LiLaBr_6$ crystals prepared for radioluminescence characterization; (c) 0.5 in. dia. $Cs_2NaLaBr_6$ (CNLB). 48
Figure 18. A typical simultaneous thermal analysis (STA) for elapsolite halides, including the thermal gravitation measurement (TGA, dotted lines) and differential thermal calorimetry (DSC, solid lines), using a cerium-doped $Cs_2NaLaBr_6$ as an example. 49
Figure 19. The thermal mechanical response and the coefficient of thermal expansion of $Cs_2LiLaBr_6:Ce^{3+}$. 50

Figure 20. Structure refinement of $Cs_2LiLaBr_6$ as a cubic elpasolite structure. 52
Figure 21. Structure refinement of the tetragonal $Cs_2NaLaBr_6$ structure. 54
Figure 22. Model of $Cs_2NaLaBr_6$ (as viewed down the c-axis) showing the relationship between the a-axis of the tetragonal cell and that of a pseudo-cubic elpasolite supercell. 55
Figure 23. Structure refinement of the orthorhombic $(Cs_{0.84}Na_{0.16})(Na_{0.5}La_{0.5})I_3$ structure. 60
Figure 24. Model of $(Cs_{0.84}Na_{0.16})(Na_{0.5}La_{0.5})I_3$ (as viewed down the a-axis) showing a distorted octahedral and the location of Cs site near the (100) and (001) plane. 61
Figure 25. The change of sample geometry for a sliced $Cs_2LiLaBr_6$ ingot (a) before and (b) after hot forging. The aspect ratio (D/t) of the sample changed from 1.4 to 24.4 after hot forging. 64
Figure 26. Hot pressed and forged samples: (a) Hot pressed Cs_2LiYCl_6 powder, (b) hot pressed Cs_2LiYCl_6 crushed particles, (c) hot forged Cs_2LiYCl_6 melt ingot, (d) hot forged $Cs_2NaLaBr_6$ under back-lighting (shadow cast by an Allen wrench). 65
Figure 27. Excitation (dotted line) and emission (red solid line) spectra of elpasolite halide compounds. 67
Figure 28. X-ray induced emission spectra of (a) $Cs_2LiEuCl_6$:5% Ce^{3+}, (b) $Cs_2NaErBr_6$, (c) $Cs_2NaErBr_6$:5%Ce^{3+}, and (d) Cs2NaGdBr$_6$:2.5%Ce^{3+} at room temperature (measured at RMD). 68
Figure 29. Pulse height spectrum of $Cs_2LiLaBr_6$:Ce^{3+} crystal excited with 663 keV gamma-rays from a ^{137}Cs source. 70
Figure 30. Pulse height spectra of (a) $Cs_2LiEuCl_6$:5% Ce^{3+}, (b) $Cs_2NaErBr_6$, (c) $Cs_2NaErBr_6$:5%Ce^{3+}, and (d) Cs2NaGdBr$_6$:2.5%Ce^{3+} at room temperature (measured at RMD). 70
Figure 31. The non-proportionality curve for $Cs_2LiLaBr_6$:Ce^{3+}, using photon yield/gamma energy with respect to the detector's light yield at 662 keV. 71
Figure 32. The non-proportionality curve and the fluorescence decay time spectrum for $Cs_2NaGdBr_6$:Ce^{3+} crystal (Measured at RMD). 71
Figure A1. Effects of charge transfer on bond length and bond energy. 74

TABLES

Table 1. Lattice constant, cohesive energy, and charge of different compound crystals. 22

Table 2. Lattice constant and cohesive energy of different elemental and compound crystals. 33

Table 3. The performance of Ce^{+3} doped elpasolite halide scintillators (RMD data). 42

Table 4. Chemical analysis data for different sections of a $Cs_2LiLaBr_6:Ce^{3+}$ single crystal. 48

Table 5. The melting and freezing points as well as enthalpy changes during solidification for some elpasolite halides (with 5 at. % of Ce^{3+}). T_u is the temperature at which the compound becomes thermally unstable, as determined by a thermal gravitational measurement (see Figure 18). 49

Table 6. Crystal structure and tolerance factor for lanthanum-based elpasolite halides (all doped compounds consist of 5 atm. % Ce^{+3}). 51

Table 7. X-ray diffraction data for cubic $Cs_2LiLaBr_6$. 53

Table 8. Crystal data for $Cs_2LiLaBr_6$ Space group: fm-3m (225), lattice parameter: a = 11.2890(6) Å, cell volume = 1438.7(2) $Å^3$, Z = 4, B_{iso} = 2.3 $Å^2$, R_p = 0.1267, density = 2.477 g/cm^3 54

Table 9. X-ray diffraction data for tetragonal $Cs_2NaLaBr_6$. 56

Table 10. Crystal data for $Cs_2NaLaBr_6$ Space group: P4/mnm (136), lattice parameters: a = 8.1416(6) Å, c = 11.580(1) Å, cell volume = 767.4(2) $Å^3$, Z = 2, B_{iso} = 3.1 $Å^2$, R_p = 0.1333, density = 2.364 g/cm^3. 57

Table 11. X-ray diffraction data for orthorhombic $(Cs_{0.84}Na_{0.16})(Na_{0.5}La_{0.5})I_3$ 58

Table 12. Crystal data for $(Cs_{0.84}Na_{0.16})(Na_{0.5}La_{0.5})I_3$ Space group: Pnma (62), lattice parameters: a = 8.762(1) Å, b = 12.436(2) Å, c = 8.627(2) Å, cell volume = 940.0(4) $Å^3$, Z = 4, B_{iso} = 2.3(2) $Å^2$, R_p = 0.1361, density = 2.455 g/cm^3. 60

Table 13. Bond lengths (Å) and angles (^{o}) for compounds. 63

Table 14. The maximum of the emission and the excitation wavelengths, as well as the amount of Stokes shift for the cerium-doped (5 mol.%) elpasolite halides. 67

Table B1. Electronegativity of elements. 75

Table B2. Calibrated pair parameters for alkali halides. Here pair type = 1 is defined by Eq. (8), and pair type = 2 is defined by Eq. (9). 75

Table B3. Full list of pair parameters of the EIM database. Here pair type = 1 is defined by Eq. (8), and pair type = 2 is defined by Eq. (9) 78

Table C1. Relative energy difference ΔE_0, minimum energy structure S_{min}, maximum energy structure S_{max}, tolerance factors t'_B, $t'_{B'}$, t', average normal distortion ε, standard deviation of halogen atoms δ, total shear distortion γ, and atomic volume Ω for all 640 compounds.t'_B t'_B. 87

1. INTRODUCTION

This work was funded by the U.S. Department of Energy Office of Nonproliferation Research to develop elpasolite materials, with an emphasis on high-atomic-number rare earth elpasolites for gamma-ray spectrometer applications. Low-cost, high-performance gamma-ray spectrometers are needed for detection of nuclear proliferation. This work was motivated by the shortcomings of available scintillation materials, which fail to meet requirements for energy resolution and sensitivity at room temperature. The workhorse alkali halides, while affordable, give poor spectroscopic performance due to their severely nonproportional response; while the still-emerging lanthanide-halide based materials, which give the desired luminosity and proportionality, have proven difficult to produce in the large sizes and low cost required due to their intrinsic brittleness and highly anisotropic nature. The difficulties and delays in commercialization of these mechanically challenging low-symmetry crystals provides strong impetus for discovery of high-luminosity cubic crystals with proportional response.

Cubic materials, such as some members of the elpasolite family (A_2BLnX_6; Ln-lanthanide and X-halogen), hold greater promise due to their high light output, proportionality, and potential for scale-up. The isotropic cubic structure leads to minimal thermomechanical stresses during single-crystal solidification, and eliminates the problematic light scattering at grain boundaries. Therefore, cubic elpasolites could be produced in large sizes as either single-crystal or transparent ceramics with high production yield and reduced costs. This class of materials seems clearly destined for important applications in nonproliferation, and they may yield the first large, low-cost gamma spectrometers approaching theoretical energy resolution.

Using both computational and experimental studies, a systematic investigation of the composition–structure–property relationships of these high-atomic-number elpasolite halides was performed, establishing a validated computational framework for advanced materials exploration and exploitation for maximum performance. Section 2 of this report details the computational effort, based on an adaptation of the embedded ion method (EIM) to predict the crystal structures over a large composition space. This section includes background on approaches to predicting structure, starting with Goldschmidt's tolerance factor and Pauling's rules, through the widely used method of bond valence sums. This discussion points to the logical progression from primitive hard-sphere models to reactive models analytically incorporating variable charge sharing effects. The culmination of this section presents a new distortion metric that successfully distinguishes stable cubic compositions from the many geometrically possible structures formed by distortions and tilts of coordination polyhedra within the unit cell.

Section 3 documents the experimental program, including details of single-crystal growth, *x*-ray structure determination, thermal analysis and structure refinement, and characterization of optical and luminescence properties. This section also includes work to evaluate ceramic processing

methods for a polycrystalline scintillator, demonstrating the feasibility of making large-area, transparent detectors by a hot forging technique similar to these reported for NaI and CsI.

The work documented in this report reduces the barrier to commercialization in growing large single crystals or processing transparent ceramics, and it will enable economical scale-up of elpasolites for high-sensitivity gamma-ray spectroscopy.

1.1 Background and Approach

The work builds upon the recent discovery of a large new class of halide scintillators. These double perovskite (elpasolite)[1,2,3] materials conform to the formula $A_2B(RE)X_6$, where A and B are alkali metals, RE is a rare earth, and X is a halogen. Many of these materials retain cubic or nearly cubic crystal structures over a range of compositions, and they have demonstrated desirable scintillation properties including pulse shape discrimination, high luminosity, and proportional response. At least one composition, Cs_2NaLaI_6, has been reported to have light yield (54,000-60,000 photons/MeV) and proportionality similar to $LaBr_3$:Ce^4. Another composition, Cs_2LiYCl_6, has been demonstrated to discriminate gammas from capture neutrons by pulse shape discrimination.[1] Therefore, this class of materials seems clearly destined for important applications in nonproliferation, and it may yield the first large, low-cost gamma spectrometers approaching theoretical energy resolution.

The number of potential scintillator compositions of the elpasolite halide system is large (thousands), and the amount of experimental research required for discovery of the most promising materials could be formidable. In order to aggressively pursue the fundamental research without losing sight of potential applications that justify the efforts, strategies to map out and zero in on the most promising scintillators materials are required. Emphasis was therefore placed on molecular static structure prediction, to narrow the scope of experimental work required to discover all cubic compositions of interest. The modeling approach expanded the capabilities of the embedded-atom method (EAM) to enable structure prediction over nearly the full composition space of interest. Ultimately these simulation results will direct us in developing new material systems with superior performance at a lower overall cost.

---

[1] C. M. Combes, P. Dorenbos, C. W. E. van Eijk, K. W. Kramer and H. U. Gudel. Optical and scintillation properties of pure and Ce^{3+}-doped Cs_2LiYCl_6 and Li_3YCl_6 : Ce^{3+} crystals. *Journal of Luminescence*, **82**:299-305, 1999.

[2] E. V. D. van Loef, J. Glodo, W. M. Higgins and K. S. Shah,"Optical and scintillation properties of Cs_2LiYCl_6 : Ce^{3+} and Cs_2LiYCl_6 : Pr^{3+} crystals." *IEEE Transactions on Nuclear Science*, **52**:1819-1822, 2005.

[3] M. D. Birowosuto, P. Dorenbos, C. W. E. van Eijk, K. W. Kramer and H. U. Gudel, "Scintillation properties and anomalous Ce^{3+} emission of $Cs_2NaREBr_6$: Ce^{3+} (RE = La, Y, Lu)." *Journal of Physics-Condensed Matter*, **18**:6133-6148, 2006.

[4] J. Glodo, E. V. D. Van Loef, W. M. Higgins, and K. S. Shah, "Scintillation properties of Cs_2NaLaI_6:Ce." *IEEE Nuclear Science Symposium Conference Record;* N30-164, 1208-1211, 2006, and Kanai Shah et al., presented at the Workshop on Radiation Detector Materials, MRS Fall Meeting, Boston, MA, (2007).

A survey of the literature on elpasolites reveals that, while scintillation properties such as light yield, decay time, and energy resolution are reported, the basic material properties such as lattice parameters, band gap, refractive index, coefficient of thermal expansion, and elastic properties are lacking. Since basic material properties are crucial to determine feasibility for the growth of large single crystals, this dearth of data represents a critical need.

The experimental and computational studies detailed below provide the necessary knowledge base and robust models to determine the boundaries of the compositional regime for cubic elpasolite materials with scintillation properties meeting NA22 mission requirements. The emphasis has been on the high-*Z* cerium-doped lanthanide–halide based materials. Strategies to increase the stopping power of these elpasolites by substituting different lanthanide and alkali cations or halide anions to increase material density and effective atomic number were explored. Studies included modeling of prototype cubic elpasolite structures, including parametric studies to elucidate sensitivity to ionic substitutions in the lattice.

Experimental studies of systematic variation of cations on octahedrally coordinated sites provided validated model points, as well as a database of trends in material structure and properties relevant to scintillation, such as band gap, fluorescence spectrum, stokes shift, and decay times. Since substitutions on the octahedral sites can produce distortions from the ideal cubic structure, which lead to manufacturing challenges as well as changes in the electronic band structure and scintillation performance, we also modeled and systematically investigated these structural effects. In addition, we investigated variation of anions in the host to modify the emission wavelength and decay time. We also determined phase diagram information to enable optimal scale-up via melt growth or ceramic processing. These data will be vital for developing and refining robust models for prediction of structure and properties and optimizing performance.

2. THEORETICAL INVESTIGATION OF ELPASOLITES STRUCTURE

Cubic elpasolites have improved manufacturability and scintillation properties. However, more than 1440 $A_2BB´X_6$ elpasolites and countless elpasolite alloys have been identified. As a result, an experimental screening of the cubic elpasolites is impractical. Below we describe our work to develop and apply a framework of atomistic simulation to predict crystal structures of elpasolites for rapid identification of cubic compositions.

2.1 Background on Ionic Structure Prediction

Depending on the material constituents, ionic compounds can exhibit a variety of crystal structures that alter the properties. This diversity provides an effective means to improve ionic compounds by manipulating their stoichiometry. On the other hand, an experimental trial-and-error method to optimize the constituents of even a quaternary system for a given desired crystal structure can become extremely expensive and time consuming. A methodology for predicting the crystal structure of an ionic compound is therefore extremely useful to promote the applications of ionic compounds.

Traditionally, the most stable crystal structure of an ionic compound has been determined topologically from relative sizes of cations and anions so that, when atoms are in contact as if they are hard spheres, the bond length between any two atoms closely matches the spacing between the corresponding lattice sites of the crystal. One representative example is the Goldschmidt criterion [1,2,3], which has been widely used to exclude ionic compounds with non-cubic perovskite crystal structures based upon environment-independent input parameters of cation and anion sizes referred to as the “ionic radius” [4].

A newer model to predict the crystal structures is called the bond valence model [5]. In this model, the bond valence is defined as a quantity specific to a bond that decays exponentially with the bond length. An atomic valence is then obtained for an atom by summing up the bond valences between this atom and all its neighbors. A global instability index (GII) is calculated as the standard deviation of the calculated atomic valence from the nominal valence (i.e., the oxidation states, e.g., +3 for aluminum and -2 for oxygen) for all the atoms in the unit cell of the crystal. The structures with low GII values are considered as possibly stable crystals. The bond valence model has been widely used, as summarized by a recent review [6], and it has been implemented in software SPuDS [7,8,9]. The bond valence model also uses parameters reflective of the relative sizes of cations and anions. The model is effective in excluding some unstable structures, but is inconclusive in predicting stable structures because some known unstable crystals are always predicted to have very low GII values by the bond valence model. One advantage of the bond valence model is that it can be applied for other crystals in addition to the perovskite structures.

In 1939, Pauling discussed the effects of valence and coordination on crystal structures [10]. He noted that when atoms of dissimilar species are brought together, they may induce charges on each other, which then change the effective radius of an atom depending on the local environment. The tendency for atoms to become charged has been characterized by the atomic property called electronegativity [10,11,12,13]. Interestingly, Mooser and Pearson discovered that different structures of AB binary ionic compounds can be well divided into different zones in an average principal quantum number vs. electronegativity difference map [14]. This phenomenon was related to angular dependence of interatomic interactions, and it is unclear if it can be related to the relative sizes of atoms.

Real atoms are not hard spheres. For instance, the hard-sphere model would imply that the three bond lengths r_{AA}, r_{BB}, r_{AB} for the three atomic pairs AA, BB, and AB are fully defined by the two ionic radii r_A and r_B through $r_{AA} = 2r_A$, $r_{BB} = 2r_B$, and $r_{AB} = r_A + r_B$. In reality, however, not only is ionic radius a function of local environment, but also atoms may exhibit multiple radii (depending on which atom it interacts with) so that the three bond lengths discussed here are independent. Large-scale molecular dynamics (MD) simulations enable crystal structures to be explored from interatomic potentials and therefore do not require the hard-sphere approximation. A systematic MD study of crystal structures, however, has not been reported in literature. This is primarily because interatomic potentials are traditionally parameterized using crystal structures as inputs rather than outputs. An approach that enables MD simulations to be used to determine the effects of independent bond lengths on crystal structures is therefore of great interest. Unlike conventional MD methods in which the interatomic potential is parameterized for a particular material, here we develop an embedded-ion method (EIM) [15] interatomic potential model that does not focus on a given material, but rather uses bond lengths directly as model parameters without fitting them and hence enables crystal structures to be explored as a function of arbitrary combinations of bond lengths.

2.2 Interatomic Potential

2.2.1 Background

The fixed-charge models commonly used for ionic compounds [16,17,18,19,20,21,22,23,24] are most accurate for defect-free stoichiometric compounds of a specific crystal structure as they do not allow environment-dependent charge variation. Because atoms remain ionized even in the vapor phase, the fixed-charge models also typically overestimate cohesive energies of compounds by 4 to 5 times [25]. In the variable-charge models [25,26,27,28,29,30,31], the equilibrium charges on atoms are solved dynamically from the minimum energy condition. The equilibrium charges vary as atoms move, and hence the variable charge models better incorporate the change of effective bond length due to the change of charges in different crystal structures. They also can correctly predict the cohesive energies of compounds. Note that ionic interatomic potentials have been derived from quantum mechanical perturbation theory [32,33,34,35,36,37]. These models typically use atomic sizes as model parameters. While some models assume fixed atomic sizes, other models allow variable atomic sizes. In the latter case,

the atomic sizes are dynamically solved to minimize the energy. Even though these models are based upon fixed charges, the effect achieved by the variable atomic size may be similar to that achieved by the variable-charge models.

The distribution of charges among atoms always changes when crystal structures change. While the variable-charge potential models [25,26,27,28,29,30,31] capture this charge transfer phenomenon, they require the recalculation of the equilibrium charges on atoms at each time step during an MD simulation. These equilibrium charges are obtained numerically by minimizing the system energy with respect to charges. To ensure energy conservation during constant energy MD simulations, the energy drop during the energy minimization calculations must be negligible. This means that the minimum energy condition (i.e., the change of energy with respect to change of charges equals zero) must be well achieved after the energy minimization, and the time step size must be small enough so that the minimum energy condition is approximately maintained prior to the next energy minimization calculation. Clearly, such simulations are computationally expensive. To overcome this problem, recent efforts have been made to incorporate the variable charge effects analytically [15,38]. The embedded-ion method [15] is one of such analytical variable-charge models. The embedded-ion method potential model used here is modified from the previous model [15].

2.2.2 Embedded-Ion Method Potential Model

The essential effect incorporated by a variable-charge model is discussed in Appendix A. Here we describe the EIM model that aims to incorporate the physics discussed in Appendix A and Figure A1. Following the previous work [15], the total system energy of the EIM is expressed as

$$E = \frac{1}{2}\sum_{i=1}^{N}\sum_{j=i_1}^{i_N}\phi_{ij}\left(r_{ij}\right) + \sum_{i=1}^{N}E_i\left(q_i,\sigma_i\right) \tag{1}$$

where $\phi_{ij}(r_{ij})$ is a pair energy between atoms i and j separated by a distance r_{ij}, $E_i(q_i,\sigma_i)$ is the embedding energy arising from embedding an atom onto a local site i, q_i is a measure of charge on atom i, σ_i is a measure of electrical potential (in unit of voltage) at site i due to neighboring atoms, $i_1, i_2, \ldots, i_N$ is a list of neighbors to atom i, and N is total number of atoms in the system. The electrical potential σ_i can be assumed to be a sum of contributions from all neighbors to atom i:

$$\sigma_i = \sum_{j=i_1}^{i_N} q_j \cdot \varphi_{ij}\left(r_{ij}\right) \tag{2}$$

where $\varphi_{ij}(r_{ij})$ is taken as an empirical pair function. The embedding energy can be simply written as*

$$E_i(q_i,\sigma_i)=\frac{1}{2}q_i\cdot\sigma_i \tag{3}$$

If we assume that η_{ji} represents the electron transfer from atom i to atom j, the charge on atom i can then be written as a sum of electrons that i loses to all its neighbors:

$$q_i=\sum_{j=i_1}^{i_N}\eta_{ji} \tag{4}$$

Note that, by definition, $\eta_{ji} = -\eta_{ij}$ (i.e., the electrons that the atom i lost to atom j equals the electrons that atom j gained from atom i), and as long as this condition is satisfied, charge balance is guaranteed by Eq. (4).

The electron transfer variable η_{ji} (and hence the charge q_i on an atom i) is a definite quantity when the environment of i and j is given. This means that η_{ji} (and q_i) can be described by environment dependent functions. A simple treatment is to assume that η_{ji} is a function of spacing between i and j. This assumption is similar to the bond valence model, where the bond valence is assumed to be a pair function. With this assumption, substituting Eqs. (2) to (4) into Eq. (1) results in a total system energy of

$$E=\frac{1}{2}\sum_{i=1}^{N}\sum_{j=i_1}^{i_N}\phi_{ij}(r_{ij})+\sum_{i=1}^{N}\left\{\left(\sum_{j=i_1}^{i_N}\eta_{ji}(r_{ij})\right)\cdot\sum_{j=i_1}^{i_N}\left[\left(\sum_{k=j_1}^{j_N}\eta_{kj}(r_{jk})\right)\cdot\varphi(r_{ij})\right]\right\} \tag{5}$$

The embedding energy defined by Eq. (5) incorporates two many-body terms $\sum_{j=i_1}^{i_N}\eta_{ji}(r_{ij})$ and $\sum_{j=i_1}^{i_N}\left[\left(\sum_{k=j_1}^{j_N}\eta_{kj}(r_{jk})\right)\cdot\varphi(r_{ij})\right]$. The $\sum_{j=i_1}^{i_N}\eta_{ji}(r_{ij})$ term is similar to the electron density term in the EAM for metals [39,40] except that $\sum_{j=i_1}^{i_N}\eta_{ji}(r_{ij})$ can be both positive and negative whereas the electron density in the EAM is always positive. The $\sum_{j=i_1}^{i_N}\left[\left(\sum_{k=j_1}^{j_N}\eta_{kj}(r_{jk})\right)\cdot\varphi(r_{ij})\right]$ term additionally incorporates an environment-dependent many-body term that requires a nested loop to compute. Despite this complexity, the efficiency of EIM force and stress calculations is still comparable to

* Note that Eq. (3) reduces to Coulomb type interactions between i and its neighbors if $\varphi_{ij}(r_{ij})$ is taken as $\sim r_{ij}^{-1}$: $E_i(q_i,\sigma_i)=\frac{1}{2}\sum_{j=i_1}^{i_N}\frac{q_i\cdot q_j}{r_{ij}}$.

that of EAM, requiring only one additional message passing during parallel simulations. This can be illustrated by writing the derivative of the embedding energy term with respect to any coordinate variable *X* as

$$\begin{aligned}\sum_{i=1}^{N}\frac{\partial E_i(q_i,\sigma_i)}{\partial X} &= \frac{1}{2}\sum_{i=1}^{N}\sum_{j=i_1}^{i_N}\left[\frac{\partial q_i}{\partial X}\cdot q_j\cdot\varphi(r_{ij})+q_i\cdot\frac{\partial q_j}{\partial X}\cdot\varphi(r_{ij})+q_i\cdot q_j\cdot\frac{\partial\varphi(r_{ij})}{\partial X}\right]\\ &= \frac{1}{2}\sum_{i=1}^{N}\left(\frac{\partial q_i}{\partial X}\cdot\sigma_i\right)+\frac{1}{2}\sum_{j=1}^{N}\left(\frac{\partial q_j}{\partial X}\cdot\sigma_j\right)+\frac{1}{2}\sum_{i=1}^{N}\sum_{j=i_1}^{i_N}\left[q_i\cdot q_j\cdot\frac{\partial\varphi(r_{ij})}{\partial X}\right]\\ &= \sum_{i=1}^{N}\left(\frac{\partial q_i}{\partial X}\cdot\sigma_i\right)+\frac{1}{2}\sum_{i=1}^{N}\sum_{j=i_1}^{i_N}\left[q_i\cdot q_j\cdot\frac{\partial\varphi(r_{ij})}{\partial X}\right]\end{aligned} \tag{6}$$

Apparently, the $\sum_{i=1}^{N}\left(\frac{\partial q_i}{\partial X}\cdot\sigma_i\right)$ term has the same calculation cost as the derivative of electron density in the EAM model if σ_i is known, and the $\sum_{i=1}^{N}\sum_{j=i_1}^{i_N}\left[q_i\cdot q_j\cdot\frac{\partial\varphi(r_{ij})}{\partial X}\right]$ term has the same calculation cost as a pair potential model if q_i and q_j are known. To implement this model in MD codes, q_i is first calculated according to Eq. (4) and passed to all processors. σ_i is next calculated using Eq. (2) and passed to all processors. The forces and stresses can then be implemented according to Eq. (6). The calculations are so similar to the EAM that only an additional message passing of σ_i needs to be added to an existing parallel EAM routine. This EIM has been implemented in the parallel MD code LAMMPS [41,42].

2.2.3 Function Forms

As described above, our objective is to understand crystal structure as a function of atomic sizes that are characterized by the "intrinsic" bond length. Here the intrinsic bond length refers to the bond length of an isolated pair of atoms at the absence of charge transfer. It is distinguishable from the "crystal" bond length that results from interaction of many atoms and is affected by the charge transfer. Note that the crystal bond lengths between different pairs of atoms are not independent but rather are related to the lattice constants. To enable crystal structure to be explored in the intrinsic bond length space, we construct our potential formalisms so that the intrinsic bond lengths use the model parameters directly rather than using other parameters to fit them.

The EIM model described above involves three pairwise functions $\phi_{ij}(r)$, $\eta_{ij}(r)$, and $\varphi_{ij}(r)$ between any pair of species i and j. These functions are assumed to cut off at designated cutoff distances. To implement the cutoff distance, all the pair functions are multiplied by a cutoff function constructed as the following:

$$f_c(r,r_p,r_c)=\left[0.510204\cdot erfc\left(\frac{1.64498(2r-r_p-r_c)}{r_c-r_p}\right)-0.010204\right] \tag{7}$$

where r_p and r_c are two parameters. This cutoff function approximately equals unity at $r \le r_p$, but decays to zero when r approaches the cutoff distance r_c. Note that some interatomic potentials apply the cutoff function over a designated cutoff range [43,44]. Such potentials do not have continuous second derivatives at the junction points of the cutoff function. The cutoff method used here has (theoretically) continuous high-order derivatives.

The characteristic properties of a pair energy function $\phi_{ij}(r)$ is the energy well $E_{b,ij}$, the intrinsic bond length $r_{e,ij}$ at which the energy well occurs, and the cutoff distance $r_{c\phi,ij}$. Here we also refer $E_{b,ij}$ to the intrinsic bond energy. As an exponential potential is typically used for metallic and covalent interactions [43,44,45,46], a Morse type of potential is adopted to represent the interactions between cation atoms or between anion atoms:

$$\phi_{ij}(r) = \left[\frac{E_{b,ij} \cdot \beta_{ij}}{\beta_{ij} - \alpha_{ij}} \cdot \exp\left(-\alpha_{ij} \cdot \frac{r - r_{e,ij}}{r_{e,ij}} \right) - \frac{E_{b,ij} \cdot \alpha_{ij}}{\beta_{ij} - \alpha_{ij}} \cdot \exp\left(-\beta_{ij} \cdot \frac{r - r_{e,ij}}{r_{e,ij}} \right) \right] \cdot f_c\left(r, r_{e,ij}, r_{c\phi,ij}\right) \tag{8}$$

Unlike an increase in the bond length between cation atoms or between anion atoms, the charge-transfer causes a reduction in the bond length between cation and anion atoms. Considering that ions are relatively incompressible, we use a Lennard-Jones type of power function with a strong, short-distance repulsion to represent the cation–anion interactions:

$$\phi_{ij}(r) = \left[\frac{E_{b,ij} \cdot \beta_{ij}}{\beta_{ij} - \alpha_{ij}} \cdot \left(\frac{r_{e,ij}}{r} \right)^{\alpha_{ij}} - \frac{E_{b,ij} \cdot \alpha_{ij}}{\beta_{ij} - \alpha_{ij}} \cdot \left(\frac{r_{e,ij}}{r} \right)^{\beta_{ij}} \right] \cdot f_c\left(r, r_{e,ij}, r_{c\phi,ij}\right) \tag{9}$$

Eqs. (8) and (9) include five parameters: intrinsic bond energy $E_{b,ij}$, intrinsic bond length $r_{e,ij}$, cutoff distance $r_{c\phi,ij}$, and two additional constant α_{ij} and β_{ij}. The concepts of $E_{b,ij}$, $r_{e,ij}$, and $r_{c\phi,ij}$, are verified in Figure 1, where (a) through (c) show respectively the effect of individually varying r_e, $r_{c\phi}$, and E_b at fixed other parameters, and the left and the right columns are calculated using Eqs. (8) and (9), respectively. Clearly, it can be seen that parameters r_e, r_c, and E_b correspond independently to their intended definitions. In this way, the physical properties r_e and E_b are directly treated as model parameters.

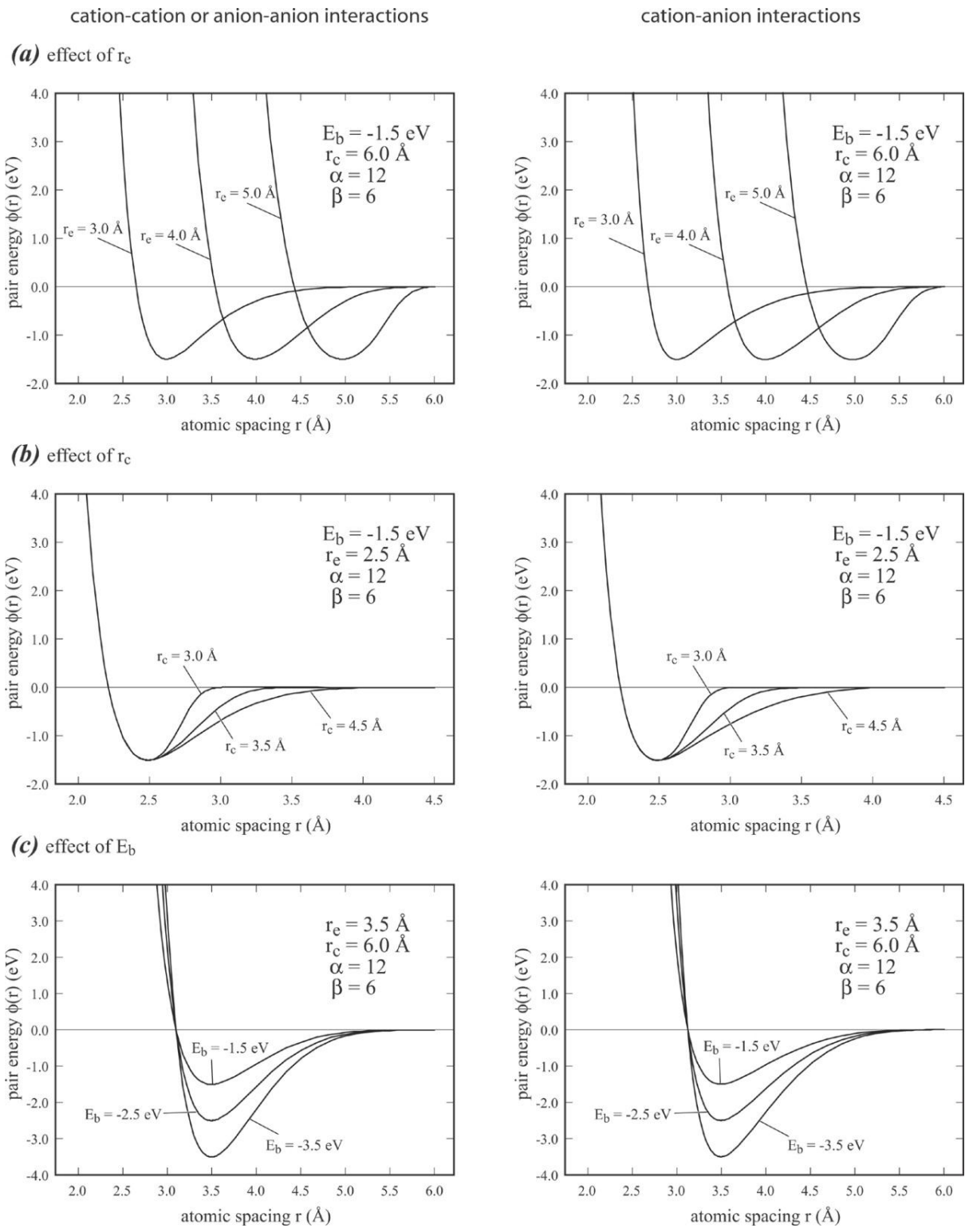

Figure 1. Effects of parameters on pair energy function $\phi(r)$.

The charge-transfer η_{ji} from atom i to atom j has been found to scale with (χ_j - χ_i) where χ_j and χ_i are electronegativities of atoms j and i respectively [25]. Hence, $\eta_{ji}(r)$ is expressed as

$$\eta_{ji}(r) = A_{\eta_{ij}}(\chi_j - \chi_i)\cdot f_c(r, r_{s\eta,ij}, r_{c\eta,ij}) \tag{10}$$

where $A_{\eta_{ij}}$, $r_{s\eta,ij}$, and $r_{c\eta,ij}$ are three parameters, and, in particular, $r_{c\eta,ij}$ is the cutoff distance for the charge-transfer function and $r_{s\eta,ij}$ is the point where the cutoff function starts to deviate from unity. Our model uses the classical concept that the charges induced by cation–cation or anion–anion interactions are negligible. This can be conveniently done by setting $A_{\eta_{ij}} = 0$ when i and j are both cations or when they are both anions.

Finally, the charge interaction function $\varphi_{ij}(r)$ is simply taken as an exponential decaying function multiplied with the cutoff function. This is expressed as

$$\varphi_{ij}(r) = A_{\varphi_{ij}} \cdot \exp(-\zeta_{ij} \cdot r)\cdot f_c(r, r_{s\varphi,ij}, r_{c\varphi,ij}) \tag{11}$$

Eq. (11) includes four parameters: constants $A_{\varphi_{ij}}$ and ζ_{ij}, cutoff distance $r_{c\varphi,ij}$, and the starting point of the cutoff $r_{s\varphi,ij}$.

In summary, the EIM model described above would contain one electronegativity parameter for each element, and 12 parameters $E_{b,ij}$, $r_{e,ij}$, $r_{c\phi,ij}$, α_{ij}, β_{ij}, $A_{\eta_{ij}}$, $r_{s\eta,ij}$, $r_{c\eta,ij}$, $A_{\varphi_{ij}}$, ζ_{ij}, $r_{s\varphi,ij}$, and $r_{c\varphi,ij}$ for each pairs. These parameters can be determined by fitting to the target lattice constants and cohesive energies of elemental and binary systems, as described below.

2.3 Monovalent Binary Systems

2.3.1 Calibrated EIM Parameters

We first explore crystal stability criteria of monovalent binary compounds AB. Specifically, we will theoretically establish effects of atomic sizes (i.e., the intrinsic bond lengths $r_{e,AA}$, $r_{e,BB}$, and $r_{e,AB}$) on the crystal structure of binary compounds over the bond length ratio range (e.g., $r_{e,AA}$/ $r_{e,BB}$) typical of alkali halides. For this purpose, reasonable values of EIM parameters need to be used. Here we derive 20 sets of calibrated parameters for the binary compound by fitting EIM to the properties of the 20 monovalent alkali halide systems (e.g., LiF, LiI, NaCl, CsCl) composed of one 1A metal atom (Li, Na, K, Rb, Cs) and one halogen atom (F, Cl, Br, I). To consistently represent the general trend of atomic sizes for the alkali halide systems, the parameterization was performed simultaneously so that the parameter for the same pair is treated as a single parameter even it is used in different alkali halides. Note that parameters obtained for each alkali halide compound are sufficient to explore the effects of crystal stability as a function of intrinsic bond lengths (as will be shown in Figure 8 below). All 20 sets of parameters are used in this work to

explore the crystal stability so that the conclusion is more robust and is less affected by the model approximation and the parameter accuracy for any individual alkali halide compound.

Note also that the crystal stability will be tested with parameters that are different from the calibrated parameters due to the use of arbitrary intrinsic bond lengths so that we are truly studying the "generic" materials. The calibrated parameters are only used for the reference values of other parameters when the intrinsic bond lengths are varied. Now we describe details of the parameterization.

The Pauling scale of electronegativities [11,47,48] are directly used in this work, and the data are listed in Table B1 of Appendix B for convenience. For the 20 alkali halide compounds, there are 9 elements (i = Li, Na, K, Rb, Cs, F, Cl, Br, I). The total number of parameters to be calibrated then contain 12 pair parameters for each of the 45 pairs of species. For the 12 pairwise parameters, $A_{\eta_{ij}}$ is set to zero for any cation–cation or anion–anion pairs so that no charges are induced between cation atoms or between anion atoms, and to a universal value for any cation–anion pairs based upon the constraint that the maximum magnitude of charge of all the compounds equals the valence of unity. ζ_{ij} is set to a universal value of 0.6, as treating it as a free parameter did not result in an improved fitting. Parameters $r_{c\phi,ij}$, $r_{s\eta,ij}$, $r_{c\eta,ij}$, $r_{s\varphi,ij}$, $r_{c\varphi,ij}$ are all related to the cutoff and are preselected following a few trial-and-errors without including them in the optimization. Note that when $A_{\eta_{ij}}$ is set to zero for cation–cation or anion–anion pairs, the values of $r_{s\eta,ij}$ and $r_{c\eta,ij}$ do not affect the results, Eq. (10). In these cases, $r_{s\eta,ij}$ and $r_{c\eta,ij}$ are both set to 0. Under these choices, only five parameters ($E_{b,ij}$, $r_{e,ij}$, α_{ij}, β_{ij}, $A_{\varphi_{ij}}$) remain to be determined. These five parameters have clear physical meanings on atomic properties, and therefore can be arbitrarily varied within physical ranges. Here they are calibrated from experimental lattice constants and cohesive energies of binary alkali halide compounds under constraints that

(a) The nine elements (Li, Na, K, Rb, Cs, F, Cl, Br, I) all have approximately the right cohesive energies, and

(b) The experimentally observed crystals of the binary compounds have the lowest cohesive energies: Li, Na, K, Rb, Cs, F, Cl, Br, I Li, Na, K, Rb, Cs, F, Cl, Br, I Li, Na, K, Rb, Cs, F, Cl, Br, ILi, Na, K, Rb, Cs, F, Cl, Br, I,and

(c) Since the binary compounds only give information to determine the cross interactions between cations and anions but not the cross interactions between different cations or between different anions, we use the following conventional mixing rule to define the parameters between different cations or between different anions [44]: $E_{b,ij} = -\sqrt{E_{b,ii} \cdot E_{b,jj}}$, $r_{e,ij} = \left(r_{e,ii} + r_{e,jj}\right)/2$, $\alpha_{ij} = \left(\alpha_{ii} + \alpha_{jj}\right)/2$, $\beta_{ij} = \left(\beta_{ii} + \beta_{jj}\right)/2$, and $A_{\varphi_{ij}} = \sqrt{A_{\varphi_{ii}} \cdot A_{\varphi_{jj}}}$.

All the 20 binary alkali halide compounds considered are listed in Table 1. Of these 20 compounds, only CsCl, CsBr, and CsI exhibit the B2 (CsCl type) crystal structure whereas all the other compounds exhibit the B1 (NaCl type) crystal [10,49]. Experimental lattice constants were taken from [10,49]. Following the previous approach [25,50], we derived the cohesive energies of both elemental and compound phases from the experimental thermochemical data of various substances [51,**Error! Bookmark not defined.**]. An objective function was defined as a weighted sum of square deviation of calculated lattice constants and cohesive energies from the corresponding experimental values for all the 20 phases being calibrated. With proper bounds for all parameters, optimization is done using four Mathematica [52] built-in methods: differential evolution, simulated-annealing, default, and Nelder-Mead algorithms to ensure a well-converged global minimum. The calibrated nominal parameters thus obtained are shown in Table B2 in Appendix B.

Table 1. Lattice constant, cohesive energy, and charge of different compound crystals.

Compound	Lattice constant (Å)		Cohesive energy (eV/atom)		|Charge|(e)
	Experiment [10,49]	EIM	Experiment [51,53]	EIM	EIM
LiF	4.018	4.018	-4.431	-4.426	0.940
LiCl	5.132	5.133	-3.570	-3.578	0.683
LiBr	5.494	5.495	-3.224	-3.194	0.621
LiI	6.050	6.050	-2.778	-2.805	0.527
NaF	4.614	4.613	-3.947	-3.876	0.956
NaCl	5.628	5.627	-3.315	-3.315	0.699
NaBr	5.962	5.954	-3.009	-3.004	0.636
NaI	6.462	6.455	-2.601	-2.597	0.542
KF	5.328	5.325	-3.817	-3.830	0.991
KCl	6.278	6.280	-3.353	-3.339	0.733
KBr	6.586	6.586	-3.082	-2.793	0.671
KI	7.052	7.052	-2.714	-2.723	0.577
RbF	5.630	5.629	-3.718	-3.677	0.990
RbCl	6.570	6.568	-3.304	-3.295	0.733
RbBr	6.868	6.868	-3.044	-2.814	0.671
RbI	7.326	7.325	-2.703	-2.506	0.577
CsF	6.010	6.010	-3.680	-3.631	1.000
CsCl	3.984	3.984	-3.320	-3.323	0.976
CsBr	4.155	4.155	-3.077	-3.056	0.894
CsI	4.414	4.414	-2.746	-2.699	0.771

2.3.2 Characteristics of Calibrated Parameters

The characteristics of the calibrated parameters are evaluated. The calculated lattice constants and cohesive energies of the 20 equilibrium alkali halide compounds are compared with the corresponding experimental data in Table 1. In addition, the calculated absolute values of charge on atoms are included. Table 1 shows that the difference between the calculated and the experimental lattice constant is in general significantly less than 0.1%, and the agreement between the calculated and the experimental cohesive energy is also very good. This excellent agreement was not trivial to achieve as it required extensive iterative parameterizations where the constraining bounds for the parameter ratio α_{ij}/β_{ij} were adjusted through trial and error while keeping them close to the ideal value of $\alpha_{ij}/\beta_{ij} = 2$ when possible. Note that, because the calibrated parameters are only used as reference points to explore "generic" materials, the exact fit is not a requirement. Our choice to pursue the good fit was mainly due to Pauling's initial work [10] where his predicted lattice constants of alkali halide compounds also precisely match the corresponding experimental values.

Table 1 shows that the calculated charges correspond to the electronegativity difference between the two elements very well. This difference can be more clearly seen in Figure 2, where the magnitude of charge is plotted as a function of difference of electronegativity between anion and cation, $\chi_{anion} - \chi_{cation}$. Figure 2 verifies that by construction, the model has the desired characteristics that the magnitude of charge linearly increases with electronegativity difference for a given crystal structure, and the maximum magnitude of charge (observed in CsF, Table 1) is bounded by unity. It is possible to fit charges of different crystals. It is not clear how to determine the target values of charges in the 20 compounds considered here, and the purpose of the calibration is not to study these 20 compounds but rather the generic materials. Hence, we leave the charge refinement for future investigation. Here we have selected the charge parameters so that the charges increase with coordination number of dissimilar species and are bounded by the valence value at short distances (as a result, it is relatively insensitive to the atomic spacing at short distances). This means that when cations are embedded in a cation-rich environment, or when anions are embedded in an anion-rich environment, the charges on atoms are low. Only when cations are embedded in anion-rich environment, or when anions are embedded in a cation-rich environment, will the atoms have a high charge. In this sense the model is in line with the variable charge concept.

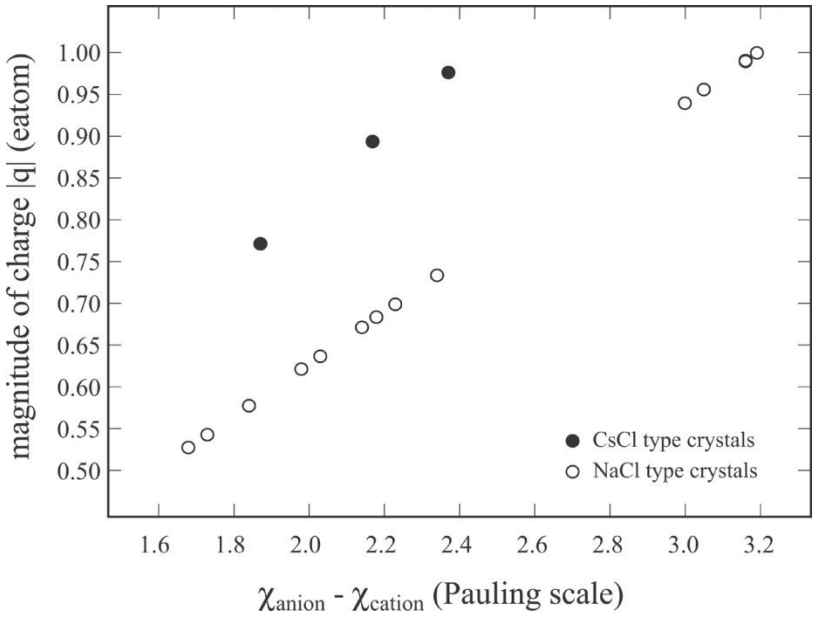

Figure 2. Magnitude of charge as a function of electronegativity difference.

Figure 3 examines bond length. The circles in Figure 3(a) show the intrinsic bond length r_e as a function of experimental crystal bond length for all the cation–anion pairs, whereas the "slope = 1" line indicates an exact match between r_e and the experimental crystal bond length. As expected, r_e does not match exactly, but correlates well to experimental crystal bond length. On the other hand, the circles in Figure 3(b) show the calculated crystal bond length as a function experimental crystal bond length for all the cation–anion pairs. In this case, the calculated and experimental crystal bond lengths match exactly, consistent with the lattice constants shown in Table 1. The good correlation between r_e and experimental crystal bond length indicates that the calibrated EIM at least captures the general trend of the atomic size effect of the alkali halide compounds.

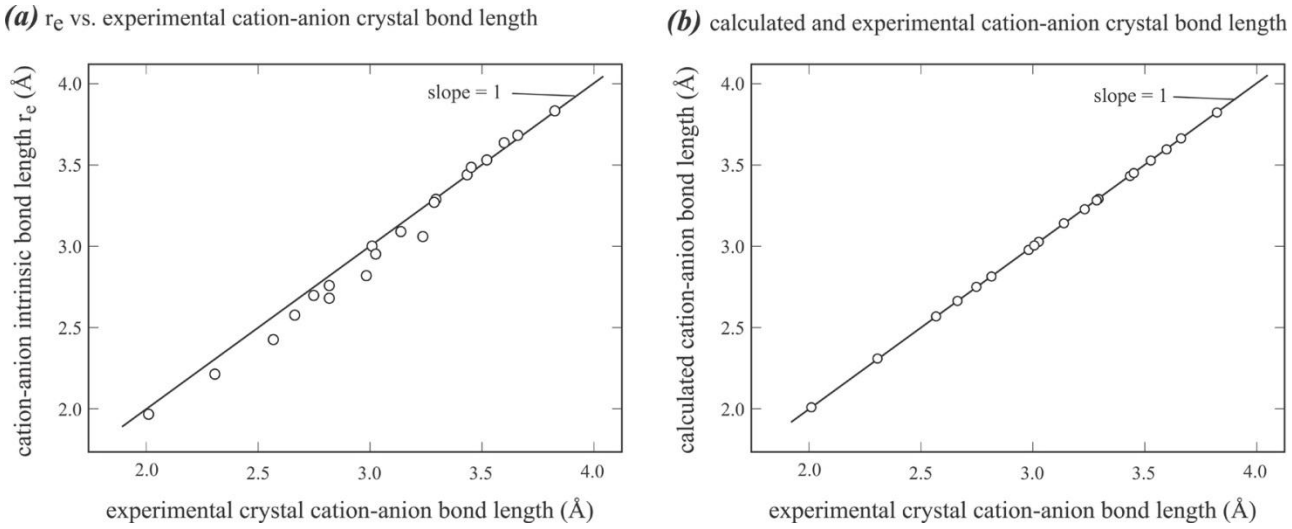

Figure 3. Parameter r_e and calculated crystal bond length as a function of experimental crystal bond length for cation–anion pairs.

Table 1 also compares the calculated cohesive energies of the 20 compounds with those obtained from experiments. To examine this aspect more clearly, the calculated cohesive energies are shown against the experimental data for both elements and compounds in Figure 4, where the "slope = 1" line indicates an exact match between the model results and the experiment. Figure 4 further confirms that the calibrated EIM agrees very well with the general trend of the cohesive energies of all of the 20 compounds as well as the nine elements. Note that our elemental calculations are based upon a face-centered-cubic (fcc) phase, whereas the experimental cohesive energies of F, Cl, Br, and I are referred to the molecular solid phases of F_2, Cl_2, Br_2, and I_2. Consequently, Figure 4 only demonstrates that the calibrated parameters are well guided by the energies of these elemental systems. The demonstrated values, however, should not be taken as the real differences between the calculated and experimental cohesive energies for the F, Cl, Br and I elements.

The charge-transfer nature of the EIM potentials is explored. The general feature was found to be the same for all of the 20 compounds, and hence only LiF is demonstrated here as an example. Various energy components are plotted against hydrostatic strain in Figure 5, where red, blue, and black lines indicate, respectively, the cohesive energy components arising from cation–cation (Li-Li), anion–anion (F-F), and cation–anion (Li-F) interactions, and the solid and dash lines correspond respectively to the energies without and with the charge-transfer embedding energy term. Note that the embedding energy equals zero when charges are zero (Eq. (3)).

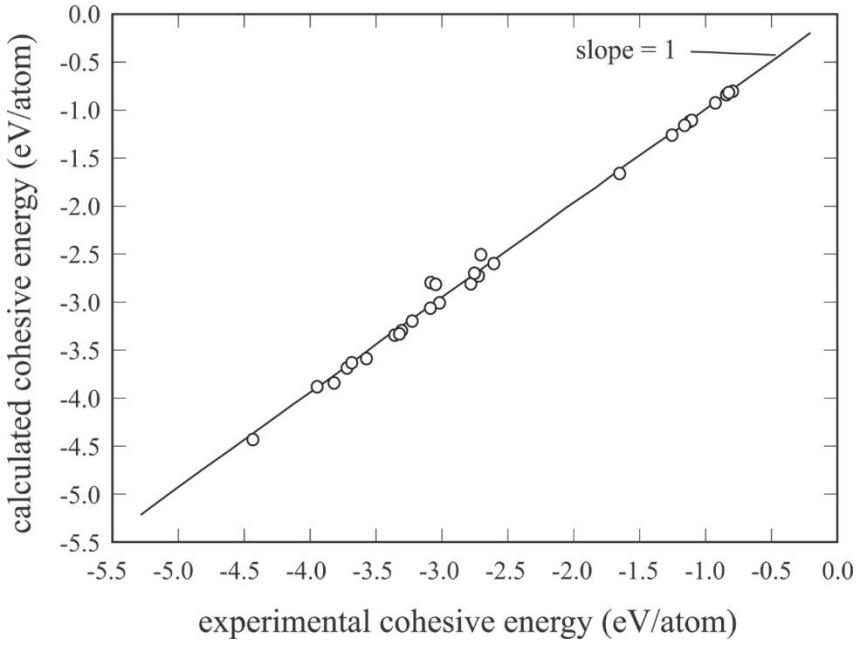

Figure 4. Calculated and experimental cohesive energies for the 20 binary compounds and the nine elements.

Imagine that if the cation (Li) sublattice is moved away from the anion (F) sublattice, then charges become zero on both cation and anion atoms. The energies for the cation and anion sublattices can therefore be exactly described by the LiLi and FF solid lines in Figure 5. When cation and anion sublattices are brought together to form the compound, charges are induced on cation and anion atoms. This charge causes an increase in the length of the Li-Li and F-F bonds and a decrease in their bond strength, as shown by the corresponding dash lines. Figure 5 also clearly shows that the induced charges cause a decrease in the bond length and an increase in the bond strength for the cation–anion (Li-F) interaction. The EIM, hence, correctly captures the charge-transfer interactions discussed in Appendix A and Figure A1 that have not been captured by conventional analytical interatomic potential methods.

We found that the extent of the charge-transfer (i.e., the change caused by the embedding energy) aligns with the electronegativity difference. In particular, the charge-transfer decreases in the anion sequence of decreasing electronegativity F, Cl, Br, and I for any given cation except from CsF to CsCl where the charge-transfer increases. This exception can be attributed to the crystal structure change going from CsF to CsCl.

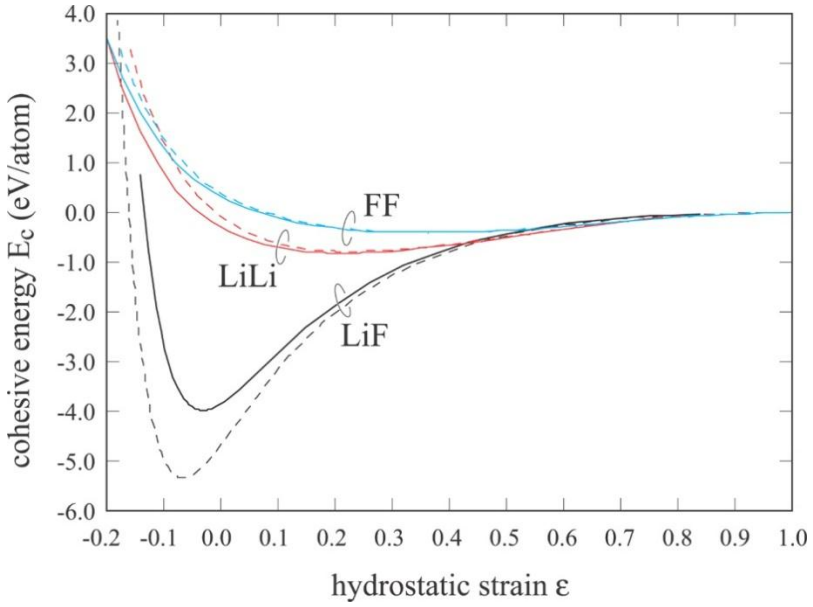

Figure 5. Various energy components as a function of hydrostatic strain for LiF.

2.3.3 Molecular Dynamics Study of Crystal Stability

The calibrated parameters developed above begin to enable atomistic simulations to be used to explore the effects of intrinsic bond length on the crystal structure of an ionic compound. Here, we explore the conditions that lead to the formation of B1 (NaCl type), B2 (CsCl type), and B3 (zinc-blende) structures commonly seen in the AB compounds. To reduce the parameter space that involves AA, BB and AB bond lengths, we start with the parameters that are calibrated to the 20 real alkali halide compounds and then systematically increase and decrease the bond lengths. To prevent the system from being trapped in any given initial configuration that might be in a metastable state with a deep local energy minimum, three molecular dynamics simulations of annealing were conducted for each of the 20 compounds using all three initial crystal configurations: B1, B2, and B3. The B1 crystal has 6×6× 6 cells and 1728 atoms. The B2 crystal has 10×10×10 cells and 2000 atoms. The B3 crystal has 8× 8× 8 cells and 4096 atoms. In each simulation, the system was initially heated up to 1400 K and then "slowly" cooled to 300 K over a 10 ns period. The lowest free-energy final configuration obtained from the three simulations of each compound was then taken as the equilibrium phase. The effectiveness of this approach in finding the lowest free energy configuration is illustrated in Figure 6 using NaCl as an example. Assume that the NaCl was initially in a wrong B2 crystal structure as shown by the (001) image of Figure 6(a) where each atom has eight nearest neighbors (i.e., the Cl atoms lie on the center of Na simple cubic cells and vice versa). After the simulated-annealing, the system was found to change to a lower-energy configuration and the same plane as Figure 6(a) is shown in Figure 6(b). This configuration exhibits a (111) type of plane of a cubic crystal where each atom has only six nearest neighbors of dissimilar species, thereby matching the equilibrium B1 crystal. In this case, the simulated-annealing identified the equilibrium crystal phase even though the initial configuration is not the correct B1 structure.

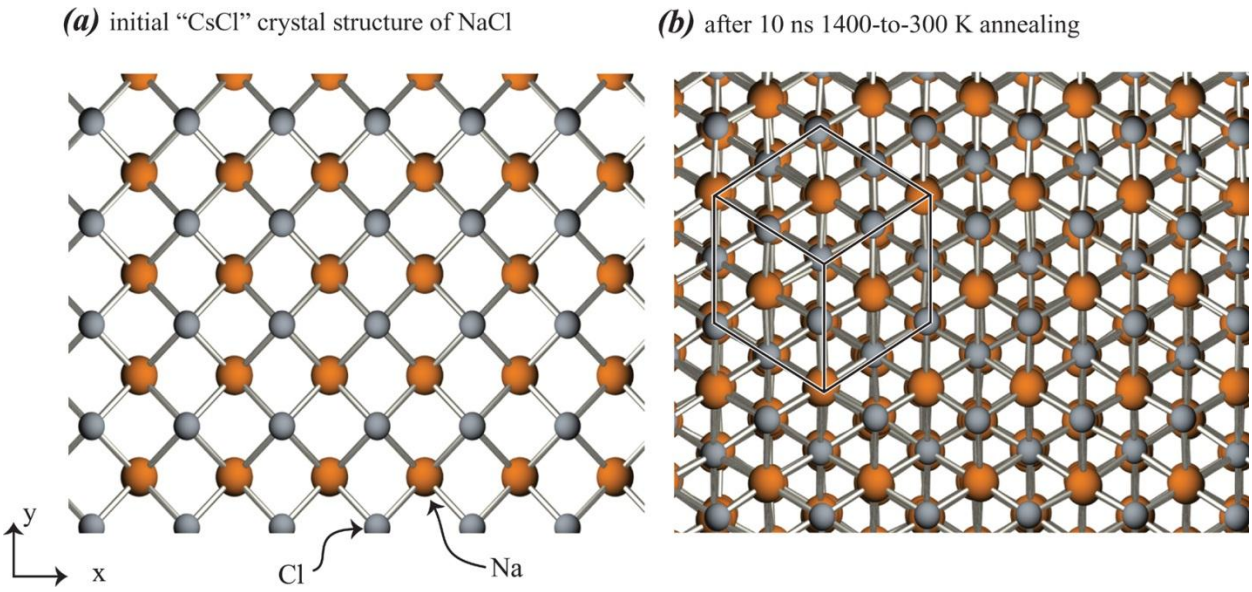

Figure 6. Change of a metastable B2 crystal of NaCl after the simulated-annealing.

Based on the equilibrium crystals identified in the simulated-annealing, different crystal vs. bond length parameter (r_e) maps were tried for best distinguishing different crystal zones. We found that if structures were mapped over a $r_{e,AB}$ vs. $(r_{e,AA}+r_{e,BB})/2$ diagram, then regions of different phases can be clearly distinguished. To illustrate this, the structures for the 20 alkali halide compounds obtained at a zero pressure are shown using unfilled circles in Figure 7(a), where the orange and blue colors represent B1 and B2 phases, respectively. Here, only three compounds (namely CsCl, CsBr, and CsI) exhibit the B2 crystal, whereas all the other compounds exhibit the B1 crystal. Interestingly, almost all the B1 crystals are below a B1/B2 boundary marked as a dash line in the figure, except for the four compounds CsF, CsCl, CsBr, and CsI, which are significantly above the line. Because CsCl, CsBr, and CsI all have the B2 crystal and CsF is likely to be close to changing to the B2 crystal, the different crystals appear to be well divided by the boundary line. The dash line can be quantified as $r^*_{e,AB} = 1.384\ (r_{e,AA}+r_{e,BB})/2 - 3.123$. Note that the parameters shown in Table B2 satisfy $0.69 < r_{e,AA}/r_{e,BB} < 1.44$. The finding in Figure 7(a) can be summarized as a crystal stability rule, as, under the condition $0.69 < r_{e,AA}/r_{e,BB} < 1.44$, the system exhibits the B2 structure when $r_{e,AB} > r^*_{e,AB}$, and the B1 structure when $r_{e,AB} < r^*_{e,AB}$.

The relatively open B1 structure of alkali halide crystals is known to transfer to the denser B2 structure under high pressure. Our literature survey indicated that experimental measurement of transformation pressure has been performed for KCl, KBr, KI, RbCl, RbBr, RbI, NaF, and NaCl [54,55]. For KCl, KBr, KI, RbCl, RbBr, and RbI, some experiments indicated that their transformation pressure can be as high as 2.5 – 10 GPa [54], whereas other experiments indicated a smaller ranger between 0.45 and 1.9 GPa [55]. For NaF and NaCl, the experimental transformation pressure is around 30 GPa or higher [55,56,57]. To test if our model qualitatively captures this pressure effect, simulations were repeated at two pressures of 25 GPa and 100 GPa, and the results are shown respectively in Figures 7(b) and 7(c).

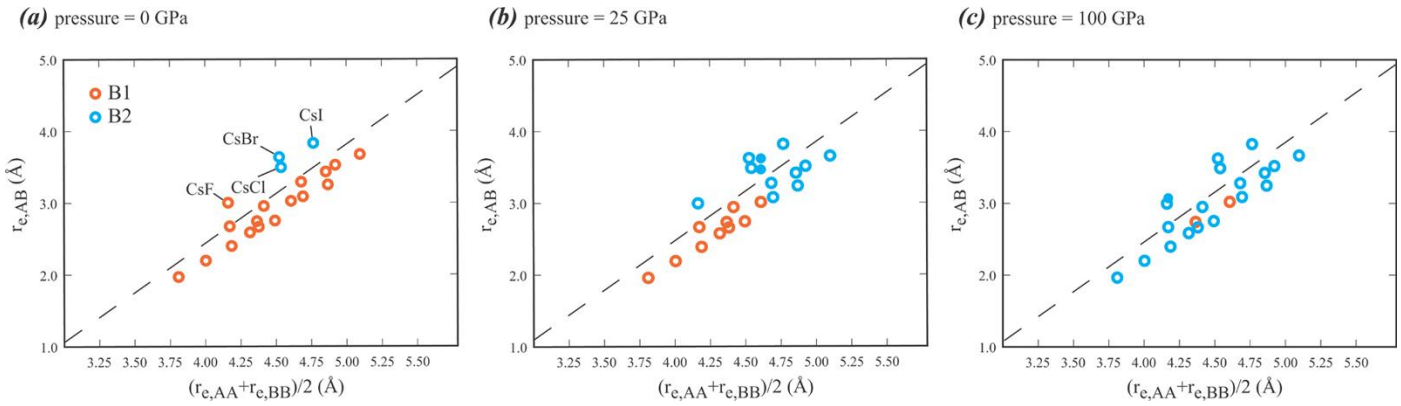

Figure 7. Crystal phase diagrams obtained at different pressures using the calibrated parameters.

For comparison, the B1/B2 phase boundary at zero pressure is included. Figure 7(b) indicates that when the pressure was increased from zero to 25 GPa, seven orange circles below the dash line turned blue. These seven circles, corresponding to CsF, KBr, KCl, KI, RbBr, RbCl, and RbI, respectively, therefore undergo a B1 to B2 transformation at a pressure below 25 GPa. Interestingly, these seven compounds cover all the six compounds mentioned above that have an experimental transformation pressure below 25 GPa. We found that when pressure was increased to 100 GPa, almost all of the 20 compounds have the B2 crystal structure. This finding is well reflected in Figure 7(c) where most circles are blue (the only two remaining orange circles correspond to NaBr and NaI). The results are consistent with experiments mentioned above showing that the transformation pressure for NaF and NaCl is between 25 and 100 GPa.

Having qualitatively validated the effect of pressure, we now further test the crystal phase diagram shown in Figure 7(a) using NaCl as an example reference point. Two series of simulations were performed. The first series progressively increased $r_{e,NaCl}$ at a constant $r_{e,NaNa}$ and $r_{e,ClCl}$; the second series progressively reduced $(r_{e,NaNa}+r_{e,ClCl})/2$ at a constant $r_{e,NaCl}$ and $r_{e,NaNa}/r_{e,ClCl}$ ratios. Note that the modified parameters no longer correspond to NaCl, but rather to a generic material system. The results are summarized in Figure 8 where the filled and unfilled circles refer respectively to modified and unmodified r_e with the B1/B2 boundary included as the dash line. It can be seen that the B1 structure of the original NaCl changed to a B2 structure when the points were moved above the boundary line whether or not it was caused by modifying $r_{e,NaCl}$ or modifying $(r_{e,NaNa}+r_{e,ClCl})/2$. This finding verifies the crystal stability rule shown in Figure 7(a).

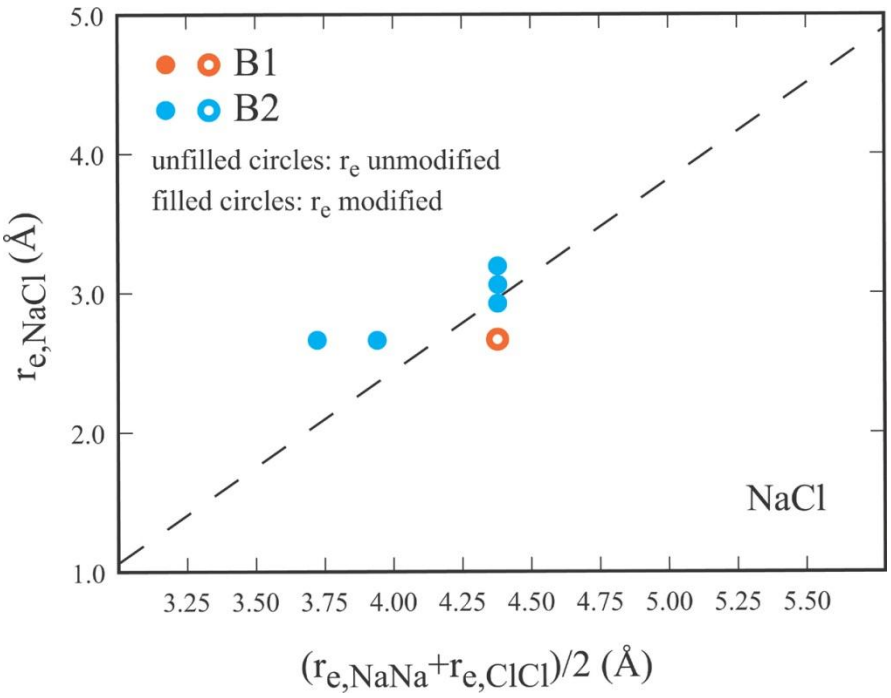

Figure 8. Structure vs. bond length map obtained from unmodified and perturbed NaCl parameters.

To more broadly verify the crystal phase diagram, simulations were repeated at increased and decreased $r_{e,AB}$ at constant $r_{e,AA}$ and $r_{e,BB}$ using each of the 20 alkali halide compounds as the starting point for parameter variation. The results thus obtained are summarized in Figure 9(a) where the unfilled circles indicate the 20 compounds and the filled circles represent the generic systems whose bond lengths were disturbed from those of the 20 compounds. In Figure 9, the orange, blue, and brown colors represent B1, B2, and B3 phases, respectively. Figure 9(a) confirms that by increasing $r_{e,AB}$, many of the data points in the B1 region moved above the B1/B2 boundary (dashed line) and the associated structures became B2. Likewise, the three B2 structures became B1 structures when $r_{e,AB}$ was reduced.

To further test the crystal stability criterion, simulations were again repeated using increased or decreased $(r_{e,AA}+r_{e,BB})/2$ values while keeping the $r_{e,AB}$ and $r_{e,AA}/r_{e,BB}$ ratios the same as those used in Figure 7(a). The results are included in Figure 9(b). It can be seen again that the crystals change from B1 to B2 when the data points are moved significantly above the B1 region. In particular, we found that the B1 structures always change to B2 structures when $(r_{e,AA}+r_{e,BB})/2$ is decreased below a certain threshold, and likewise B2 structures always change to B1 structures when $(r_{e,AA}+r_{e,BB})/2$ is increased above a certain threshold. Furthermore, when the data points are moved below a second boundary (dotted line), B1 structures change to B3 structures. The crystal zone map revealed in Figure 9, therefore, is a robust representation of the crystal stability criterion.

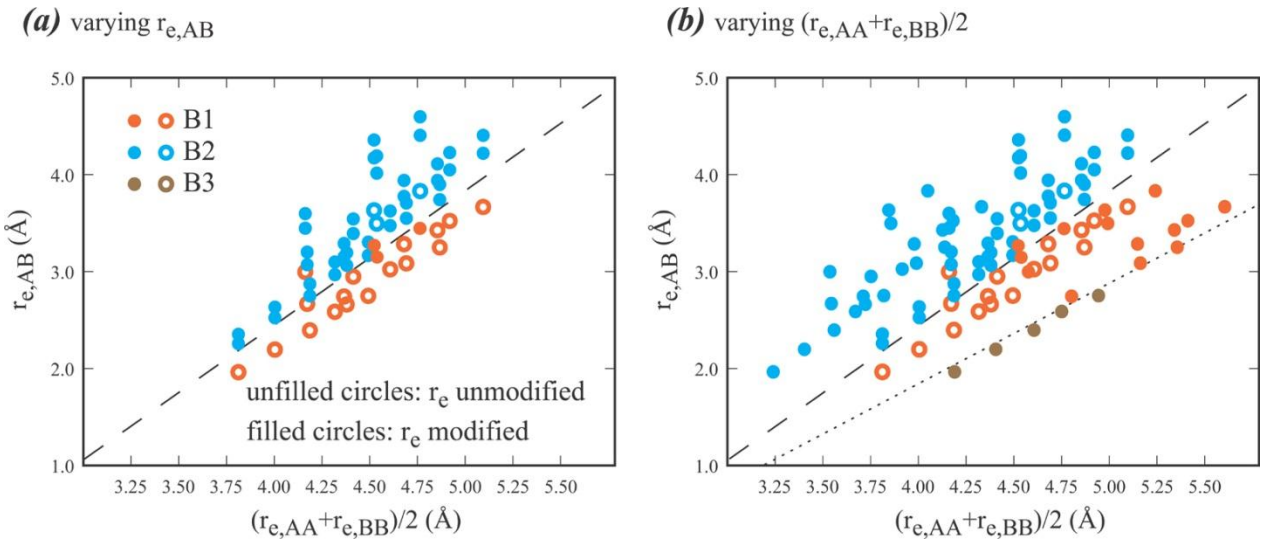

Figure 9. Crystal phase diagrams obtained at zero pressure using all calibrated and perturbed parameters.

It should be noted that in the hard-sphere model, $r_{e,AB} \equiv (r_{e,AA}+r_{e,BB})/2$. As a result, the $r_{e,AB}$ vs. $(r_{e,AA}+r_{e,BB})/2$ data reduce to a "slope = 1" line regardless compounds and the associated combinations of ionic radii. It is for this reason that the hard-sphere model cannot distinguish B1, B2, and B3 crystals.

Note that we do not fit the charges in our potential parameterization as described above. The net effect of the refined charges is to change the bond length according to Figure 5, which in turn may shift the location of the phase boundaries shown in Figures 7 through 9. However, Figures 7 through 9 were obtained from extensive MD simulations (combinations of 20 compounds, 3 crystal structures, numerous alterations of bond lengths, and 3 pressures) with each going through 1400 to 300 K temperature variation over a 10 ns period. The general trend of the crystal stability rule is hence rather robust and should not be affected by the charge refinement.

While the present work enables a relatively reliable analysis of crystal structures as a function of the intrinsic bond length r_e, caution should be taken when using the calibrated parameters to study specific compound because of the following:

(a) We did not fit the charges in this work other than demonstrating that the model correctly captures the charge transfer phenomenon shown in Figures 5 and A1, and

(b) Although the parameters were calibrated using the lattice constants and cohesive energies of the 20 alkali halide compounds, the intent is not to study these compounds but rather to study the generic materials.

Likewise, we assume an fcc lattice as the ground state structure for F, Cl, Br, and I, rather than their molecular gas phases. Improvement of the potential for a given compound can be made by

fitting other properties such as elastic constants and surface energies of the lowest energy phase, and lattice constants and cohesive energies of metastable phases; and by ensuring the lowest energy F_2, Cl_2, Br_2, and I_2 phases if possible.

In conclusion, the work performed in this project has enabled empirical atomistic simulations to be used to explore crystal stability rules. Our method is based upon a computationally efficient embedded-ion method based on interatomic potential. This potential analytically incorporates the charge-transfer interactions between atoms with different electronegativities, calibrates well with the lattice constants and cohesive energies of the 20 alkali halide compounds, and can be used for systems with any combinations of bond lengths. Preliminary atomistic simulations indicate that the crystal structure of ionic AB binary compounds is sensitive to the AA, BB, and AB intrinsic bond lengths $r_{e,AA}$, $r_{e,BB}$, and $r_{e,AB}$. Defining a critical AB bond length as $r^*_{e,AB}$ = 1.384 $(r_{e,AA}+r_{e,BB})/2$ – 3.123, we found that under the condition $0.69 < r_{e,AA}/r_{e,BB} < 1.44$, the system exhibits the B2 structure when $r_{e,AB} > r^*_{e,AB}$, and the B1 structure when $r_{e,AB} < r^*_{e,AB}$. Such a crystal zone diagram cannot be captured by the hard-sphere model.

2.4 Quaternary Elpasolite Systems

2.4.1 Development of the EIM Database

The chemical formula of elpasolite compounds can be expressed as A_2BLnX_6, where A and B are two different alkali elements, Ln is a lanthanide, and X is a halogen. To use atomistic simulation approaches to explore crystal structures of elpasolites, we developed an EIM database composed of all five alkali elements Li, Na, K, Rb, , and Cs, all four halogen elements F, Cl, Br, and I, and eight selected lanthanide elements La, Nd, Eu, Er, Ce, Sc, Y, and Gd. This enables us to cover 5×4×4×8 = 640 compounds. Note that here we explore the actual materials rather than the generic materials as described above for the monovalent binary systems.

The Pauling scale of electronegativities (listed in Table B1 of Appendix B) are again directly used. For the 17-element super system, there are 153 different pairs. As described above, $A_{\eta_{ij}}$, ζ_{ij}, $r_{c\phi,ij}$, $r_{s\eta,ij}$, $r_{c\eta,ij}$, $r_{s\varphi,ij}$, $r_{c\varphi,ij}$ are all pre-selected, resulting in only five parameters ($E_{b,ij}$, $r_{e,ij}$, α_{ij}, β_{ij}, $A_{\varphi_{ij}}$) per pair to be determined. Furthermore, interactions between different cations or between different anions are defined using the conventional mixing rule [44]: $E_{b,ij} = -\sqrt{E_{b,ii} \cdot E_{b,jj}}$, $r_{e,ij} = (r_{e,ii} + r_{e,jj})/2$, $\alpha_{ij} = (\alpha_{ii} + \alpha_{jj})/2$, $\beta_{ij} = (\beta_{ii} + \beta_{jj})/2$, and $A_{\varphi_{ij}} = \sqrt{A_{\varphi_{ii}} \cdot A_{\varphi_{jj}}}$, resulting in further reduction in unknown parameters. Here the remaining parameters are determined from experimental lattice constants [10,49] and cohesive energies [51,53,58] of elements and ionic binary (AX and LnX_3) compounds using the same approach described above. The parameters thus obtained are shown in Table B3 in Appendix B.

2.4.2 Characteristics of the EIM Database

The characteristics of the EIM database are evaluated by calculating lattice constants and cohesive energies of all the elements and ionic compounds and comparing them with the corresponding experimental data in Table 2.

Table 2. Lattice constant and cohesive energy of different elemental and compound crystals.

Material	Structure	Lattice constant a,b,c(Å), β(°)		Cohesive energy (eV/atom)	
		Experiment [10,49]	EIM	Experiment [51,53,58]	EIM
Li	fcc	4.404,-----,-----,-----	4.509,-----,-----,-----	-1.625[a]	-1.392
Na	fcc	5.350,-----,-----,-----	5.388,-----,-----,-----	-1.086[a]	-1.031
K	bcc	5.344,-----,-----,-----	5.164,-----,-----,-----	-0.897	-1.001
Rb	bcc	5.630,-----,-----,-----	5.503,-----,-----,-----	-0.813	-0.903
Cs	bcc	6.091,-----,-----,-----	4.776,-----,-----,-----	-0.767	-0.732
F	fcc[b]	-----,-----,-----,-----	5.056,-----,-----,-----	-0.792	-0.904
Cl	fcc[b]	-----,-----,-----,-----	6.238,-----,-----,-----	-1.231	-1.202
Br	fcc[b]	-----,-----,-----,-----	6.281,-----,-----,-----	-1.134	-1.136
I	fcc[b]	-----,-----,-----,-----	6.773,-----,-----,-----	-1.081	-0.912
La	fcc	5.307,-----,-----,-----	5.306,-----,-----,-----	-4.441[c]	-3.973
Nd	hcp	3.650,-----,5.890,-----	3.636,-----,5.937,-----	-3.370	-3.215
Eu	bcc	4.582,-----,-----,-----	4.458,-----,-----,-----	-1.791	-2.252
Er	hcp	3.559,-----,5.587,-----	3.519,-----,5.746,-----	-3.261	-3.371
Ce	fcc	5.153,-----,-----,-----	5.158,-----,-----,-----	-4.354	-4.452
Sc	hcp	3.309,-----,5.273,-----	3.159,-----,5.159,-----	-3.891	-3.676
Y	hcp	3.629,-----,5.750,-----	3.589,-----,5.861,-----	-4.376	-4.658
Gd	hcp	3.634,-----,5.781,-----	3.608,-----,5.893,-----	-4.094	-4.146
LiF	B1	4.018,-----,-----,-----	4.022,-----,-----,-----	-4.426	-4.266
LiCl	B1	5.133,-----,-----,-----	5.126,-----,-----,-----	-3.578	-3.561
LiBr	B1	5.495,-----,-----,-----	5.493,-----,-----,-----	-3.194	-3.167
LiI	B1	6.050,-----,-----,-----	6.046,-----,-----,-----	-2.805	-2.578
NaF	B1	4.613,-----,-----,-----	4.614,-----,-----,-----	-3.876	-3.865
NaCl	B1	5.627,-----,-----,-----	5.626,-----,-----,-----	-3.315	-3.175
NaBr	B1	5.954,-----,-----,-----	5.956,-----,-----,-----	-3.004	-2.960
NaI	B1	6.455,-----,-----,-----	6.458,-----,-----,-----	-2.597	-2.397
KF	B1	5.325,-----,-----,-----	5.326,-----,-----,-----	-3.830	-3.782
KCl	B1	6.280,-----,-----,-----	6.281,-----,-----,-----	-3.339	-3.299
KBr	B1	6.586,-----,-----,-----	6.582,-----,-----,-----	-2.793	-2.937
KI	B1	7.052,-----,-----,-----	7.053,-----,-----,-----	-2.723	-2.538
RbF	B1	5.629,-----,-----,-----	5.625,-----,-----,-----	-3.677	-3.727
RbCl	B1	6.568,-----,-----,-----	6.569,-----,-----,-----	-3.295	-3.321
RbBr	B1	6.868,-----,-----,-----	6.870,-----,-----,-----	-2.814	-2.745

Material	Structure	Lattice constant a,b,c(Å), β(°)		Cohesive energy (eV/atom)	
		Experiment [10,49]	EIM	Experiment [51,53,58]	EIM
RbI	B1	7.325,-----,-----,-----	7.322,-----,-----,-----	-2.506	-2.345
CsF	B1	6.010,-----,-----,-----	6.008,-----,-----,-----	-3.631	-3.672
CsCl	B2	3.984,-----,-----,-----	3.982,-----,-----,-----	-3.323	-3.313
CsBr	B2	4.155,-----,-----,-----	4.155,-----,-----,-----	-3.056	-3.089
CsI	B2	4.414,-----,-----,-----	4.420,-----,-----,-----	-2.699	-2.677
LaF_3	$P6_3/mcm$	7.185,-----,7.351,-----	3.834,-----,5.253,-----	-6.108	-4.782
$LaCl_3$	UCl_3	7.468,-----,4,366,-----	7.426,-----,4.319,-----	-4.809	-4.894
$LaBr_3$	UCl_3	7.951,-----,4.501,-----	7.875,-----,4.445,-----	-4.311	-4.497
LaI_3	$PuBr_3$	10.05,14.10,4.330,-----	10.01,15.18,4.246,-----	-3.649	-3.842
NdF_3	$P6_3/mcm$	7.021,-----,7.196,-----	3.703,-----,5.245,-----	-5.788	-4.487
$NdCl_3$	UCl_3	7.381,-----,4.231,-----	7.390,-----,4.140,-----	-4.465	-4.474
$NdBr_3$	$PuBr_3$	9.150,12.63,4.100,-----	9.121,14.03,3.926,-----	-3.955	-4.068
NdI_3	$PuBr_3$	9.948,13.98,4.284,-----	10.37,15.05,4.126,-----	-3.310	-3.655
EuF_3	$P6_3/mcm$	6.916,-----,7.091,-----	3.915,-----,4.665,-----	-5.146	-4.404
$EuCl_3$	UCl_3	7.369,-----,4.133,-----	7.260,-----,4.165,-----	-3.796	-3.694
$EuBr_3$	BiI_3[b]	-----,-----,-----,-----	7.727,-----,4.276,-----	-3.249	-3.104
EuI_3	BiI_3[b]	-----,-----,-----,-----	7.464,-----,21.78,-----	-----	-2.777
ErF_3	Pnma	6.354,6.846,4.380,-----	6.740,6.903,3.907,-----	-5.798	-5.779
$ErCl_3$	$AlCl_3$	6.800,11.79,6.390,111	9.049,11.62,6.722,108	-4.316	-4.281
$ErBr_3$	UCl_3[b]	-----,-----,-----,-----	7.713,-----,-----,-----	-----	-3.604
ErI_3	BiI_3	7.451,-----,20.78,-----	7.149,-----,20.56,-----	-----	-3.844
CeF_3	$P6_3/mcm$	7.114,-----,7.273,-----	3.674,-----,6.890,-----	-6.059	-4.410
$CeCl_3$	UCl_3	7.436,-----,4.304,-----	7.418,-----,4.303,-----	-4.742	-4.727
$CeBr_3$	UCl_3	7.936,-----,4.435,-----	7.834,-----,4.383,-----	-4.226	-4.159
CeI_3	$PuBr_3$	10.02,14.00,4.341,-----	9.915,15.44,4.281,-----	-3.583	-3.616
ScF_3	AlF_3	5.667,-----,7.017,-----	4.086,-----,16.17,-----	-5.743	-5.316
$ScCl_3$	BiI_3	6.384,-----,17.78,-----	7.041,-----,20.776,-----	-4.293	-4.299
$ScBr_3$	BiI_3[b]	-----,-----,-----,-----	6.458,-----,18.82,-----	-3.743	-3.743
ScI_3	BiI_3	7.149,-----,20.40,-----	7.698,-----,23.083,-----	-3.251	-3.684
YF_3	Pnma	6.353,6.850,4.393,-----	6.121,6.208,3.612,-----	-6.140	-10.67
YCl_3	$AlCl_3$	6.920,11.940,6.440,111	8.917,11.45,6.556,108	-4.608	-4.787
YBr_3	BiI_3[b]	-----,-----,-----,-----	6.779,-----,19.98,-----	-----	-5.307
YI_3	BiI_3	7.505,-----,20.880,-----	7.344,-----,22.06,-----	-3.503	-3.588
GdF_3	Pnma	6.570,6.984,4.393,-----	6.823,7.034,3.955,-----	-6.020	-5.798
$GdCl_3$	UCl_3	7.363,-----,4.105,-----	7.327,-----,4.096,-----	-4.559	-4.523
$GdBr_3$	UCl_3[b]	-----,-----,-----,-----	7.871,-----,4.122,-----	-4.021	-4.165
GdI_3	BiI_3	7.539,-----,20.83,-----	7.397,-----,22.17,-----	-3.374	-3.282

[a] Cohesive energy is for bcc phase.
[b] No experimental structure was found so model structure is used.
[c] Cohesive energy is for $P6_3/mmc$ phase.

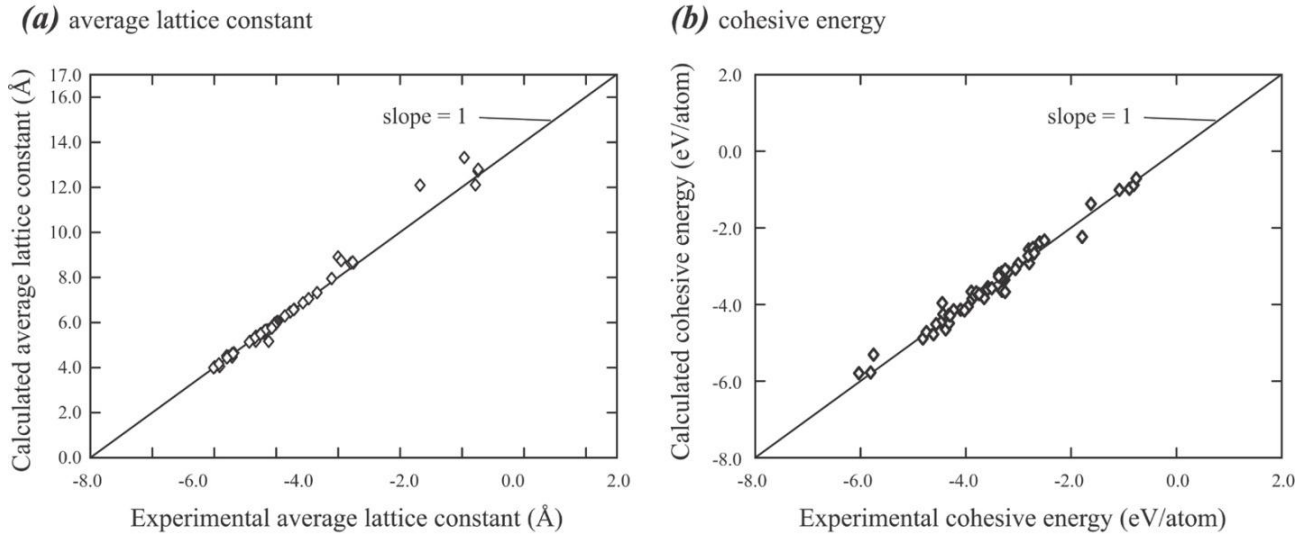

Figure 10. Comparison of calculated and experimental lattice constants and cohesive energies.

Table 2 gives numerical references of the lattice constants and cohesive energies. To more clearly examine the data, the calculated results are compared with the corresponding experimental values in Figures 10(a) and 10(b), respectively, for lattice constant and cohesive energy. Here when a lattice has more than one lattice constant, a geometric mean of these lattice constants are used. In Figure 10, the $P6_3/mcm$ structures are not included. In addition, Cs (bcc) and ScF_3 (AlF_3) are not included in Figure 10(a) and the YF_3 (Pnma) structure is not included in Figure 10(b). They were excluded because these structures cannot be well fitted by EIM while capturing the trends of other structures. (For example, our EIM predicts $P6_3/mmc$ to be more stable than $P6_3/mcm$.) Other than these rare anomalies, Figures 10(a) and 10(b) verify that the lattice constants and cohesive energies predicted by the EIM method are very close to the corresponding experimental values (i.e., the data points are close to the "slope = 1" line). Capturing the general trends of bond lengths of different materials is the key for EIM to predict crystal structures.

2.4.2.1 Molecular Statics Study of Crystal Stability

Our objective is to use molecular statics energy minimization to determine the lowest-energy crystal structure of elpasolite compounds. To prevent the system from being trapped in any given initial configuration that might be in a metastable state with a deep local energy minimum, a variety of initial configurations are used for each compound. To create a meaningful set of initial configurations, possible crystal structures of elpasolite compounds are first examined.

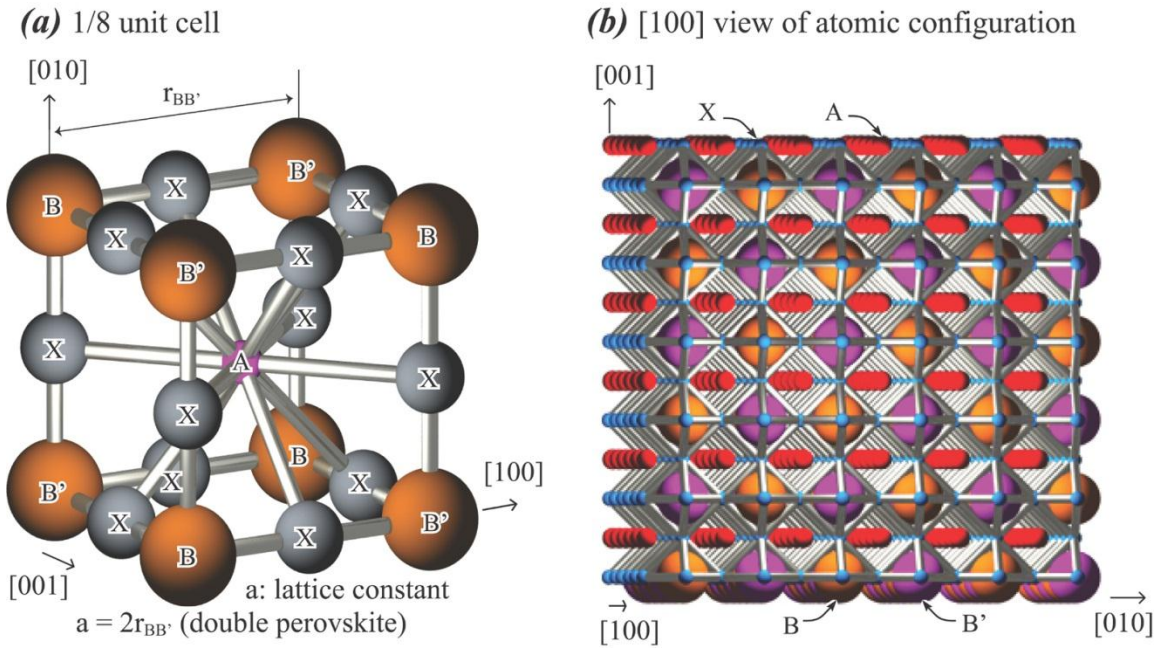

Figure 11. Schematic of perovskite structure.

$A_2BB'X_6$ elpasolite compound usually exhibits double perovskite structure [59]. This structure is illustrated in Figure 11(a) using 1/8 of the unit cell, which is essentially a cube with A atoms occupying the center site, B and B´ atoms occupying alternative corner sites, and X atoms occupying the edge sites. A larger view of the structure along the [100] direction is presented in Figure 11(b), where bonds between X atoms are displayed with sticks. Figure 11(b) shows that the X (halogen) atoms essentially form octahedrons surrounding each B and B´ atom.

In real elpasolites, the configurations of halogen octahedrons are usually not ideal as shown in Figure 11(b), but are rather tilted [60,61,62]. The tilting can occur along the three cubic directions, and two examples of tilts about the c [001] axis are shown in Figures 12(a) and 12(b). Figure 12 shows that for any layer of octahedrons perpendicular to the tilting axis, successive octahedrons are constrained to have opposite tilts about that axis. Thus, a positive tilt about the [001] axis of magnitude α in the first octahedron makes a negative tilt about the [001] axis of equal magnitude in the nearest-neighbor octahedrons along the [100] and [010] directions. However, successive octahedrons along the tilting axis may have either the same or opposite tilts, as shown respectively in Figures 12(a) and 12(b). Glazer [60,61] uses three letters to represent the tilting about the three cubic axes [100], [010], and [001]. Each letter is followed by a superscript (+, -, or 0) to indicate whether successive octahedrons along the corresponding axis have the same tilt, opposite tilt, or no tilt about that axis. For example, the symbol $a^-b^0c^+$ means that successive octahedrons have opposite tilts along [100] axis, no tilts along [010] axis, and the same tilts along [001] axis. The symbol $a^0a^0a^0$ means that there are no tilts in any axis so the structure remains cubic. Note that the same letter is used for all axes in $a^0a^0a^0$ because the lattice constants in the three axes are the same.

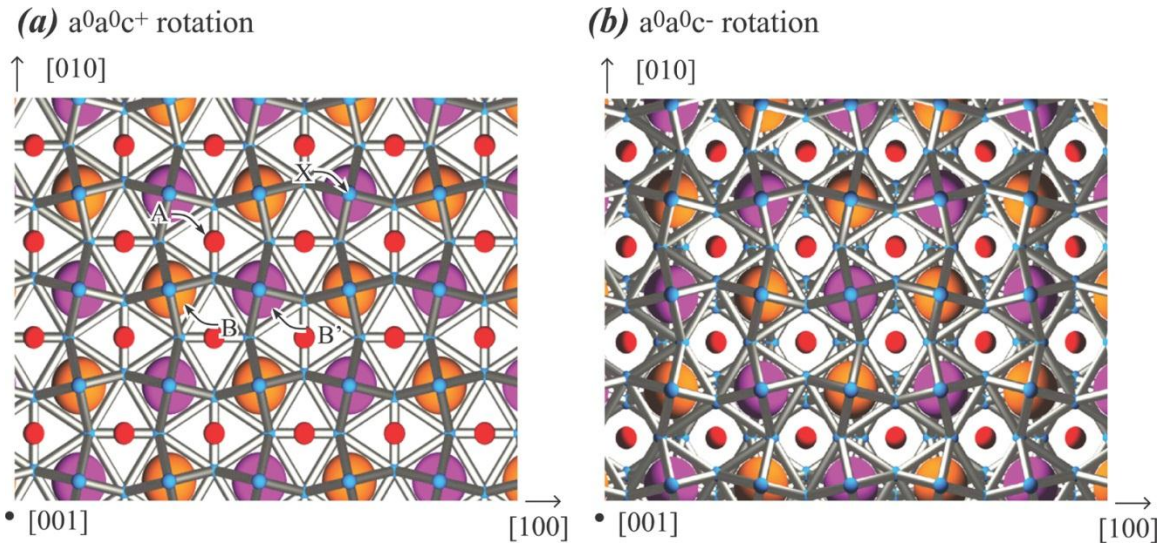

Figure 12. Two different tilts of halogen octahedrons.

In addition to double perovskite, some elpasolites may exhibit other structures such as the $BaNiO_3$ structure [63]. $BaNiO_3$ has a hexagonal lattice with face-sharing (alternative BX_6 or $B´X_6$) octahedrons stacked along the [001] axis. This structure can be represented with an orthogonal coordinate system as shown in Figure 13(a). Note that the $a^0a^0a^0$ double perovskite structure can also be represented in a similar hexagonal orientation using an orthogonal coordinate system, as shown in Figure 13(b).

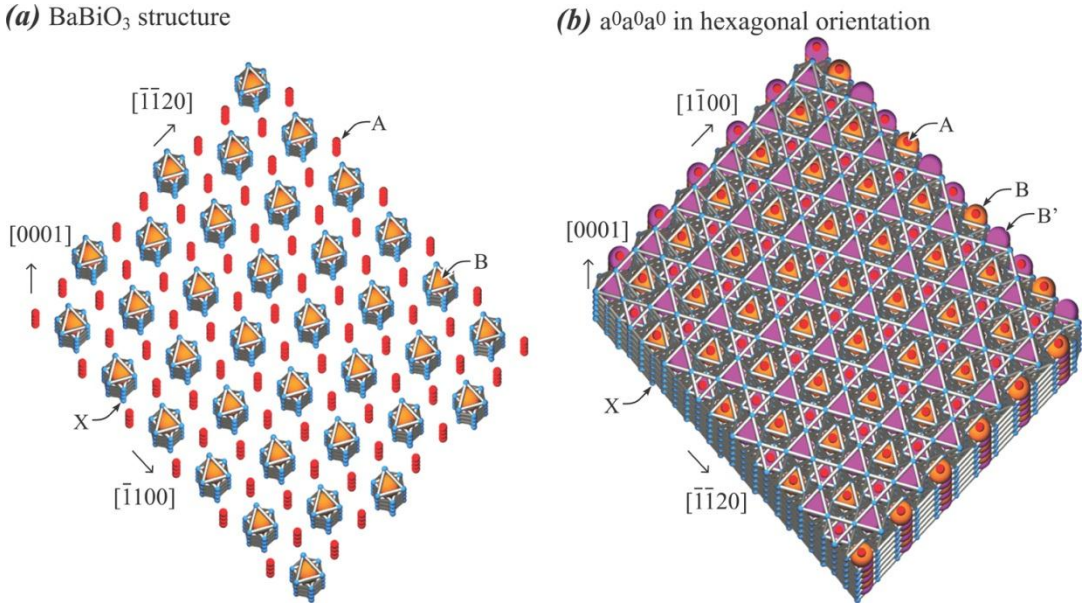

Figure 13. $BaBiO_3$-structure and hexagonal orientation of $a^0a^0a^0$ structure.

Using the molecular dynamics codes LAMMPS [42,41] under the variable volume and shape condition [64], 10,880 molecular statics simulations were performed to relax the structures of 17 different initial crystals of all the possible 640 elpasolite compounds within our EIM database. The 17 initial crystals include 15 tilting systems of the double perovskite structures $a^0a^0a^0$, $a^0a^0c^-$, $a^0a^0c^+$, $a^0b^+b^+$, $a^0b^+c^-$, $a^+a^+a^+$, $a^+a^+c^-$, $a^-b^0a^-$, $a^-b^0c^-$, $a^+b^+c^+$, $a^-a^-a^-$, $a^-a^-c^-$, $a^+b^-b^-$, $a^-b^-c^-$, and $a^-b^+c^-$. These crystals are created in the cubic directions with cubic dimensions (i.e., the length l_x, l_y, and l_z in the three coordinate directions are equal), and contain 1080 atoms. In addition, the $BaNiO_3$ structure (notated as $BaNiO_3$) and the hexagonal orientation of the $a^0a^0a^0$ structure (notated $a^0a^0a^0H$) are also used as the initial crystals. The $BaNiO_3$ structure contains 720 atoms, and the hexagonally orientated $a^0a^0a^0$ structure contains 4320 atoms. The use of the hexagonally orientated $a^0a^0a^0$ structure provides verification that the observed cubic structure is not an artifact of constraints on configuration relaxation due to the periodic boundary conditions.

To evaluate the equilibrium crystal structure, several structure-determining factors are determined from the simulations for each compound:

1. The initial structure S_{min} that gives the lowest energy after relaxation;

2. The initial structure S_{max} that gives the maximum energy after relaxation;

3. Relative energy ΔE_0, defined as the difference of the relaxed energies between the $a^0a^0a^0$ (note that the structure may no longer be $a^0a^0a^0$ after relaxation) and S_{min} structures;

4. The EIM tolerance factor t'_B for B element, defined as $t'_B = \sqrt{2}r_{e,AX}/(2r_{e,BX})$, where $r_{e,ij}$ (ij = AX, BX etc.) are EIM parameters listed in Table B3;

5. The EIM tolerance factor $t'_{B'}$ for B´ element, defined as $t'_{B'} = \sqrt{2}r_{e,AX}/(2r_{e,B'X})$;

6. The average EIM tolerance factor t´ for both B and B´, defined as $t' = \sqrt{2}r_{e,AX}/(r_{e,BX} + r_{e,B'X})$;

7. The average normal distortion ε, defined for the 15 cubic systems as $\varepsilon = \sqrt{(\varepsilon_x^2 + \varepsilon_y^2 + \varepsilon_z^2)/3}$, where $\varepsilon_i = (l_i - l_0)/l_0$ (i = x, y, z), and $l_0 = (l_x \cdot l_y \cdot l_z)^{1/3}$ (note that for the 15 cubic systems, the lengths l_x, l_y, and l_z are initially equal but may become different after relaxation);

8. Total shear distortion γ, defined as $\gamma = |\gamma_{xy}| + |\gamma_{xz}| + |\gamma_{yz}|$, where $|\gamma_{ij}|$ (ij = xy, xz, yz) are shear components; and

9. Standard deviation δ of halogen (X) atoms from their ideal octahedron positions. These quantities are listed in Table C1 for all the compounds in decreasing order of ΔE_0.

The quantities list in Table C1 may each be indicative of the stability of the cubic structure $a^0a^0a^0$. For instance, small ΔE_0 indicates that $a^0a^0a^0$ is likely to be more stable than other (non-cubic) structures. Small ΔE_0 alone is not sufficient to guarantee the cubic structure because the initial $a^0a^0a^0$ may relax to a non-cubic configuration during energy minimization. Other quantities, such as normal and shear distortion, ε and γ, as well as deviation of halogen atoms from their non-distorted positions, δ, must all be small in order to insure that the relaxed structure remains $a^0a^0a^0$. Furthermore, we found that the tolerance factors t'_B, $t'_{B'}$, and t' must also satisfy certain conditions to ensure a cubic structure. Note that these tolerance factors are derived from $r_{e,ij}$ parameters of the EIM potential. As a result, they do not suffer from the hard-sphere limitation that interatomic spacing of atoms A and B is constrained by ionic radii through $r_{AA} = 2r_A$, $r_{BB} = 2r_B$, and $r_{AB} = r_A + r_B$.

Through a few trial-and-error experiments, we found that the structural quantities t', ΔE_0, and ε can be combined to formulate a distortion metric $\eta = \eta(t', \Delta E_0, \varepsilon)$ that can distinguish cubic compounds from other compounds. In particular, η is given as

$$\eta(t', \Delta E_0, \phi) = \eta_1(t') + \eta_2(\Delta E_0) + \eta_3(\varepsilon) \tag{12}$$

where

$$\eta_1(t') = \begin{cases} 3t', & t' \le 0.9 \\ t', & 0.9 < t' \le 1, \\ t'^{10}, & t' > 1 \end{cases} \eta_2(\Delta E_0) = \begin{cases} \Delta E_0, & \Delta E_0 \le 0.1 \\ 3\Delta E_0, & \Delta E_0 > 0.1 \end{cases}, \eta_3(\varepsilon) = \begin{cases} \varepsilon, & \varepsilon \le 0.05 \\ 0.2\varepsilon^3, & \varepsilon > 0.05 \end{cases}.$$

All compounds are ranked according to this metric and the results are shown in Figure 14. Note that the metric undergoes a sharp drop at the rank number near 60. So far, we have grown 9 elpasolites in the small-metric end (the green lines in the figure), and all of these compounds were found to be cubic using X diffraction measurement. We have also grown 4 compounds in the high-metric region. All 4 of these compounds were found to be non-cubic with X diffraction measurement. These results are strong validation that the EIM method can be used to sort out the cubic elpasolites.

In conclusion, the work presented in this project has resulted in an EIM potential database that covers 17 elements Li, Na, K, Rb, Cs, F, Cl, Br, I, La, Nd, Eu, Er, Ce, Sc, Y, and Gd. This finding allows us to use molecular statics simulations to explore crystal structures. In particular, a distortion metric has been developed to screen out cubic crystals of 640 elpasolite compounds. So far, 13 elpasolite compounds have been grown. All 9 elpasolites that are predicted to be cubic were experimentally found to be cubic, and all 4 elpasolites that are predicted to be non-cubic were experimentally found to be non-cubic.

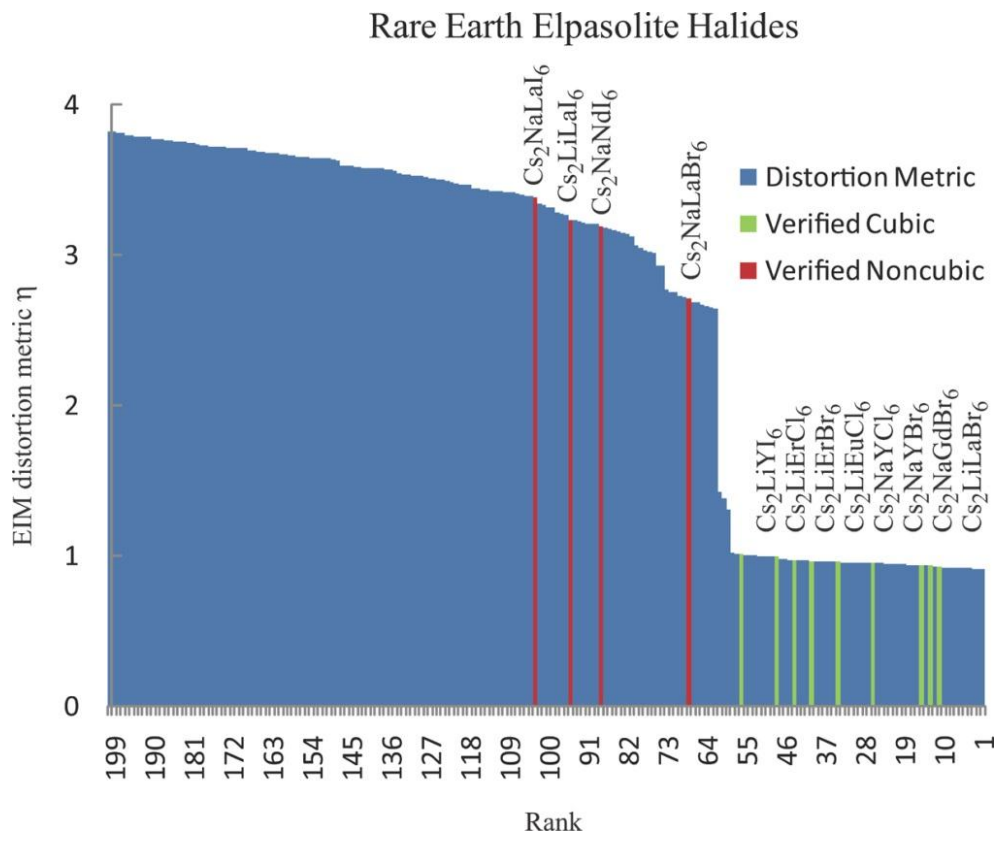

Figure 14. EIM distortion metric η as a function of rank number sorted with this metric.

3. EXPERIMENTAL INVESTIGATION OF ELPASOLITE STRUCTURE: SYNTHESIS AND CHARACTERIZATION

Section 3 documents experimental work for compound synthesis, crystal growth, hot pressing/forging, and provides structural refinement data for some of the elpasolite halides simulated in the previous section. One of the main objectives is to provide direct validation of our embedded-ion model, particularly on structure prediction. In addition, photoluminescence and radioluminescence, proportionality, and energy resolution of a few selected elpasolite halide compounds are reported.

We have synthesized and grown single crystals of more than ten different elpasolite halide compounds. Most of these compounds were doped with Ce^{3+} to study their scintillation performance, and some compounds were synthesized without Ce^{3+} activator to evaluate their crystal structure and lattice distortion in order to verify our embedded-ion model. Structural refinement data of these compounds were shown to be consistent with our model prediction. In addition, a single crystal of cubic isovalent solid solution of $Cs_2Na(Yb_{0.5}Ce_{0.5})Br_6$ was grown. Some cubic compounds, such as Cs_2LiYCl_6 and $Cs_2LiLaBr_6$, were hot-pressed and forged to explore the feasibility of fabrication of polycrystalline scintillator materials. The optical quality of these polycrystalline materials was degraded due to internal fractures from the high-temperature deformation process. Optimizing the deformation process is the key to improving the optical quality of these polycrystalline scintillators and unleashing their potential for radiation detection applications.

3.1 Background and Introduction

The past decade has seen an extensive effort to explore new scintillation materials for radiation detection applications due to needs in nuclear nonproliferation and homeland security. In addition, inorganic scintillators have always played an important role in nuclear and particle physics research, medical imaging, and geological exploration applications [65]. The workhorse alkali halides, including NaI and CsI, while affordable, are poor spectrometers due to severe nonproportionality responses. Recent studies have indicated that the lanthanum halide family is rich in high-performance scintillators, including many tri-halides (LnX_3) [66,67,68,69,70] and elpasolite halides (A_2BLnX_6, [71,72,73,74,75,76]. See the structure model in Figure 11 above). The emerging tri-halide compounds, such as $LaBr_3$ [67] and GdI_3 [70], while having the desired luminosity and proportionality, have proven difficult to produce in large size with low cost due to their intrinsic brittleness and highly anisotropic nature. For example, the coefficients of thermal expansion (CTE) for the hexagonal $LaBr_3$ (space group: P63/m) along its c axis and normal to the prismatic plane are 13.46 $X10^{-6}$/°C and 28.12 $X\ 10^{-6}$/°C, respectively [77]. The large difference in CTE can create enormous thermomechanical stresses in the crystal during the solidification process, making it hard to grow in large sizes. Furthermore, these materials have

extremely limited ductility and low fracture toughness in comparison to traditional halide salts. Cracks can be easily initiated and propagate along their prismatic planes [77]. These factors limit the available crystal sizes, increase manufacturing costs, and hamper the widespread of these materials for radiation detection applications.

This work focuses on a large new class of elpasolite halide compounds (space group Fm-3m), which usually crystallize in the ordered double perovskite structure [78]. Many of these materials retain cubic or near-cubic structures over a range of compositions, and they have demonstrated desirable scintillation properties including pulse shape discrimination [79,80,81], high light yield, and excellent proportional response (see Table 3). The features of these cubic, isotropic compounds are desired to minimize the complex thermomechanical stresses during solidification and facilitate the growth of practical-size crystals for detector applications.

Table 3. The performance of Ce^{+3} doped elpasolite halide scintillators (RMD data).

Material	Density (g/cm^3)	Light output (Photons/MeV)	Decay time (ns)	Non-proportionality (60-1275 keV)
Cs_2NaLaI_6 [11]	~ 4.2	54,000 – 60,000	50	< 1
Cs_2LiLaI_6	~ 4.3	> 50,000	51	1.6
$Cs_2LiLaBr_6$	~ 4.1	50,000 – 55,000	65	1.7
$Cs_2NaLaBr_6$	~ 3.9	12,000	55	2.9

Furthermore, optically isotropic materials can effectively eliminate problematic light scattering at the grain boundaries of a polycrystalline ceramic body. Therefore, cubic symmetry can greatly improve optical quality and potentially boost the energy resolution for ceramic detectors. These features make elpasolite halide compounds extremely competitive to the tri-halide scintillators in terms of manufacturability challenges.

In this work we focused on compound synthesis, crystal growth, and thermal stability with respect to processing conditions. The initial study concentrated on compounds that were thermally stable and exhibited no self-activity for single crystal growth or ceramic fabrication. Special emphasis was placed on supporting and validating the structural prediction effort based on our embedded ion model (EIB). The structural information was also used to correlate luminescence properties of these new compounds.

3.2 Experimental Procedure

3.2.1 Compound Formation and Synthesis

Three different approaches, solution synthesis [82,83] solid-state reaction, and melt synthesis, were explored to fabricate the Ce^{3+} (5 mol %) doped lanthanum-based elpasolite halides. Initial attempts to synthesize these compounds by salt-acid [82] and metal-acid [84] reactions followed

by vacuum dehydration were unsuccessful. X ray diffraction and thermal analysis results indicated that these synthesized powders were a mixture of salts, presumably due to a large difference in solubility of these salts in the acid solution. As a result, halide salts, including CsI, NaI, LiI, LaI_3, CeI_3, CsBr, NaBr, LiBr, $LaBr_3$, and $CeBr_3$, were used to directly synthesize these elpasolites. For these processes, high-purity anhydrous bromide and iodide salts (> 99.999%; except LaI_3 which is 99.9%) from Alfa-Aldrich were weighed according to their chemical formulations. These salts were mixed and ground with mortar and pestle for two hours. In addition, these halide salts, in particular the $LaBr_3$ and the LaI_3, were found to be extremely oxophilic. They tend to reduce the refractory materials in the box furnace and form oxyhalides (LaOBr and LaOI) during solid-state reactions.

To prevent such a reaction, the ground, mixed salts were loaded into a fused quartz ampoule in an argon-filled glovebox and subsequently vacuum sealed for the melting synthesis. Sometimes the ground powder in the ampoule was first heated to 200 °C under vacuum to remove any residual hydrates. After dehydration, the powder was heated to about 70% of the highest melting point of initial salt in a double quartz tube for solid-state reaction. X-ray data indicated the formation of compound and some residual phases. The purpose of this approach was to form a desirable compound at a lower temperature to prevent any decomposition. However, it involved additional complexity in the process, and the resulting powder was quite reactive and prone to absorb water during subsequent handling. Lanthanum-based elpasolite halides were finally successfully synthesized by melting and solidifying these halide salts (either from powder or beads) in the vacuum-sealed quartz ampoules. Experimental results indicated that adequate mixing during melting and controlling the reaction kinetics are critical for achieving phase-pure elpasolites (see next section for details). In addition, small single crystals of lanthanum-based elpasolite halides produced by small-scale growth methods from Radiation Monitoring Devices, Inc. (RMD, Watertown, MA) have been provided for initial crystal structure determination.

3.2.2 Single Crystal Growth

Small, laboratory-scale single crystals (~ 1 cm to ~2 cm diameters) of elpasolite halides were grown by a vertical Bridgman method using an in-house built two-zone furnace. The temperatures of these two zones were controlled independently by two programmable thermal controllers (Watlow SD). An “adiabatic” zone approximately 1 in. thick was placed between the two temperature zones to control the thermal gradient and to provide a stable solid–liquid interface during crystal growth. The temperature at the top and the bottom of the adiabatic zone as well as pulling speed were closely monitored and controlled by a LabView program. The melting point and the freezing point for a new compound were determined by a differential scanning calorimetric measurement (Netzsch, DSC404 F3) prior to the crystal growth process. These temperatures were used for the temperature settings for the Bridgman furnace. A typical thermal gradient across the 1 in. adiabatic zone was controlled between 60 °C to 70 °C; control was achieved by adjusting the temperature settings between the top and the bottom zones in the furnace. The growth rate was controlled by lowering the fused quartz ampoule from the top zone (above melting point) to the bottom zone (below freezing point) at 1.2 mm per hour. Sometimes

this furnace was also used to homogenize and assist in the compound formation from its constituent halide salts. In this process, the mixed powder was melted in an inverted thermal gradient for 10 hours (temperature setting for the top and bottom zones were below and above compound's melting point) where the thermally induced convectional flow in the ampoule assisted the mixing and prevented the gravitation separation in the melt prior to crystal growth. This method was found to be quite effective to produce phase-pure elpasolite halides for ceramic processing.

3.2.3 Hot Pressing

Hot pressing was performed to consolidate the elpasolite halide powders synthesized by solid-state reaction and melt synthesis, using a graphite die in an argon back-filled resistant heating furnace. It was quickly learned that the fine powder made by solid-state reaction was prone to darken due to its high surface area. In subsequent hot pressing or forging experiments, two fused quartz spacers were used to prevent the powder from directly contacting the graphite rams. The darkening problem was also effectively suppressed by using coarse powder made by solid-state reaction. Additional improvement was achieved by direct hot forging of a solidified ingot from melt synthesis. Hot pressing (consolidate the powder) and hot forging (deform and further densify the melt ingot) were generally performed at the temperature about 50 °C below the compound's melting point with 6.5 ksi (or 44.8 MPa) pressure.

3.2.4 Thermal Analysis and Structural Refinement

A differential calorimeter (DSC) was used to detect the thermal events during synthesis and melting. The DSC unit was first calibrated with a sapphire standard before measurements were made. Powder of halide salts or elpasolite halide sample was loaded in a platinum crucible and heated at 10 °C/min under flowing argon and subsequently cooled back to room temperature at 10 °C/min. The onset of melting was reported and the enthalpy change was determined by directly integrating the area under the DSC curve.

Powder x-ray diffraction was performed using a Siemens D500 diffractometer equipped with a sealed tube x-ray source (Cu Ka) and a diffracted beam graphite monochromator. Fixed slits were employed for the measurement, and generator settings were 40 kV and 30 mA, respectively. Typical scan parameters were 10-90^{o} 2θ with a step size of 0.04^{o} and various count times ranging from 1 to 20 seconds. Due to the hygroscopic nature of the synthesis salts and subsequent elpasolite structures, a special beryllium dome (BeD) holder was employed for isolating the powder specimen from the atmosphere [84]. Structure refinement of isolated phases was performed using GSAS software [85,86]. Since the ionic size of Ce (activator) and La is very close and $CeBr_3$ and $LaBr_3$ form a completely solid solution [87] throughout the whole composition range, we expect the small substitution of Ce (5 mol %) with La in these elpasolites would have a minimal impact on their crystal structures. The theoretical density of these compounds was directly calculated from lattice parameter(s) of a unit cell.

3.2.5 Photoluminescence and Radioluminescence

The photo-excitation and emission spectra of elpasolite halide samples were measured by a standard fluorometer (PTI QuantaMaster, Birmingham, NJ), using a Xe arc lamp as a light source. This system was equipped with a double monochromator on the excitation side and a single monochromator on the emission side. The radioluminescence spectrum was recorded using x-ray radiation from a Philips x-ray generator operated at 40 keV and 20 mA. The scintillation light was passed through a McPherson 0.2-m monochromator and detected with a cooled Burle C31034 photomultiplier tube (PMT) tube with a GaAs:Cs phtotocathode. The energy spectra and light output measurements were performed by coupling the crystals to a super bialkali R6233-100 PMT operating at a voltage of -650 V. Pulse height spectra for the $Cs_2NaGdBr_6$ samples were recorded under 662 keV gamma-ray excitation from a ^{137}Cs source. Scintillation decay time spectra were measured under 511 keV gamma-ray excitation (^{22}Na source) using the coincident technique. All these scintillation characterizations were measured at room temperature and some of the data were collected at RMD.

3.3 Results and Discussion

3.3.1 Synthesis, Crystal Growth, and Thermal Measurements

Preliminary experiments showed that phase-pure elapsolite halides could not be produced by a quick melting and solidification of the ground alkaline and lanthanum halide salts. Differential scanning calorimetric data indicated that there were some residual, unreacted halide salts in the melt as evidenced by several thermal events observed during the solidification process. The presence of these salts was later confirmed by x-ray diffraction analysis. However, these events progressively disappeared as the material went through thermal cycles, while the exothermic peak corresponding to the solidification of elpasolite halide increased in the expanse of these residual unreacted phases. These observations are illustrated in Figure 15 for the Cs_2NaLaI_6, where the dotted, dashed, and solid lines represent the first, the second, and the third cooling cycles, respectively. Close examination of these thermal events indicates that none of these temperatures correspond to the melting points of the starting materials (i.e., LaI_3 – 778 °C, NaI – 654 °C, and CsI – 624 °C); instead, they are close to the eutectic points in the three constituent binary systems for the CsI-NaI-LaI_3 ternary system.

For example, major thermal events found at 543 °C, 454 °C and 429 °C are well matched to the eutectic points found in Cs_3LaI_6-CsI (539°C) [88], NaI-LaI_3(454°C) [89], and CsI-NaI (426 °C) [89] binary phase diagrams. However, the most dominate thermal event (the highest peak) observed in the cooling cycle is the solidification of the elpasolite phase near 540 °C. This peak becomes sharper as the number of thermal cycle increases. Finally, the melting point of Cs_2NaLaI_6 was well defined at 540 °C with no detectable foreign phases present on the solidification curve. The merging and disappearing of some of exothermal peaks on Figure 15 depict the reaction kinetics involved with the Cs_2NaLaI_6 elpasolite formation, as the chemical reaction approaches completion through the subsequent thermal cycles. These observations

immediately suggest that reaction kinetics is important for the formation of elpasolites and a longer reaction time or higher temperature is required to complete the reaction.

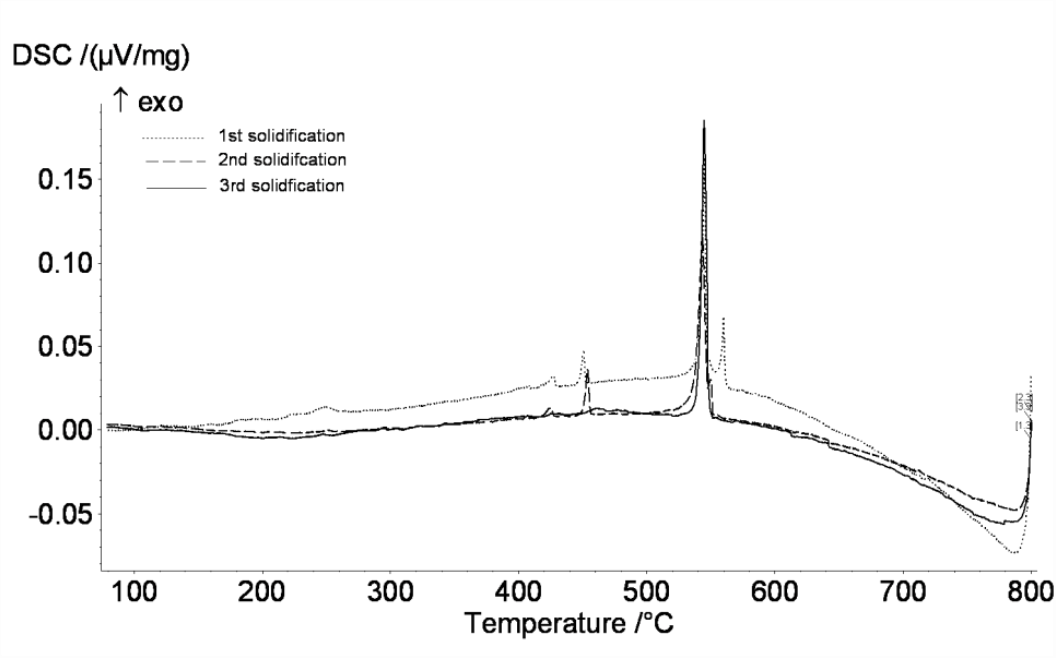

Figure 15. The differential scanning calorimetric data during the solidification cycles for the Cs_2NaLaI_6. Data were collected at 3 °C/min under a flowing argon condition.

Several initial attempts to form a phase-pure Cs_2NaLaI_6 from the melt, based on the aforementioned observations, were unsuccessful. X-ray diffraction data indicated that these samples still have traces of foreign phases after being melted at 30 °C above the highest melting point of the salts ($LaBr_3$ at 788 °C or LaI_3 at 778 °C) for 10 hours. It was found that adding agitation to the melt (by shaking the ampoule in the furnace) at a higher temperature helped the elpasolite phase formation, presumably due to the density difference between these molten salts. To minimize this gravitational separation , a two-zone, vertical furnace was used and configured with a thermal gradient of about 50 °C per inch from bottom (hot end) to top (cold end) of the ampoule to provide additional convection mixing. A phase-pure solidified Cs_2NaLaI_6 ingot, as determined by the powder x-ray diffraction data, was obtained after melting at 850 °C (the maximum temperature at the bottom of the ampoule) for 10 hours. After melting, the furnace was slowly cooled to room temperature. The process of removing these residual phases was occasionally quite challenging. For example, both the top and the bottom sections of a single crystal of $Cs_2LiLaBr_6:Ce^{3+}$ have a trace of LiBr and CsBr residual phases, respectively (see Figure 16 and Table 4). Occasionally, a trace of $Cs_3Ln_2X_9$ (sorohalide) has also been detected in the x-ray diffraction pattern. These sections were generally slightly milky in appearance, in contrast to the transparent middle section, which was most close to its stoichiometry.

Single crystals of various elpasolite halides were grown in different sizes. Most of these crystals were slightly milky and occasionally cracks were also observed (see Figure 17). Improvement on our crystal growth facility and vacuum bake-out can definitely improve the optical quality and scintillation performance of these materials.

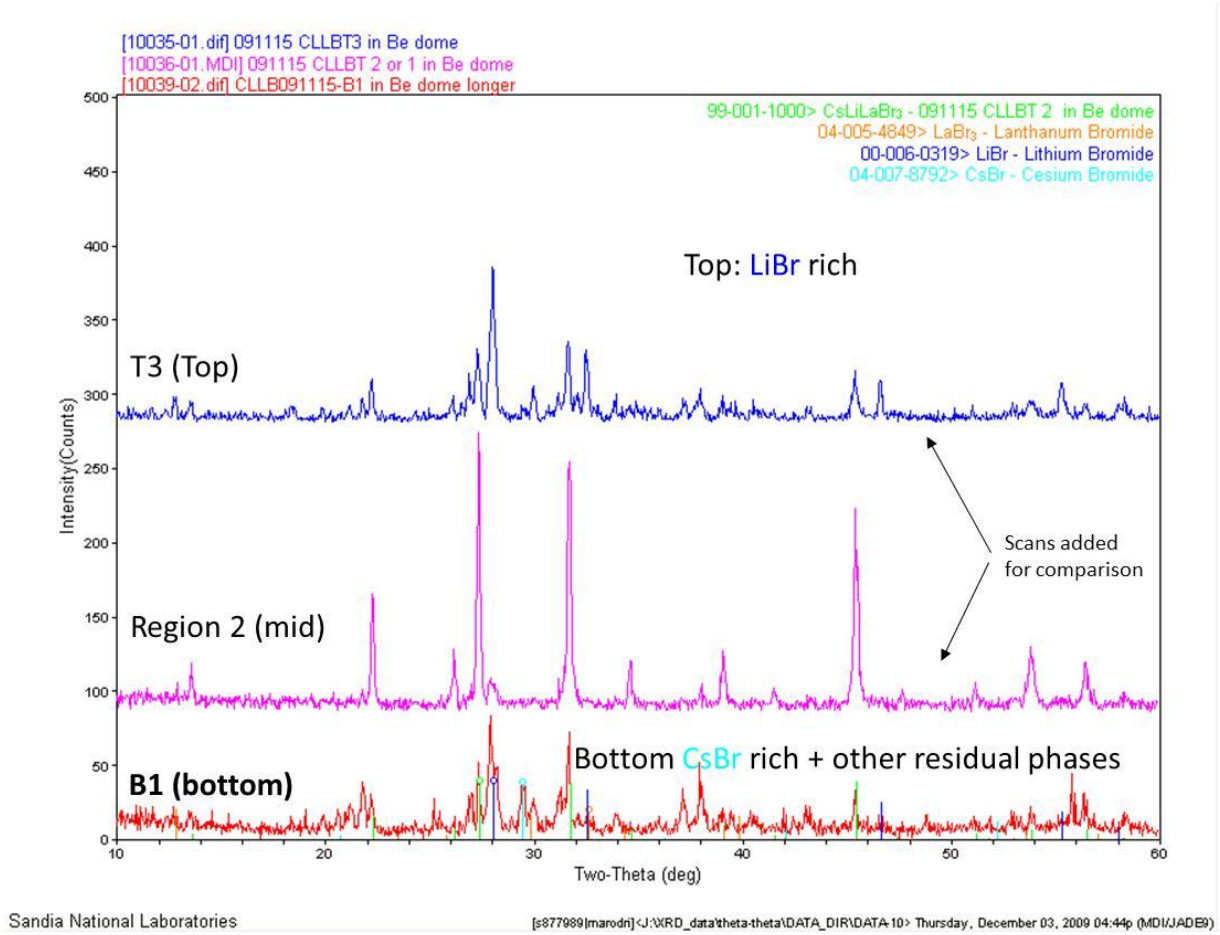

Figure 16. X-ray diffraction data illustrate compositional variations for a single crystal $Cs_2LiLaBr_6:Ce^{3+}$ grown by a Bridgman technique. Crushed powder of these sections was collected from the top (milky), middle (mid, transparent) and bottom (milky) of the crystal for the x-ray diffraction study.

Table 5 lists the melting and the freezing points, as well as the enthalpy changes associated with phase change during solidification for different elpasolite halides (see Figure 18). It was found most of these compounds began to decompose or sublime at 80 to 85% of their melting points, as indicated by the weight loss during the thermal gravitational measurement. Difficulties were experienced in determining the enthalpy change for some compounds as thermal decomposition or volatility contaminated the thermal analysis system (not available (N/A) in Table 5).

Table 4. Chemical analysis data for different sections of a $Cs_2LiLaBr_6:Ce^{3+}$ single crystal.

Element	B1 (bottom)		M2 (middle)		T3 (top)		Avg wt%	Stoich. wt%
	Conc (Wt.%)	B1 normal	Conc (Wt.%)	M2 normal	Conc (Wt.%)	T3 normal		
Ce (ICP-MS)	0.892	0.973	0.902	1.018	0.386	0.424	0.805	0.786
Cs (ICP-MS)	33.300	36.330	29.500	33.284	23.700	26.050	31.888	29.828
La	13.810	15.067	14.670	16.552	16.220	17.828	16.482	14.808
Li	0.500	0.545	0.800	0.903	1.310	1.440	0.963	0.779
Avg. Br	43.160	47.087	42.770	48.257	49.370	54.265	49.870	53.799
Sum		100.002		100.014		100.007	100.000	100.000
Total	91.660	100.000	88.630	100.000	90.980	100.000		

Note: Compositions were determined by an induction-coupled plasma technique. Due the emission interference between Ce and Cs in the optical emission spectra (Conc. Wt.%), results were re-calibrated with other wavelengths and final data are given in the normalized columns (normal).

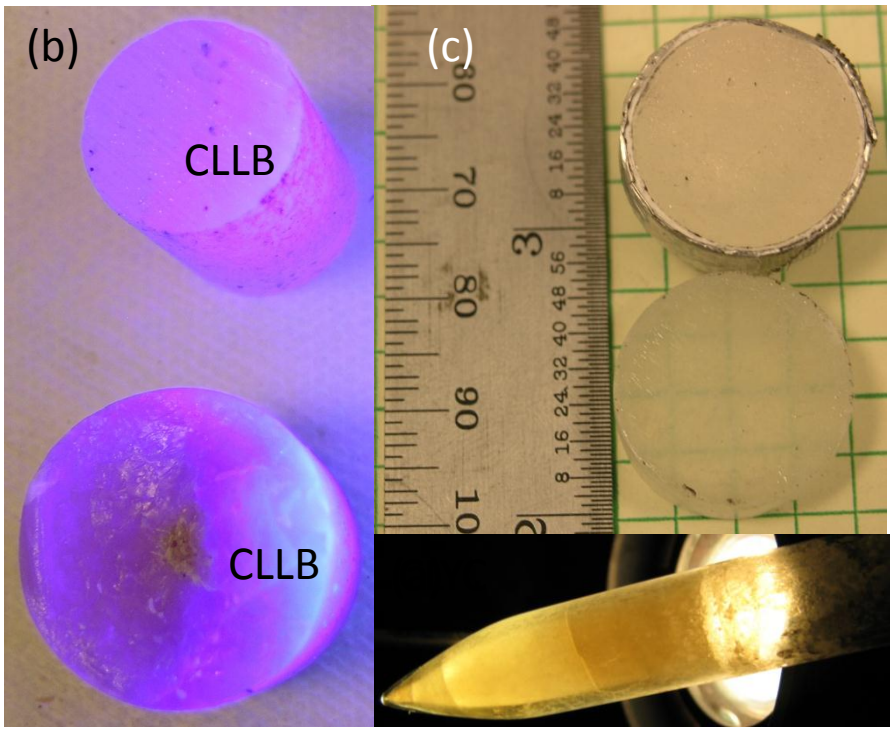

Figure 17. Single crystals of elpasolite halides grown to different sizes: (a) 0.75 in. dia. Cs_2LiYCl_6 (CLYC) and 1 in. dia. $Cs_2LiLaBr_6$ (CLLB), both shown under black light excitation; (b) two 0.75 in. dia., 0.5 in. thick $Cs_2LiLaBr_6$ crystals prepared for radioluminescence characterization; (c) 0.5 in. dia. $Cs_2NaLaBr_6$ (CNLB).

Table 5. The melting and freezing points as well as enthalpy changes during solidification for some elpasolite halides (with 5 at. % of Ce^{3+}). T_u is the temperature at which the compound becomes thermally unstable, as determined by a thermal gravitational measurement (see Figure 18).

Material	Melting point (°C)	Freezing point (°C)	T_u (°C)	Enthalpy (J/g)
$Cs_2LiLaBr_6$	492.8	471.5	>460	55.6
Cs_2LiLaI_6	469.8	457.8	>350	N/A
Cs_2LiYCl_6	647.2	622.3	>540	N/A
$Cs_2NaLaBr_6$	626.1	600.1	>510	68.77
Cs_2NaLaI_6	540.6	530.7	>420	44.92
$Cs_2NaErBr_6$	653.7	655.5		166.3
$Cs_2NaGdBr_6$	704.2	693.4		144.6

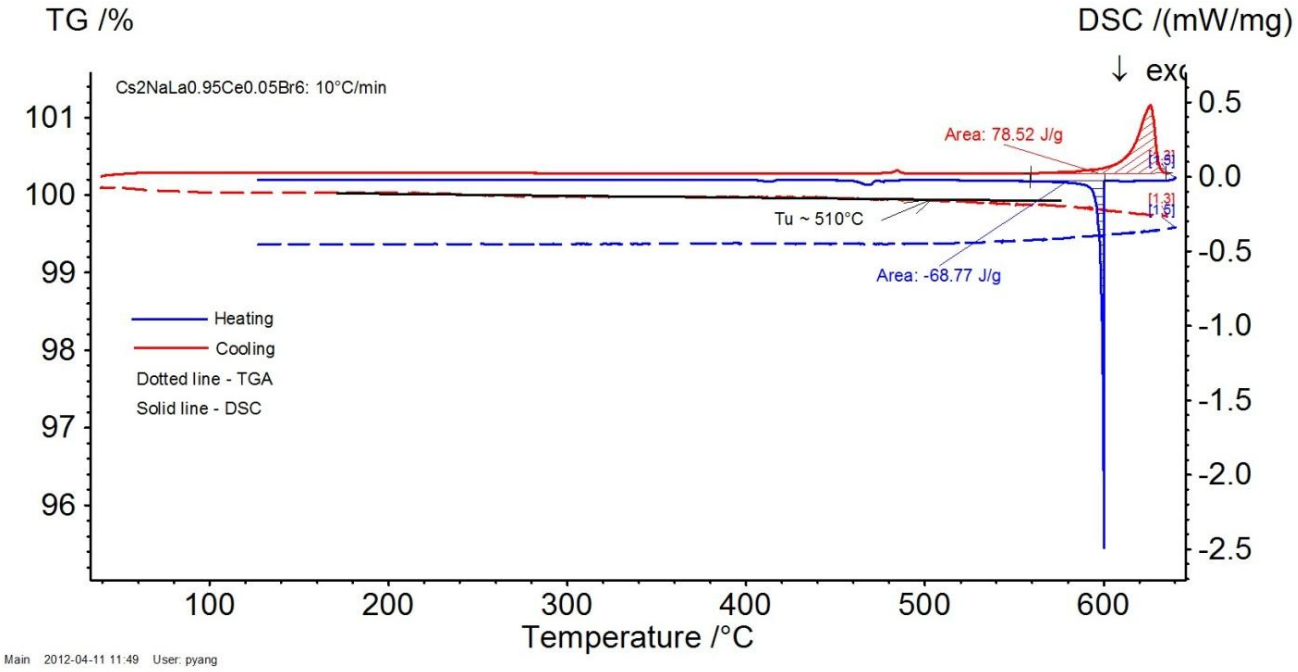

Figure 18. A typical simultaneous thermal analysis (STA) for elapsolite halides, including the thermal gravitation measurement (TGA, dotted lines) and differential thermal calorimetry (DSC, solid lines), using a cerium-doped $Cs_2NaLaBr_6$ as an example.

The thermomechanical response ($\Delta l/l$ versus temperature) for $Cs_2LiLaBr_6:Ce^{3+}$ was measured by a dilatometer from room temperature to 450 °C at a heating rate of 3 °C/min. The result is given in Figure 19. The coefficient of thermal expansion (CTE) was determined from the slope of the thermal expansion curve. Results indicate that the CTE for $Cs_2LiLaBr_6$ at this temperature range is approximately 38.52 to 44.68 ppm/K, which is quite high in comparison to most ionic materials.

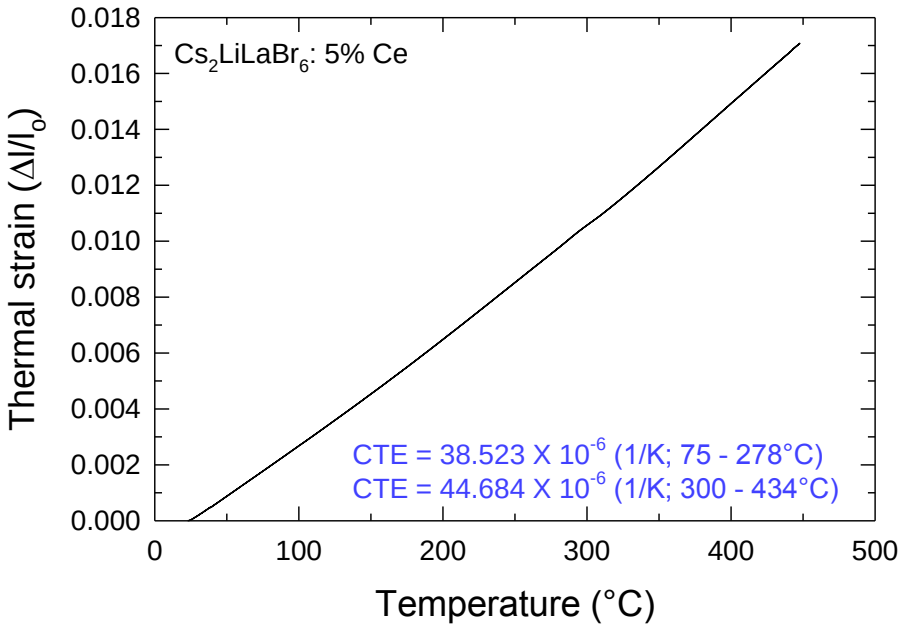

Figure 19. The thermal mechanical response and the coefficient of thermal expansion of $Cs_2LiLaBr_6:Ce^{3+}$.

3.3.2 Structural Refinement

Initial structural refinements of these elpasolites were performed on our samples and on crushed single crystals obtained from RMD. After we established our synthesis and growth capability, new compounds in addition to these crystals from RMD (including Cs_2LiLaI_6, $Cs_2LiLaBr_6$, Cs_2NaLaI_6, and $Cs_2NaLaBr_6$) were characterized by powder x-ray diffraction pattern. We explored the use of smaller lanthanide ions (such as Eu^{3+}, Gd^{3+} and Er^{3+}), and a rare earth cation (Y^{3+}) and a solid solution (Ce^{3+} and Yb^{3+}) to examine the change of crystal structure and confirm with our EIM model. It was also expected that the energy gap of the scintillation materials will change by varying the ionic radius of cations and anions, thereby producing scintillators with different light yields. In the same time period, the ligand field around the octahedrally coordinated Ce^{3+} activator (at the Ln site, coordination number = 6) would be modified and would produce a red-shift in emission wavelength. If these substitutions would induce a lattice distortion and create non-centrosymmetric environments for the activator, changes in Stokes shift and relaxation time would be also anticipated.

This section presents the crystallographic data of these compounds, which will be correlated to their spectroscopic and scintillation properties in the future. The Goldschmidt tolerance factor (*t*) [90] of these new elpasolite halides will also be calculated and compared with structural refinement results, based on a large database of experimental ionic radii and the coordination number (CN) of the cations and anions in the lattice [91]. The tolerance factor (*t*) is a simple

geometric factor (see Eq. [13]) that gives a necessary but not sufficient condition for the formation of perovskite-type complex halides, based on a hard-sphere model.

$$t = \frac{\sqrt{2}(R_{X^{-1}} + R_{A^{+1}})}{[R_{X^{-1}} + 0.5(R_{B^{+1}} + R_{RE^{+3}})]} \quad (13)$$

A tolerance factor that is equal or close to unity would be observed for perovskites with no distortion from the ideal cubic structure. Therefore, this factor can provide a preliminary estimation in terms of possible lattice distortion from a cubic cell, which is closely related to the degree of structural anisotropy in the lattice. Implications can be drawn for material selection in order to minimize the anisotropic thermomechanical stresses developed in single crystal growth or to reduce the amount of light scattering in polycrystalline ceramics.

Table 6. Crystal structure and tolerance factor for lanthanum-based elpasolite halides (all doped compounds consist of 5 atm. % Ce^{+3}).

Material	Crystal structure	Lattice parameters (Å)			Tolerance factor (*t*)
		a	b	c	
$Cs_2LiEuCl_6$	Cubic (Fm-3m)	10.544(1)	10.544(1)	10.544(1)	0.980
$Cs2LiYCl_6$	Cubic (Fm-3m)	10.479(1)	10.479(1)	10.479(1)	0.988
$Cs_2LiErCl_6$	Cubic (Fm-3m)	10.446(1)	10.446(1)	10.446(1)	0.990
$Cs_2LiLaBr_6:Ce^{3+}$	Cubic (Fm-3m)	11.2890	11.2890	11.2890	0.951*
$Cs2LiYBr_6$	Cubic (Fm-3m)	11.017(1)	11.017(1)	11.017(1)	0.973
$Cs_2LiLaI_6:Ce^{3+}$	Non-cubic	n/a	n/a	n/a	0.935*
$Cs_2NaEuCl_6:Ce^{3+}$	Cubic (Fm-3m)	10.552(2)	10.552(2)	10.552(2)	0.934*
$Cs_2NaLaBr_6:Ce^{3+}$	Tetragonal	8.1416	8.1416	11.580	0.909*
$Cs_2NaErBr_6$	Cubic (Fm-3m)	11.262(1)	11.262(1)	11.262(1)	0.931
$Cs_2NaErBr_6:Ce^{3+}$	Cubic (Fm-3m)	11.269(1)	11.269(1)	11.269(1)	0.931*
$Cs_2NaLaI_6:Ce^{3+}$	Orthorh. (Pnma)	8.7615	12.4361	8.6270	0.897*
$Cs_2NaGdBr_6$	Cubic (Fm-3m)	11.351(2)	11.351(2)	11.351(2)	0.924
$Cs_2NaGdBr_6:Ce^{3+}$	Cubic (Fm-3m)	11.360(1)	11.360(1)	11.360(1)	
$Cs_2Na(Yb_{0.5}Ce_{0.5})Br_6$	Cubic (Fm-3m)	11.360(1)	11.360(1)	11.360(1)	0.924

* Calculated *t* does not include cerium concentration.

Lattice parameters and the tolerance factors of these Sandia- and RMD-grown compounds are reported in Table 6. A comparison of the x-ray diffraction data and theoretically calculated intensity for $Cs_2LiLaBr_6$ is given in Figure 20. In this report, we use the structural refinement data of this compound as an example for a typical cubic elpasolite.

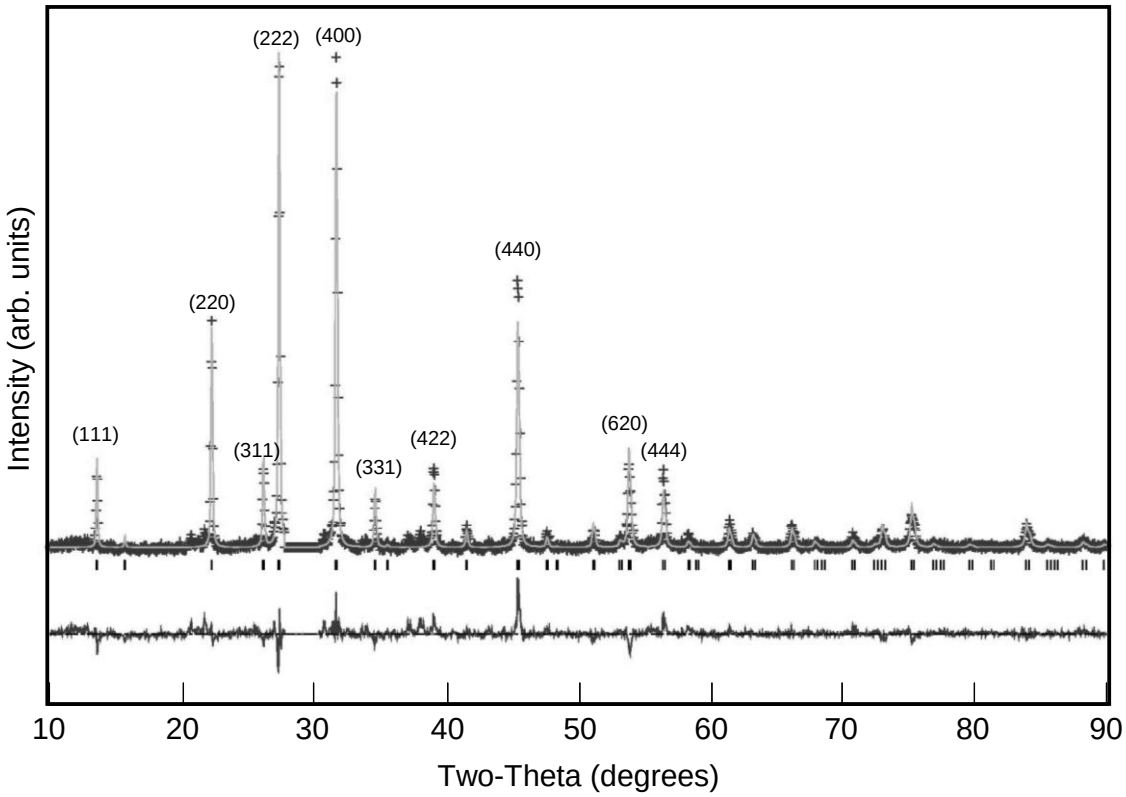

Figure 20. Structure refinement of $Cs_2LiLaBr_6$ as a cubic elpasolite structure.

The powder x-ray diffraction pattern refined well as a cubic elpasolite (Fm-3m), similar in structure to chloride elpasolites previously reported by Publete et al. [92] and Villafuerte-Castrejon et al. [82], except with an expanded a-axis of 11.289 Å. Figure 20 shows the simulated pattern based on the model structure plotted on top of the observed powder data (shown as + symbols). The major peaks of the pattern are labeled with their respective hkl indices. A difference pattern is displayed underneath the fit data. The final residual error (Rp) for the fit was 12.67 %. The region from 27.8 to 30.4^o 2θ that was removed from the histogram as residual salt phases, namely CsBr and LiBr, had peaks in this range. There were no predicted elpasolite peaks in this range, so the additional salt peaks could be removed to improve the fit to the elpasolite structure without loss of structural information.

X-ray diffraction data are shown in Table 7, listing the observed peak positions and relative intensities for the indexed reflections. The structural parameters for the $Cs_2LiLaBr_6$ elpasolite lattice are shown in Table 8. Individual atomic displacement parameters were not refined for the atoms. Instead, an overall atomic displacement parameter for the structure (B_{iso}) was refined and is reported. Table 8 shows the La being located on the origin of the lattice (which replicates to the face center as well). The La is octahedrally coordinated to the Br atoms with a bond length of La-Br = 2.935(5) Å, which is reasonable for this atom pair. The Li is located at (½ ½ ½), thus displaying octahedral coordination to Br as well; in this case with a smaller bond length of Li-Br = 2.710(5) Å.

Table 7. X-ray diffraction data for cubic $Cs_2LiLaBr_6$.

2θ (°)	*d* (Å)	I/I_o	*h*	*k*	*l*
13.562	6.524	11	1	1	1
15.685	5.645	< 1	2	0	0
22.249	3.992	40	2	2	0
26.148	3.405	13	3	1	1
27.351	3.258	95	2	2	2
31.668	2.823	100	4	0	0
34.586	2.591	9	3	3	1
35.482	2.528	1	4	2	0
39.049	2.305	17	4	2	2
41.521	2.1731	5	3	3	3
45.407	1.9958	55	4	4	0
47.581	1.9095	3	5	3	1
48.329	1.8817	<1	4	4	2
51.165	1.7839	3	6	2	0
53.182	1.7209	2	5	3	3
53.808	1.7023	18	6	2	2
56.419	1.6296	17	4	4	4
58.273	1.5821	3	5	5	1
58.942	1.5657	<1	6	4	0
61.424	1.5082	6	6	4	2
63.205	1.4700	3	5	5	3
66.117	1.4121	5	8	0	0

The difference in the La-Br as compared to the Li-Br bond lengths demands that the Br atom shift from the (¼ 0 0) site to draw closer to the Li atom. Hence, the Li-Br octahedral is smaller than that of the La-Br. This result is in contrast to the Cs_2KTbCl_6 and Cs_2KeuCl_6 structures reported by Villafuerte-Casterjon, et al [82] where the K-Cl octahedral was significantly larger in comparison to the Tb-Cl and Eu-Cl octahedral. The Cs atom displays a 12-fold coordination to Br, being located in a distorted dodecahedral site defined by the shared corners of Li-Br and La-Br octahedral. The distortion of the Cs-Br dodecahedral site is due to the shift of the Br atom from its ideal (¼ 0 0) position. The Cs-Br bond length of 3.993(1) Å is the longest of the cation–Br bond lengths and rounds out the structure of this new elpasolite compound.

Table 8. Crystal data for $Cs_2LiLaBr_6$ Space group: fm-3m (225), lattice parameter: a = 11.2890(6) Å, cell volume = 1438.7(2) $Å^3$, Z = 4, B_{iso} = 2.3 $Å^2$, R_p = 0.1267, density = 2.477 g/cm^3

	Site	x	y	z	Occ.
Cs	8*c*	¼	¼	¼	1
Li	4*b*	½	½	½	1
La	4*a*	0	0	0	1
Br	24*e*	0.2603(4)	0	0	1

The cerium-activated $Cs_2NaLaBr_6$ has a very similar diffraction pattern to that of the $Cs_2LiLaBr_6$ (see Figure 21) and initial refinements were attempted as the cubic elpasolite phase. However, it quickly became apparent that this compound showed considerable discrepancies between the model and observed pattern when using the cubic elpasolite form.

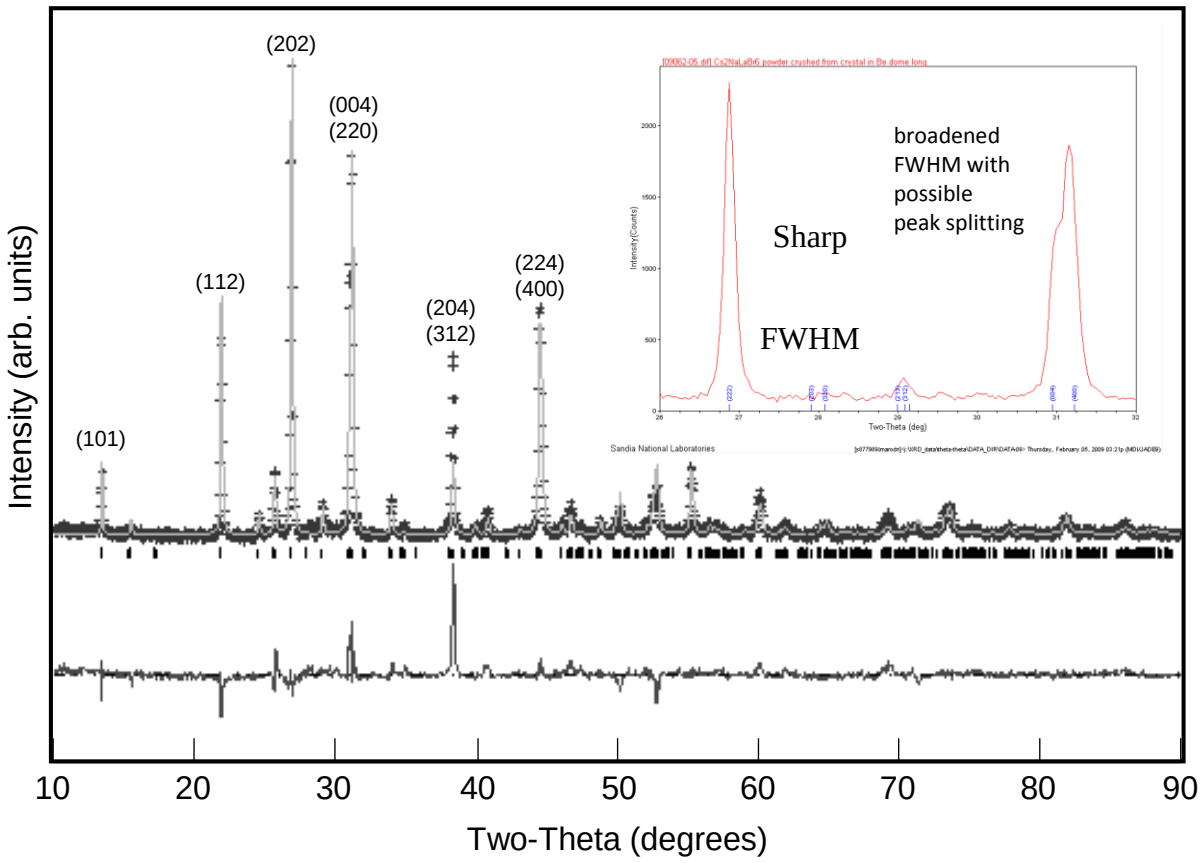

Figure 21. Structure refinement of the tetragonal $Cs_2NaLaBr_6$ structure.

In particular, the peak at ~30.9° 2θ showed significant broadening from what would otherwise be a cubic (400) peak. Careful inspection of the peak suggested a shoulder on the low-angle side of the peak that hinted at a distortion of the structure away from cubic symmetry (see insert in Figure 21, near 31°). Indexing the pattern as tetragonal confirmed these suspicions, showing a good match to a unit cell with a-axis ≈ 8.14 Å and a c-axis ≈ 12.58 Å. This tetragonal sub-cell corresponds to a reduction of the a-axis of a pseudo-cubic elpasolite lattice by √2, as illustrated by Figure 22. The space group $P4_2/mnm$ (136) predicted all of the observed peaks for the pattern. Subsequent unit cell refinement of the lattice resulted in the x-ray diffraction data for the tetragonal $Cs_2NaLaBr_6$ structure, as given in Table 9. Due to the tetragonal distortion of the cell, it was often difficult to separate overlapping peaks. Hence, several of the peaks in Table 9 are labeled with a (+) symbol to indicate the presence of more than one reflection contributing to the peak intensity.

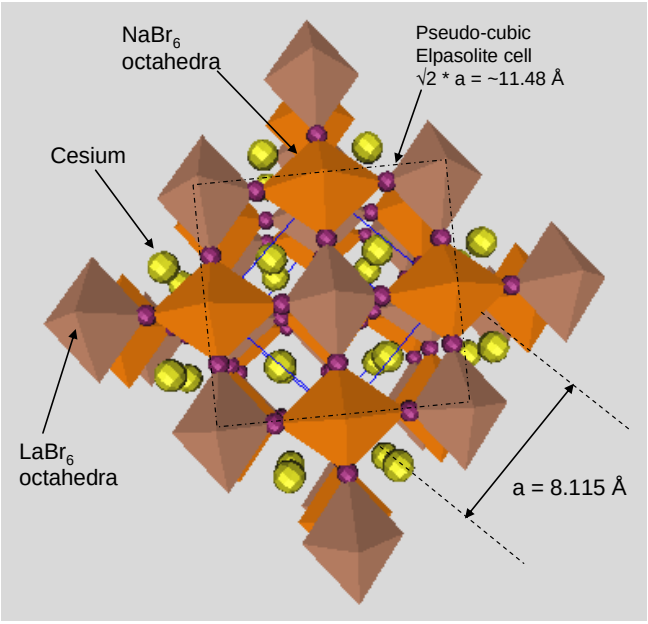

Figure 22. Model of $Cs_2NaLaBr_6$ (as viewed down the c-axis) showing the relationship between the a-axis of the tetragonal cell and that of a pseudo-cubic elpasolite supercell.

Diagnosis of the $P4_2/mnm$ space group indicated reasonable assignment of the atom positions as listed in Table 10. Note that the cations are all on special positions while the Br atoms have a degree of freedom to displace in either the x or z directions. Site occupancies for all the atoms refined to full occupancy with the resulting chemical composition matching the expected stoichiometry of $Cs_2NaLaBr_6$. The final Rp value was 13.33% and only one peak (~38.2° 2θ) showed substantial deviation between model and observed data. We attribute this excess intensity to be associated with a possible Al metal peak from the BeD holder base, or perhaps a result of inadequate grinding of the powder sample during specimen preparation within the glove box. Whatever the ultimate cause of this excess intensity, the model as shown in Figure 22 and listed in Table 10 is structurally and chemically reasonable, and fits within the context of the overall elpasolite-type behavior.

Table 9. X-ray diffraction data for tetragonal $Cs_2NaLaBr_6$.

2θ (^{o})	*d* (Å)	I/I_o	*h*	*k*	*l*
13.302	6.651	12	1	0	1
15.319	5.779	2^+	0	0	2
21.779	4.078	40^+	1	1	2
24.439	3.639	4	2	1	0
25.531	3.486	9	1	0	3
25.618	3.474	11	2	1	1
26.764	3.328	100	2	0	2
28.948	3.082	5	2	1	2
30.866	2.895	52	0	0	4
31.048	2.878	80	2	2	0
33.829	2.648	7	2	1	3
33.913	2.641	5	3	0	1
34.686	2.584	1	1	1	4
38.120	2.359	19	2	0	4
38.214	2.353	36	3	1	2
40.449	2.2282	3^+	1	0	5
40.660	2.2172	5^+	3	2	1
44.344	2.0411	51	2	2	4
44.506	2.0341	19	4	0	0
45.932	1.9742	3	4	1	0
46.423	1.9544	4	2	1	5
46.505	1.9512	5	3	2	3
46.601	1.9474	6	4	1	1
48.679	1.8686	3	4	1	2
49.825	1.8287	3	1	1	6
50.031	1.8216	6	3	3	2
50.076	1.8201	6	4	2	0
51.975	1.7580	2	4	1	3
52.430	1.7436	8	2	0	6
52.692	1.7357	10	4	2	2
55.114	1.6650	16	4	0	4
56.379	1.6306	2	4	1	4
56.768	1.6204	2	1	0	7
59.854	1.5440	7	3	1	6
59.989	1.5408	8	4	2	4

Intensities with + symbols indicate overlapping reflections.

Table 10. Crystal data for $Cs_2NaLaBr_6$ Space group: P4/mnm (136), lattice parameters: a = 8.1416(6) Å, c = 11.580(1) Å, cell volume = 767.4(2) $Å^3$, Z = 2, B_{iso} = 3.1 $Å^2$, R_p = 0.1333, density = 2.364 g/cm^3.

Atom	Site	x	y	z	Occ.
Cs	4*d*	0	½	¼	1
Na	2*a*	0	0	0	1
La	2*b*	0	0	½	1
Br1	4*g*	0.286(1)	0.714(1)	0	1
Br2	4*e*	0	0	0.233(1)	1
Br3	4*f*	0.769(1)	0.769(1)	0	1

Analysis of the powder pattern from the nominally prepared composition Cs_2NaLaI_6 yielded a diffraction pattern similar in appearance to the compound $CsTmI_3$ published by G. Schilling, et al. (1992) [93]. Attempts to index the diffraction pattern yielded a similar unit cell to the $CsTmI_3$ prototype lattice. Employing the indexed unit cell as a guide for peak location, x-ray diffraction data for the observed pattern was obtained and documented in Table 11. The raw data were fit using the $CsTmI_3$ model, where La was substituted on the Tm site and the Cs site was assumed to be partially occupied by Na atoms. The refinement converged quickly and it was evident that, while the iodine sites were fully occupied, the La site showed significant deficiency. Cs and Na were both placed on the 4*c* site location, as shown in Table 12, and the occupancy was constrained to unity. The refined occupancy for this site yielded 0.84 Cs and 0.16 Na for this cation site. In addition, the La site occupancy was refined to determine the extent of La deficiency. At this point in the refinement, it was clear that sodium was significantly lacking in comparison to the nominal composition. Hence, it also seemed likely that Na had substituted in the 6-fold La position of the lattice as well. Na and La (CN=6; La^{3+} =1.032 Å, Na^{1+} = 1.02 Å) [91] were both placed on the 4*a* site (origin) and the occupancy for this site was constrained to unity. Refinements indicated a near 50/50 ratio between the two cations.

This ratio made sense in terms of charge balance (bringing the structure to a neutral condition) so the occupancies for La and Na on the 4a site were fixed to a 0.5 value. The final refinement resulted in the observed fit as shown in Figure 23. The final Rp value was 13.61% and the appearance of the difference curve was reasonably flat. As in the other refinements, an overall atomic displacement parameter was refined for the structure.

Table 11. X-ray diffraction data for orthorhombic $(Cs_{0.84}Na_{0.16})(Na_{0.5}La_{0.5})I_3$.

2θ (^{o})	*d* (Å)	I/I_o	*h*	*k*	*l*
12.497	7.077	9	0	1	1
14.247	6.211	4	0	2	0
14.417	6.139	6	1	0	1
16.035	5.523	3	1	1	1
20.285	4.374	10	1	2	1
20.611	4.306	4	0	0	2
22.741	3.907	11	2	0	1
22.947	3.873	12	1	0	2
23.794	3.737	9	0	3	1
23.856	3.727	29	2	1	1
24.064	3.695	19	1	1	2
24.858	3.579	100	2	2	0
25.106	3.544	63	0	2	2
25.912	3.436	4	1	3	1
26.961	3.304	24	2	2	1
27.109	3.287	17	1	2	2
28.683	3.110	86	0	4	0
29.035	3.073	98	2	0	2
29.632	3.012	8	2	3	0
29.901	2.986	6	2	1	2
31.421	2.845	9	2	3	1
31.646	2.825	7	1	3	2
31.892	2.804	6	0	1	3
32.238	2.775	5	1	4	1
32.327	2.767	9	3	0	1
32.470	2.755	4	2	2	2
32.806	2.728	4	1	0	3
33.167	2.699	7	3	1	1
33.602	2.665	1	1	1	3
35.395	2.534	13	2	4	0
35.488	2.528	12	3	2	1
35.562	2.522	12	0	4	2
35.871	2.501	16	1	2	3
36.990	2.428	6	2	4	1
37.149	2.418	5	3	0	2
37.396	2.403	5	2	0	3
37.611	2.390	6	0	5	1
38.089	2.361	4	0	3	3

2θ (°)	*d* (Å)	I/I_o	*h*	*k*	*l*
39.468	2.281	2	1	3	3
39.968	2.254	1	3	2	2
41.184	2.1901	26	4	0	0
41.278	2.1854	39	2	4	2
41.849	2.1569	6	4	1	0
42.547	2.1231	5	4	0	1
43.066	2.0987	10	2	5	1
43.168	2.0940	21	1	0	4
43.273	2.0891	15	3	3	2
43.525	2.0776	7	2	3	3
43.806	2.0649	9	1	1	4
44.082	2.0526	3	1	4	3
45.102	2.0086	6	4	2	1
45.731	1.9824	4	1	2	4
46.522	1.9505	2	4	0	2
46.998	1.9319	3	2	5	2
48.143	1.8886	3	4	3	1
48.347	1.8811	2	0	5	3
48.579	1.8726	5	2	6	0
48.708	1.8680	8	0	6	2
48.840	1.8632	8	4	2	2
49.338	1.8456	4	2	2	4
49.539	1.8386	2	1	5	3
50.950	1.7909	10	4	4	0
51.577	1.7706	5	0	4	4
51.687	1.7671	6	4	3	2
52.146	1.7526	2	2	3	4
52.581	1.7391	4	0	7	1
52.668	1.7365	4	1	4	4
53.281	1.7179	1	3	1	4
54.638	1.6784	2	4	2	3
54.886	1.6714	2	3	2	4
55.355	1.6584	2	3	6	1
55.539	1.6533	2	4	4	2
55.656	1.6501	4	1	6	3
55.886	1.6439	7	4	5	0

Table 12. Crystal data for $(Cs_{0.84}Na_{0.16})(Na_{0.5}La_{0.5})I_3$
Space group: Pnma (62), lattice parameters: a = 8.762(1) Å, b = 12.436(2) Å,
c = 8.627(2) Å, cell volume = 940.0(4) $Å^3$, Z = 4, B_{iso} = 2.3(2) $Å^2$,
R_p = 0.1361, density = 2.455 g/cm^3.

Atom	Site	x	y	z	Occ.
Cs	4*c*	0.459(1)	¼	0.015(1)	0.84(2)
Na1	4*c*	0.459(1)	¼	0.015(1)	0.16(2)
Na2	4*a*	0	0	0	0.5
La	4*a*	0	0	0	0.5
I1	8*d*	0.2063(8)	0.0293(6)	0.2951(8)	1
I2	4*c*	0.502(1)	¼	0.558(1)	1

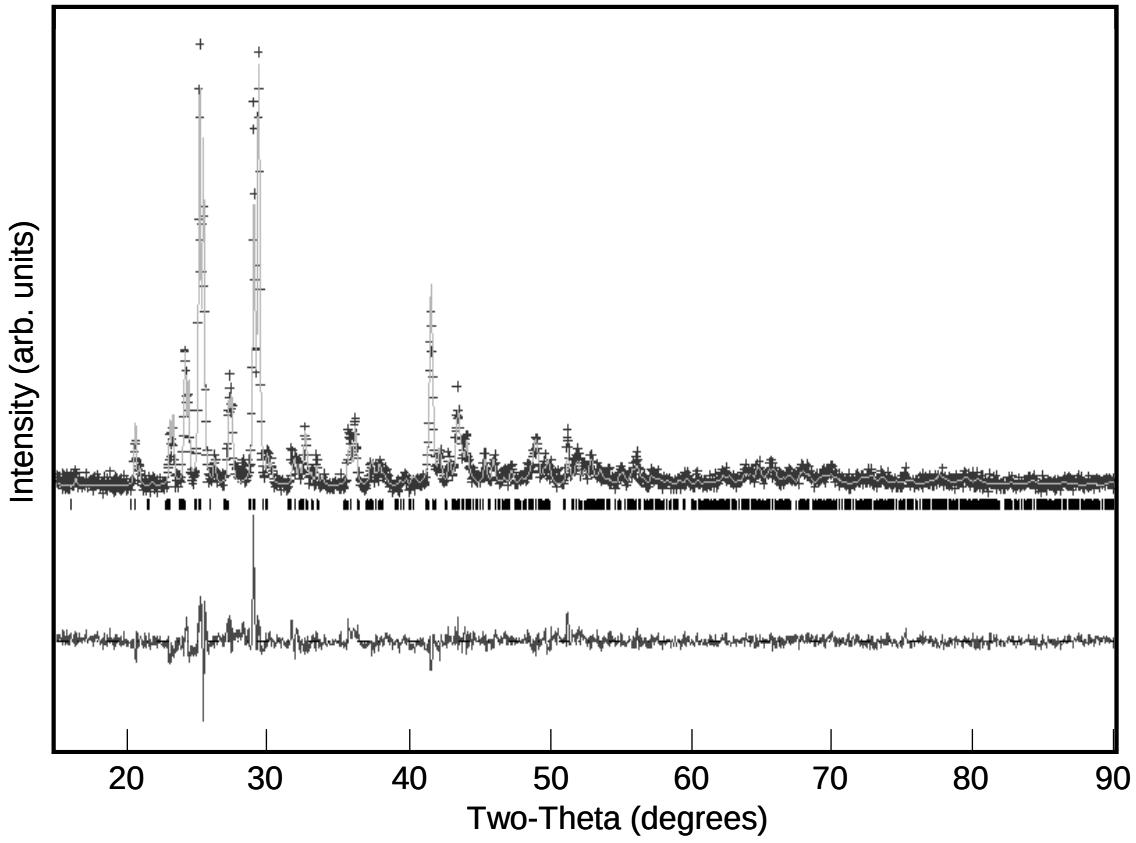

Figure 23. Structure refinement of the orthorhombic $(Cs_{0.84}Na_{0.16})(Na_{0.5}La_{0.5})I_3$ structure.

The final refined composition for the phase was $(Cs_{0.84}Na_{0.16})(Na_{0.5}La_{0.5})I_3$, which implies a slightly Na-rich, slightly Cs-deficient composition as compared to the nominal mixture. It could also be possible that the La site contains significant cation vacancies to accommodate the decreased scattering determined from this site, as shown in the refinements. Tests using such a model would suggest a 2/3 occupancy for La on the 4a site with the remainder as cation vacancy sites. While this model is plausible, it would imply significant Na deficiency as compared to nominal composition, and so is viewed as a less likely favorable model for this phase.

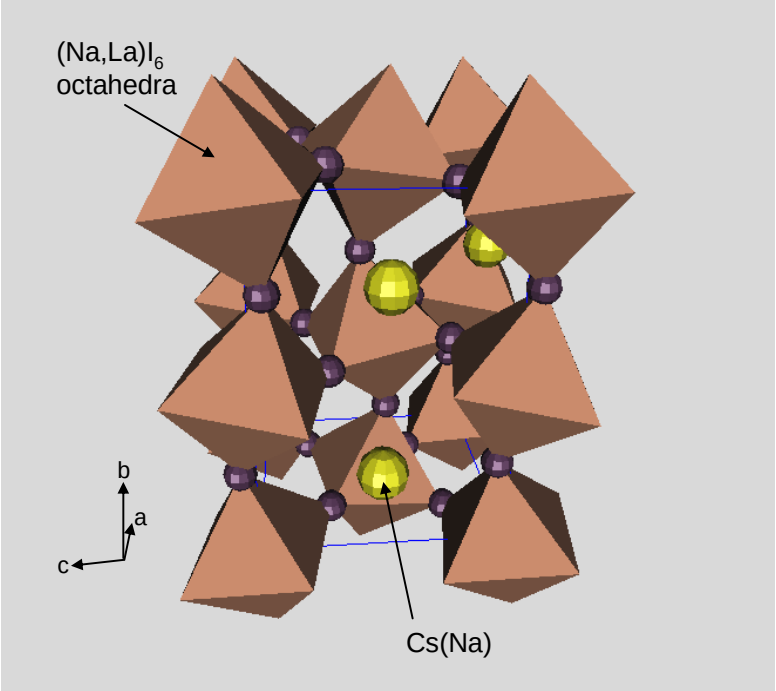

Figure 24. Model of $(Cs_{0.84}Na_{0.16})(Na_{0.5}La_{0.5})I_3$ (as viewed down the a-axis) showing a distorted octahedral and the location of Cs site near the (100) and (001) plane.

Figure 24 illustrates the $CsTmI_3$-type structure for the refined $(Cs_{0.84}Na_{0.16})(Na_{0.5}La_{0.5})I_3$ lattice, illustrating the single (mixed cation) octahedral site along with the larger (distorted) dodecahedral location for the Cs/Na cation. The iodide structure is very similar to the tetragonal $Cs_2NaLaBr_6$ structure in that it displays a sub-cell (or single, distorted perovskite cell) of the larger elpasolite structure. The Cs atoms show similar location in this cell to that of the tetragonal structure, in that Cs resides at or near the plane generated by the long axis (i.e., ≈ 12 Å) and one short axis (i.e., $\sqrt{2} * \approx 12$ Å). For the case of the tetragonal $Cs_2NaLaBr_6$, this would be the (100) and its equivalent (010) plane. In the case of the $(Cs_{0.84}Na_{0.16})(Na_{0.5}La_{0.5})I_3$ phase the Cs atoms reside on the (100) and (001) planes (see Figure 24) since the b-axis of this orthorhombic structure is the long dimension (b = 12.426(2) Å), and the a-axis (8.761(1) Å) and the c-axis (8.627 (1) Å) define the two shorter dimensions of the elpasolite sub-cell. The now nonequivalent a- and c-axes are likely a result of the tilting/rotation behavior of the La(Na)-I octahedral, as shown in Figure 24.

Additionally, the distortion of the dodecahedral site in the orthorhombic iodide phase is substantially enhanced over that of the tetragonal $Cs_2NaLaBr_6$ due to the substantial reorientation of the octahedral. Table 13 shows bond lengths and angles associated with the various sites for Cs, Li/Na, and La coordination. Most notable in this table is the elongated Cs-I1 bond length of 5.27(1) Å, which suggests a strongly distorted dodecahedral site. In addition, the I-Cs-I angles show significant deviation from the typical 60, 90, 120 and 180^o values. Interestingly, the La-Br octahedral site for the tetragonal structure shows greater variation in bond length than that of the orthorhombic iodide lattice. This likely is derived from the fact that the tetragonal structure still maintains ordered Na and La sites and does not display significant tilting/rotation of the Na-Br and La-Br octahedral, while in the case of the iodide, there is only one (mixed) site location for the 6-fold La and Na atoms and stability of the overall lattice is driven by tilt/rotation between neighboring octahedrals in the structure. As the above examples illustrate, the crystal structure of low-tolerance-factor compounds such as $Cs_2NaLaBr_6$ (t = 0.909) and Cs_2NaLaI_6 (t = 0.897) can deviate from its cubic elpasolite structure. However, the exact tolerance value where these compounds will deviate from the cubic structure still needs a large amount of experimental data to define it. Our embedded model has shown to be effective to predict and screen out cubic compounds in the large elpasolite halide family.

Table 13. Bond lengths (Å) and angles (°) for compounds.

Cubic $Cs_2LiLaBr_6$			**Tetragonal $Cs_2NaLaBr_6$**			**Orthorhombic $(Cs_{0.84}Na_{0.16})(Na_{0.5}La_{0.5})I_3$**		
La-Br	x6	2.938(5)	La-Br1	x2	2.46(2)	La-I1	x2	3.144(8)
			La-Br2	x2	3.10(1)		x2	3.142(8)
			La-Br3	x2	3.10(1)	La-I2	x2	3.150(2)
Li-Br	x6	2.706(5)	Na-Br1	x2	3.30(1)			
			Na-Br2	x2	2.69(1)			
			Na-Br3	x2	2.66(2)			
Cs-Br	x12	3.993(1)	Cs-Br1	x2	4.103(2)	Cs-I1	x2	3.86(1)
			Cs-Br2	x2	4.075(1)		x2	4.22(1)
			Cs-Br3	x2	4.088(1)		x2	4.28(1)
							x2	5.27(1)
						Cs-I2		3.96(2)
								4.06(2)
								4.70(1)
								4.79(1)
Br-La-Br		90	Br-La-Br		90.0(1)	I1-La-I1		89.9(1)
		180			180.0(1)		x2	90.1(1)
								180.0(1)
Br-Li-Br		90	Br-Na-Br		90.0(1)	I2-La-I2		180.0(1)
		180			180.0(1)	I1-La-I2	x2	88.8(3)
							x2	89.3(3)
							x2	90.7(3)
							x2	91.2(3)
Br-Cs-Br	x12	57.3(1)	Br1-Cs-Br1	x2	90.3(1)			
	x12	62.7(1)		x4	119.9(1)	I1-Cs-I1	x2	63.1(1)
	x12	90.0(1)	Br2-Cs-Br2	x4	90.1(1)		x2	66.1(2)
	x24	120.0(1)		x2	174.3(4)		x2	78.4(1)
	x6	176.7(1)	Br3-Cs-Br3	x2	89.8(1)			79.9(3)
				x4	120.1(1)			90.7(3)
			Br1-Cs-Br2	x4	57.9(2)			110.9(3)
				x4	62.7(2)		x2	120.6(3)
				x4	112.9(1)		x2	127.6(3)
				x4	127.0(1)		x2	165.9(2)
			Br1-Cs-Br3	x4	57.8(1)	I1-Cs-I2	x2	64.9(2)
				x4	62.3(1)		x2	65.4(2)
				x4	90.0(1)		x2	65.7(2)
				x4	177.2(4)		x2	111.7(3)
			Br2-Cs-Br3	x4	55.3(2)		x2	127.6(3)
				x4	64.9(2)		x2	128.3(2)
				x4	119.7(2)	I2-Cs-I2		86.3(3)
				x4	120.0(2)			

3.3.3 Hot Pressing

$Cs_2LiLaBr_6$ was chosen for the first hot forging experiment because it has a cubic structure among all these elpasolite halides. A preliminary hot forging experiment was conducted for $Cs_2LiLaBr_6$ at 478 °C for 4 hours, which was 10 °C below its T_m and 17 °C above T_u. Therefore, it is important to ensure that full density can be achieved within a short time span by the hot forging process. A solidified $Cs_2LiLaBr_6$ ingot with a diameter of 0.98 cm and thickness of 0.7 mm (see Figure 25 (a)) was hot forged at 478 °C with a pressure ramping rate at 100 psi/min. The polycrystalline ingot was centered in a 2.54 cm diameter graphite die with graphite foil liner and spacers toprevent the sample from coming into direct contact with the graphite die assembly. The cylinder specimen was found to be completely deformed into a thin disk (2.54 cm diameter, 0.104 cm thick) and the densification was completed within the first 5 minutes. The forged sample is shown in Figure 25 (b). Because graphite foil was still attached to the sample, the transparency of the material could not be determined. Attempts to remove the foil from the thin disk by a razor blade were unsuccessful, and the sample broke into pieces.

However, this experiment demonstrates that the hot forging technique can offer a short processing time and an effective densification process for these elpasolite halides. These factors are important to remove pores in a ceramic body and to produce highly transparent ceramics without causing significant weight loss or deviation from its stoichometry. The ability to sustain such a large plastic deformation for the $Cs_2LiLaBr_6$ can be attributed to its relatively soft heavy ionic nature, as well as many active slip systems available in the face-center-cubic structure. This experiment demonstrates the feasibility of making large-area, transparent detectors by a hot forging technique similar to these reported for NaI and CsI.

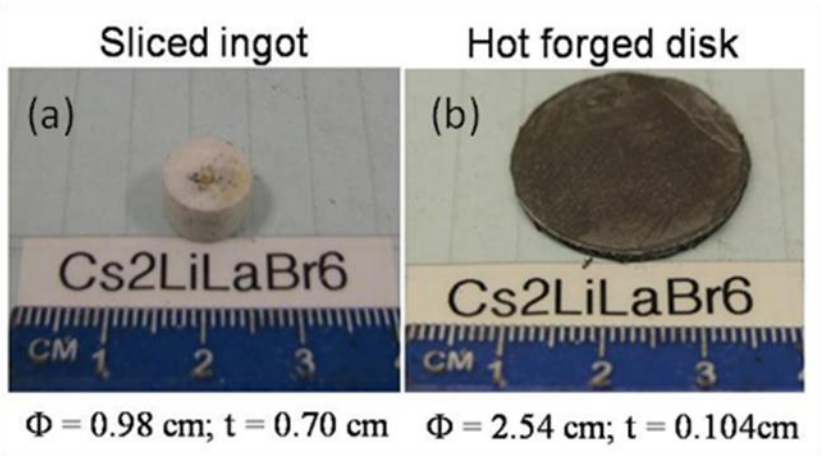

Figure 25. The change of sample geometry for a sliced $Cs_2LiLaBr_6$ ingot (a) before and (b) after hot forging. The aspect ratio (D/t) of the sample changed from 1.4 to 24.4 after hot forging.

Based on the results of the first attempt, two fused quartz plates were introduced as spacers between the raw material and graphite rams to avoid direct contact with the graphite during hot pressing or hot forging. However, after hot pressing, samples made from crushed powder (fine and coarse powders from Cs_2LiYCl_6:$Ce3^+$) had a tinted black appearance with darkened grain boundaries (see Figure 26(a) and (b)), presumably due to carbon from the graphite die preferentially diffusing into these grain boundary regions. In contrast, samples that were hot forged from melted ingots that had a diameter (0.75 in. dia.) close to the graphite die (1.0 in. dia.) had almost no darkening (see Figure 26(c)). Part of this improvement can be attributed to the higher thermal stability of Cs_2LiYCl_6 and $Cs_2NaLaBr_6$ in comparison to $Cs_2LiLaBr_6$ (Table 5). However, thermomechanically healed cracks in the hot forged $Cs_2NaLaBr_6$ sample were visible, as illustrated in Figure 26(d). These healed cracks can affect the optical quality, but could be reduced or avoided if sample was forged at a lower strain rate at higher temperature (by a slow creeping deformation). These samples were believed to have achieved a full density after hot forging, yet they were still milky and were not able to achieve full optical quality for detection applications. Therefore, other factors besides density, such as impurity and residual phase, must play an important role in the optical quality of the hot forging ceramic samples.

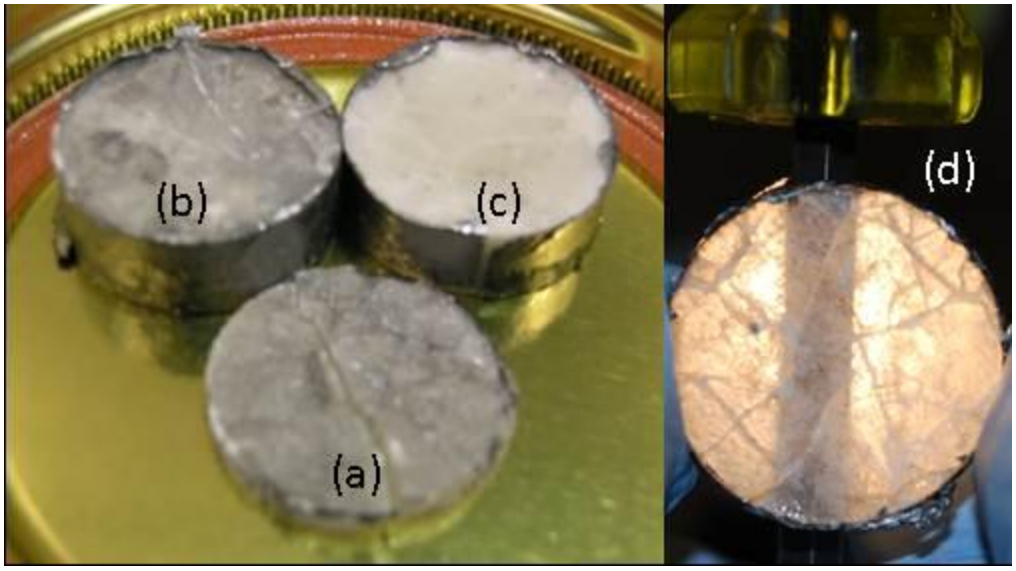

Figure 26. Hot pressed and forged samples: (a) Hot pressed Cs_2LiYCl_6 powder, (b) hot pressed Cs_2LiYCl_6 crushed particles, (c) hot forged Cs_2LiYCl_6 melt ingot, (d) hot forged $Cs_2NaLaBr_6$ under back-lighting (shadow cast by an Allen wrench).

3.3.4 Photoluminescence and Radioluminescence

3.3.4.1 Optical Spectroscopy

The optical emission and excitation of Ce^{+3} doped elpasolite halides were measured front-face with a steady state spectrofluorimeter (QuantaMaster, Photon Technology International). Figure 27 shows the emission and excitation spectra for the Cs_2LiLaI_6 crystal. The data indicate that the main Ce^{+3} emission band (solid line) is located between 420 nm and 530 nm with a maximum at 435 nm. The excitation scan monitored at 435 nm from 190 nm to 415 nm exhibits a double band with maximum excitation emission (dashed line) at 397 nm. Both the excitation and the emission spectra correspond to the 5d-4f transition for the Ce^{+3} in the elpasolite halide lattice [94].

The maximum emission and the excitation wavelengths, as well as the amount of Stokes shift and optical quantum efficiency for the elpasolite bromides and iodides, are summarized in Table 14. The data illustrate that the luminescence characteristics are strongly dependent on the type of halogen anions in the lattice, and to a lesser degree on the alkaline cations. For example, the excitation wavelengths for both of the bromides as well as the two iodides are at 358-366 nm and 397-398 nm, respectively. A similar trend can be seen for the emission spectra where the maximum emission for the bromides and iodides is at 414-417 nm and 422-435 nm, respectively. These values are compared to the elpasolite chlorides [73] where their excitation maxima are centered at 210-355 and the emission maxima are in the 337-339 nm range. The results suggest that as the size of the anions increases from Cl^- to I^-, both the excitation and the emission maxima shift to longer wavelengths. This systematic red-shift can be attributed to the differences in ionic radius as well as the polarizability of the coordinating anions to the Ce^{+3} residing in the high-symmetry O_h (octahedral) sites, as predicted by the crystal field model for strong ionic solids [73]. A larger octahedron consisting of the highly polarizable anion I^-, in comparison to smaller, less polarizable Cl^- or Br^- ions, can effectively reduce the field splitting between the 5d and 4f energy levels for Ce^{+3} and cause a red-shift for the emission spectrum. The alkaline cation, such as Na^+ or Li^+ in the elpasolite lattice, is at the second neighbor position relative to the octahedrally coordinated Ce^{+3}; therefore, it is less effective than the halogen anions in the field splitting and consequently the emission spectrum. These observations are consistent with spectroscopic studies of other elpasolite halides [95].

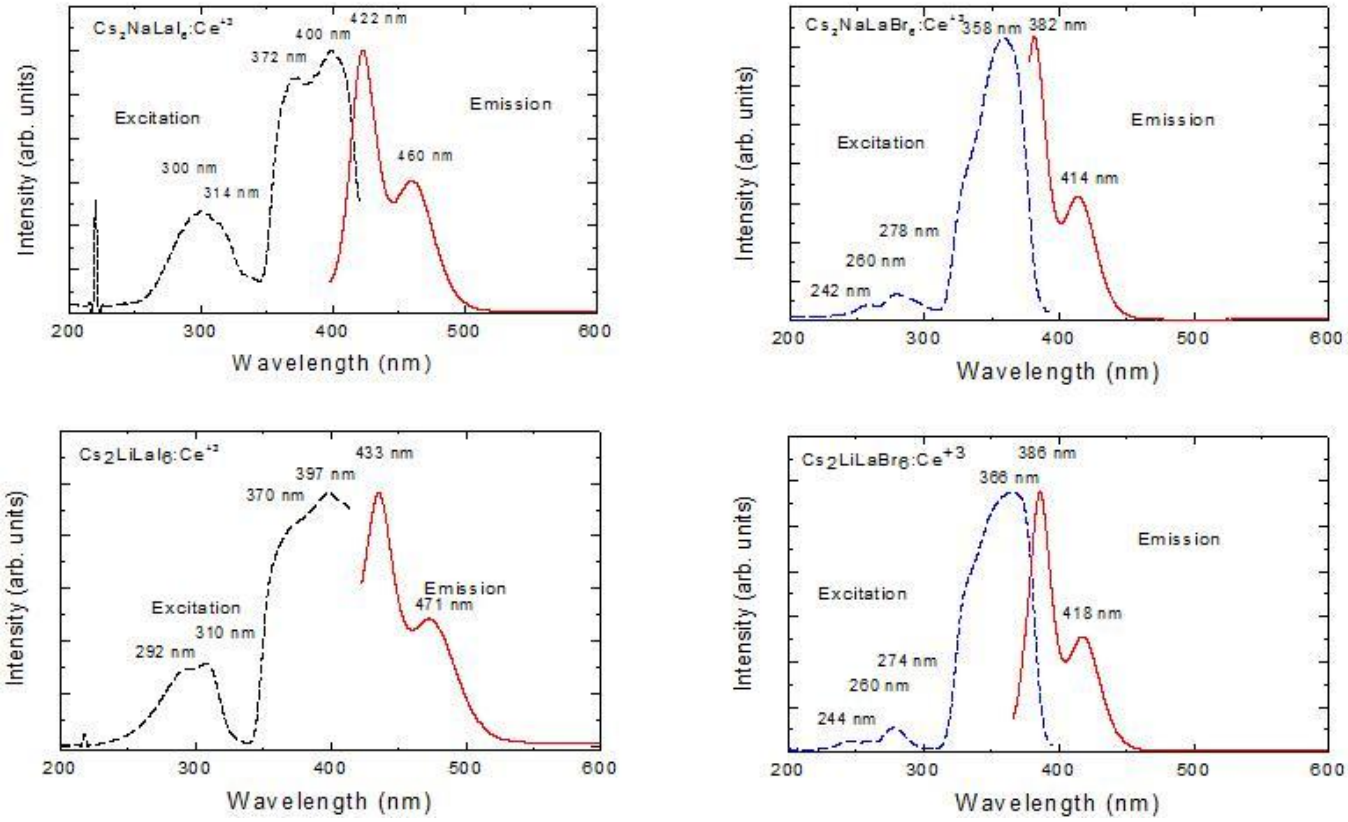

Figure 27. Excitation (dotted line) and emission (red solid line) spectra of elpasolite halide compounds.

Table 14. The maximum of the emission and the excitation wavelengths, as well as the amount of Stokes shift for the cerium-doped (5 mol.%) elpasolite halides.

Material	Excitation maximum (nm)	Emission maximum (nm)	Stokes shift (nm)	Optical quantum efficiency (%)
Cs_2NaLaI_6	400	422	22	57
Cs_2LiLaI_6	397	433	36	69
$Cs_2NaLaBr_6$	358	382	24	58
$Cs_2LiLaBr_6$	366	366	20	70
$Cs_2NaGdBr_6$	351	382	32	51

3.3.4.2 Radiation Characterization

X-ray induced emission spectra for some of the doped and undoped elpasolite halides, including $Cs_2LiEuCl_6$:5% Ce^{3+}, $Cs_2NaErBr_6$, $Cs_2NaErBr_6$:5%Ce^{3+} and Cs2NaGdBr6:2.5%Ce^{3+} are given in Figure 28. After subtracting the quartz cup signal, the spectrum of $Cs_2LiEuCl_6$:5% Ce^{3+} shows that emission from Ce^{3+} activator has been complete quenched and only two Eu^{3+} f-f ($^5D_1$ and

$^5D_0$ to $^7F_0$) transitions peaking at 591 nm and 613 nm are observed (black line). These spectra also indicate the inhomogeneity of the crystal as the emission spectrum varied from position to position (tip, middle, and top, as shown in Figure 28(a)). Since the excited Ce^{3+} (5d) has a higher energy than the Eu^{+3} (4f states), it is believed that the excitation energy is transferred nonradiatively to Eu^{3+} prior the final relaxation. For undoped $Cs_2NaErBr_6$, the emission spectrum exhibits all the sharp f-f transitions, including the de-excitation from $^2H_{9/2}$, $^4F_{7/2}$, $^2H_{11/2}$, $^4S_{3/2}$, $^4F_{9/2}$, and $^4I_{9/2}$ to the $^4I_{15/2}$ ground state (see Figure 28(b)). When this compound is activated with Ce^{3+} (Figure 28(c)), together with a few weak f-f- emissions, an addition broad band near 421 nm with a shoulder was observed. This could be the Ce^{3+} emission. For the Cs2NaGdBr$_6$:2.5%Ce^{3+} sample, the x-ray-induced emission spectrum mirrors to its photoemission spectrum (not shown). The spectrum shows two emission peaks at 382 nm and 415 nm. This emission, which can be attributed to Ce^{3+} ions, is caused by the transition from the 5d excited state to the two spin-orbit split $^2F_{5/2}$ and $^2F_{7/2}$ ground state levels. Additional small emission peaks at 310 nm and 621 nm are from the host Gd f-f transitions that can be correlated to the $^6P_{7/2}$ to $^8S_{7/2}$ ground state and the $^6G_{7/2}$ to ^6P_j transition, respectively.

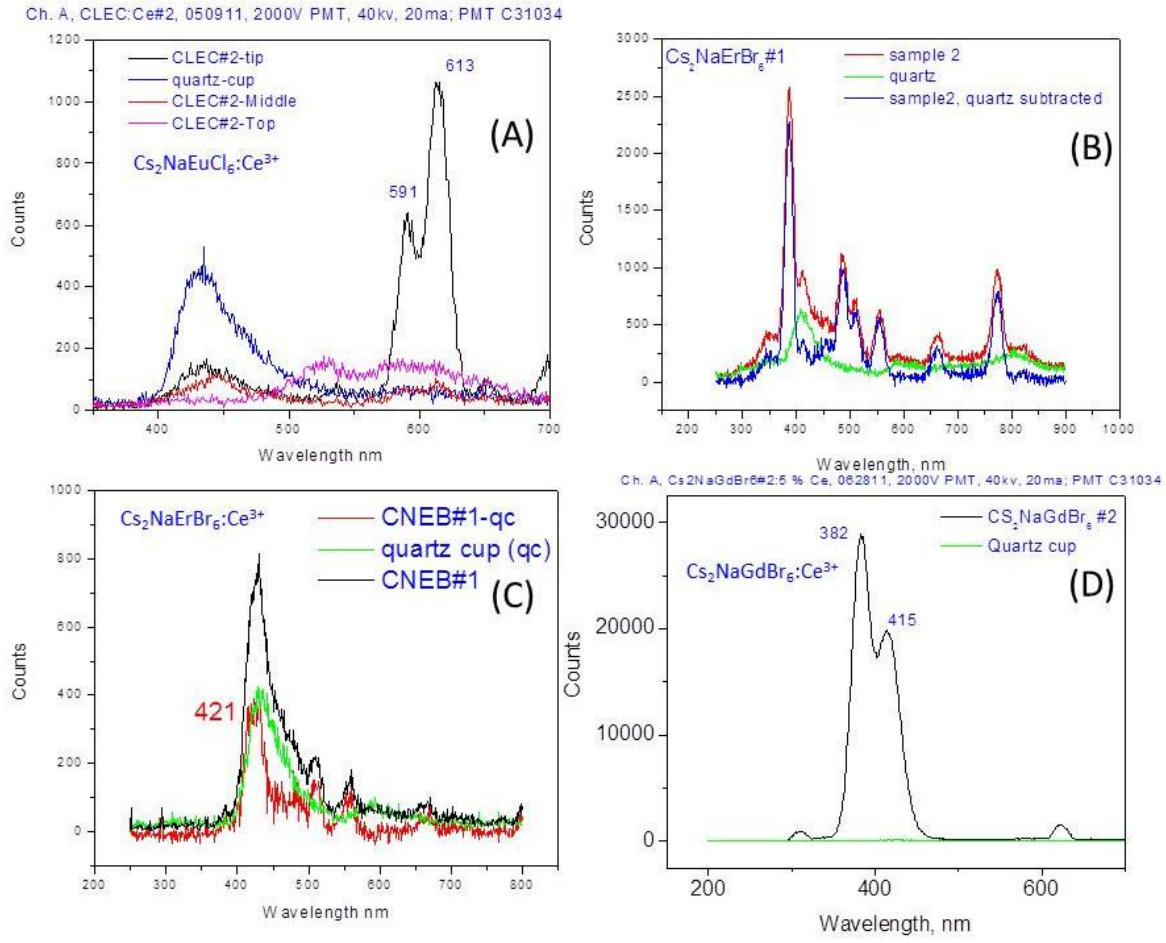

Figure 28. X-ray induced emission spectra of (a) $Cs_2LiEuCl_6$:5% Ce^{3+}, (b) $Cs_2NaErBr_6$, (c) $Cs_2NaErBr_6$:5%Ce^{3+}, and (d) Cs2NaGdBr$_6$:2.5%Ce^{3+} at room temperature (measured at RMD).

Energy resolution is an important property for gamma-ray spectroscopy. In Figure 29(a), the pulse height spectrum of a Sandia-grown Cs2LiLaBr$_6$:Ce^{3+} single crystal (Figure 17(b)) under 662 keV gamma-ray excitation, recorded with a shaping time of 6 μs, is shown. At room temperature we obtained an energy resolution of 8.96% (FWHM) at 662 keV. This resolution is lower than data reported by RMD, presumably due to the quality of our single crystal, but is comparable with that of NaI:Tl and BGO. Further improvement in the energy resolution of the $Cs_2LiLaBr_6$ could be achieved with good-quality crystal. The pulse height spectra of other elpaoslite halide compounds measured at RMD are given in Figure 30. These results indicate that Cs_2LiEuCl6: 5%Ce^{3+}, $Cs_2NaErBr_6$, and Cs_2NaEr$_6$:5%Ce^{3+} are not good scintillators, presumably due to their poor photon yield, as indicated by Figure 28.

Figure 31 shows the non-proportionality response of $Cs_2LiCeBr_6$ single crystal grown in Sandia. The non-proportionality is determined busing different radioactive sources. In Figure 31 the relative light yield are obtained from the pulse height spectra recorded with a photomultiplier (PMT) tube. The values obtained are then normalized to the incident energy and plotted relative to the 662 keV results. It is clear from Figure 31 that the energy resolution is less than 1.7% counting the ^{137}Cs x-ray peak) is within 2% over the 26.3 to 2614.5 keV energy range. For a comparison purpose, the insert in Figure 31 shows the non-proportionality of other common scintillators. Results indicate that the non-proportionality of $Cs_2LiLaBr_6$ is better than the state-of-the-art $LaBr_3$:Ce^{3+} and $LaCl_3$:Ce^{3+} crystals, which showed 4% and 7% non-proportionality, respectively, in a similar range [96][97]. Additional measurements for the non-proportionality and decay time for $Cs_2NaGdBr_6$:Ce^{3+} are given in Figure 32. Results show that the non-proportionality of $Cs_2NaGdBr_6$:Ce^{3+} is less than 4% (Figure 32(a)), which is also better than $LaBr_3$:Ce^{3+} and $LaCl_3$:Ce^{3+}. The coincident measurement results indicate that the fast decay time for $Cs_2NaGdBr_6$:Ce^{3+} can be well approximated by a two-component exponential decay curve ($R^2 > 0.998$). The fast-decay component has a lifetime of 102 ns, which is slower than other elpasolite halide compounds listed in Table 3, but is shorter than CsI;Na and CsI:Tl scintillators, which are about 640 ns and 1 μs, respectively.

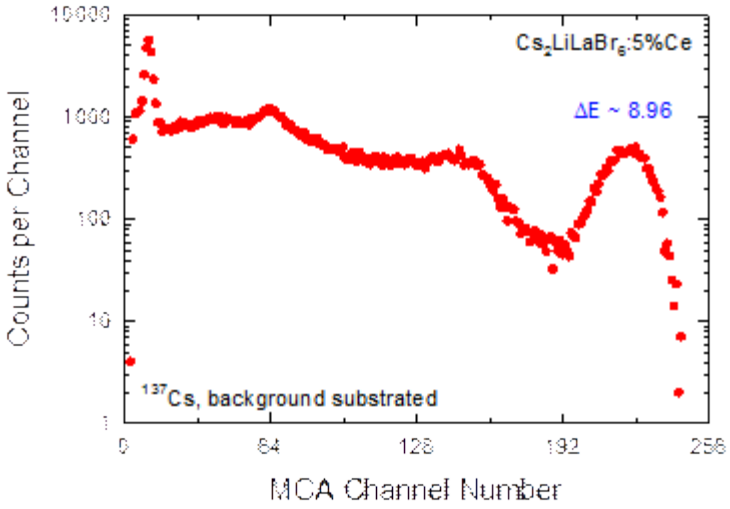

Figure 29. Pulse height spectrum of $Cs_2LiLaBr_6:Ce^{3+}$ crystal excited with 663 keV gamma-rays from a ^{137}Cs source.

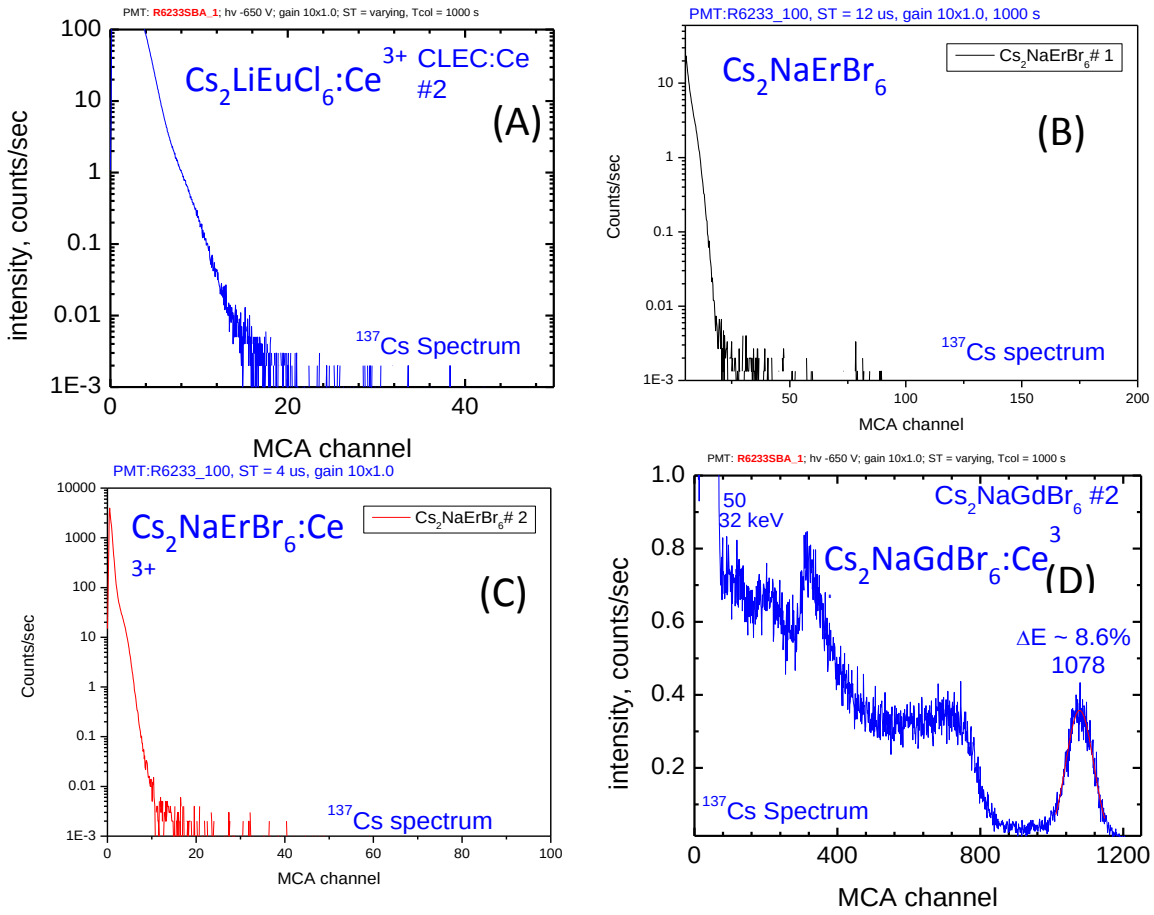

Figure 30. Pulse height spectra of (a) $Cs_2LiEuCl_6$:5% Ce^{3+}, (b) $Cs_2NaErBr_6$, (c) $Cs_2NaErBr_6$:5%Ce^{3+}, and (d) Cs2NaGdBr$_6$:2.5%Ce^{3+} at room temperature (measured at RMD).

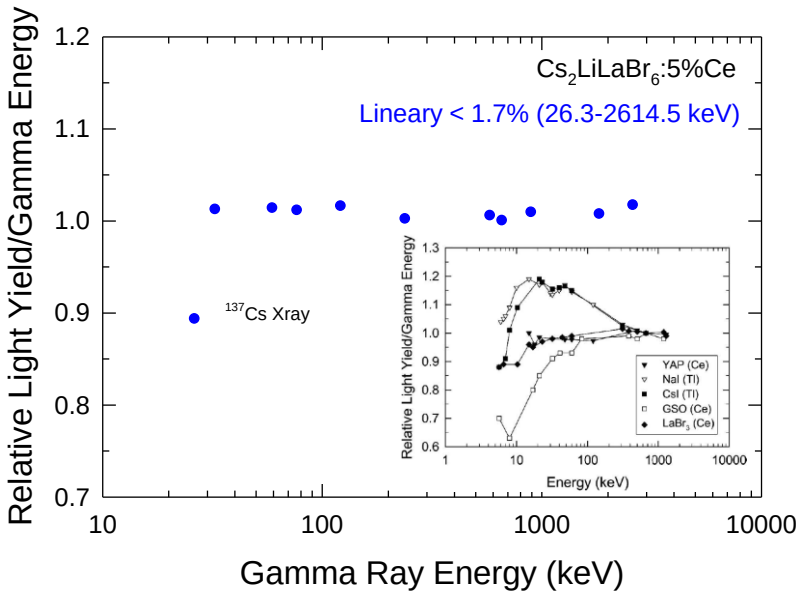

Figure 31. The non-proportionality curve for $Cs_2LiLaBr_6:Ce^{3+}$, using photon yield/gamma energy with respect to the detector's light yield at 662 keV.

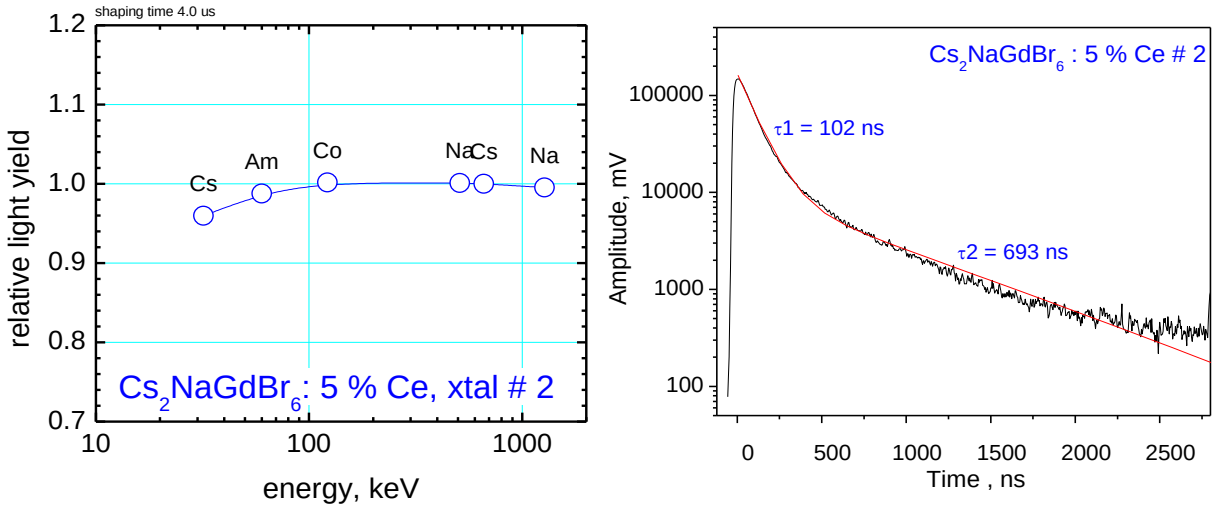

Figure 32. The non-proportionality curve and the fluorescence decay time spectrum for $Cs_2NaGdBr_6:Ce^{3+}$ crystal (Measured at RMD).

APPENDIX A: EFFECT OF VARIABLE CHARGE MODELS

To incorporate the variable charge effect in an analytical model, the distinctive effect incorporated by a variable charge model as compared with a fixed-charge model is explored using an ion pair of cation (atom 1) and anion (atom 2) with opposite point charges of +q and –q, respectively. Without a loss of generality, a Lennard-Jones type of power function can be used to represent the charge-independent component of the energy. The total energy of the pair of atoms can then be written according to the variable charge model [25] as

$$E = (\chi_1 - \chi_2)q + \left(\frac{J_1 + J_2}{2} - \frac{k}{r}\right)q^2 + \frac{E_b \cdot \beta}{\beta - \alpha} \cdot \left(\frac{r_e}{r}\right)^{\alpha} - \frac{E_b \cdot \alpha}{\beta - \alpha} \cdot \left(\frac{r_e}{r}\right)^{\beta} \tag{A-1}$$

Here χ_i and J_i are electronegativity and atomic hardness of atom i (i = 1, 2), r is spacing between the two atoms, k is the Coulomb constant, and E_b, α, β, r_e are the four parameters for the power potential. The charge q can be solved from equilibrium condition $\partial E/\partial q = 0$ as

$$q = \frac{\chi_2 - \chi_1}{J_1 + J_2 - \dfrac{2k}{r}} \tag{A-2}$$

Substituting Eq. (A-2) in Eq. (A-1), the total energy is expressed as

$$E = -\frac{(\chi_2 - \chi_1)^2}{2(J_1 + J_2) - \dfrac{4k}{r}} + \frac{E_b \cdot \beta}{\beta - \alpha} \cdot \left(\frac{r_e}{r}\right)^{\alpha} - \frac{E_b \cdot \alpha}{\beta - \alpha} \cdot \left(\frac{r_e}{r}\right)^{\beta} \tag{A-3}$$

Using example values of χ_1 = -3.402 eV, χ_2 = 2.000 eV, J_1 = 10.216 eV, J_2 = 13.992 eV [25], and power potential parameters E_b = -0.8 eV, r_e = 2.5 Å, α = 12, β = 6, the bond energy defined by Eq. (A-3) is shown as a function of the atomic spacing r in Figure A1 using a solid line. For comparison, a similar bond energy curve without the charge transfer (i.e., only the power potential) is also shown using a dashed line. The values in the figure indicate the minimum energy points. The essential effect of the charge transfer in the variable charge models [25,26,27,28,29,30,31] is to cause an increase in the magnitude of the equilibrium (minimum) bond energy and a decrease in the equilibrium bond length (which gives the minimum energy) for the cation–anion bond. This is because the charge transfer causes the cation to become a positive charge and the anion to become a negative charge, which results in a negative (attractive) Coulomb interaction. Clearly, the charge transfer also causes an increase in bond length and a decrease in the magnitude of bond energy for the cation–cation bond or the anion–anion bond where the Coulomb interactions are positive (repulsive).

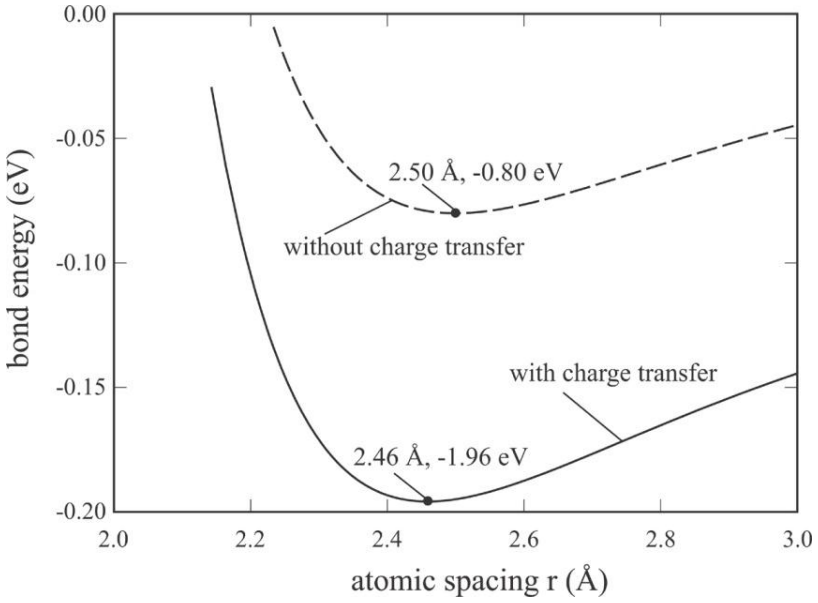

Figure A1. Effects of charge transfer on bond length and bond energy.

APPENDIX B: EIM DATABASE

The Pauling scale of electronegativities [13,47,48] are used for all the elements in this work, and the data are listed in Table B1. The calibrated pair parameters for the binary alkali halide systems are listed in Table B2. A full list of the pair parameters for our EIM database used to explore the quaternary elpasolites is shown in Table B3.

Table B1. Electronegativity of elements.

i	Li	Na	K	Rb	Cs	F	Cl	Br	I
χ_i	0.98	0.93	0.82	0.82	0.79	3.98	3.16	2.96	2.66
i	La	Nd	Eu	Er	Ce	Sc	Y	Gd	
χ_i	1.10	1.14	1.20	1.24	1.12	1.36	1.22	1.20	

Table B2. Calibrated pair parameters for alkali halides. Here pair type = 1 is defined by Eq. (8), and pair type = 2 is defined by Eq. (9).

ij	**LiLi**	**LiNa**	**LiK**	**LiRb**	**LiCs**	**LiF**	**LiCl**
Pair type	1.00000	1.00000	1.00000	1.00000	1.00000	2.00000	2.00000
$E_{b,ij}$ (eV)	-0.25330	-0.21173	-0.19593	-0.18748	-0.18290	-1.26810	-1.17267
$r_{e,ij}$ (Å)	3.61755	3.81071	4.12429	4.29974	3.96874	1.96436	2.39567
$r_{c\phi,ij}$ (Å)	6.04900	6.25500	6.55000	6.68700	6.14600	4.50000	4.50000
α_{ij}	7.55362	7.65018	8.35595	8.82530	9.76019	13.46720	13.11550
β_{ij}	3.50169	3.90660	4.14574	4.13805	5.57665	5.22720	5.00039
$A_{\varphi_{ij}}$ (eV)	0.33271	0.41481	0.31840	0.47482	0.59605	0.69987	1.57173
ζ_{ij}	0.60000	0.60000	0.60000	0.60000	0.60000	0.60000	0.60000
$r_{s\varphi,ij}$ (Å)	2.00000	2.00000	2.00000	2.00000	2.00000	2.00000	2.00000
$r_{c\varphi,ij}$ (Å)	7.06372	7.23908	7.46698	7.56898	7.33505	5.48400	5.97500
$A_{\eta_{ij}}$	0.02178	0.02178	0.02178	0.02178	0.02178	0.02178	0.02178
$r_{s\eta,ij}$ (Å)	2.00000	2.00000	2.00000	2.00000	2.00000	2.00900	2.56600
$r_{c\eta,ij}$ (Å)	0.00000	0.00000	0.00000	0.00000	0.00000	5.43000	6.93600
ij	**LiBr**	**LiId**	**NaNa**	**NaK**	**NaRb**	**NaCs**	**NaF**
Pair type	2.00000	2.00000	1.00000	1.00000	1.00000	1.00000	2.00000
$E_{b,ij}$ (eV)	-0.85748	-0.87986	-0.17698	-0.16377	-0.15671	-0.15288	-1.16205
$r_{e,ij}$ (Å)	2.67275	2.95365	4.00386	4.31745	4.49289	4.16190	2.19744
$r_{c\phi,ij}$ (Å)	4.75800	5.23900	6.46100	6.75600	6.89300	6.35200	4.50000
α_{ij}	14.43590	17.36230	7.74674	8.45251	8.92186	9.85675	11.04890
β_{ij}	9.15927	10.90430	4.31150	4.55065	4.54295	5.98155	4.14238

$A_{\varphi_{ij}}$ (eV)	1.98268	1.96608	0.51719	0.39698	0.59201	0.74315	0.49728
ζ_{ij}	0.60000	0.60000	0.60000	0.60000	0.60000	0.60000	0.60000
$r_{s\varphi,ij}$ (Å)	2.00000	2.00000	2.00000	2.00000	2.00000	2.00000	2.00000
$r_{c\varphi,ij}$ (Å)	6.13500	6.37800	7.41443	7.64234	7.74434	7.51041	5.73100
$A_{\eta_{ij}}$	0.02178	0.02178	0.02178	0.02178	0.02178	0.02178	0.02178
$r_{s\eta,ij}$ (Å)	2.74700	3.02500	2.00000	2.00000	2.00000	2.00000	2.30700
$r_{c\eta,ij}$ (Å)	7.42500	8.17700	0.00000	0.00000	0.00000	0.00000	6.23600
ij	**NaCl**	**NaBr**	**NaI**	**KK**	**KRb**	**KCs**	**KF**
Pair type	2.00000	2.00000	2.00000	1.00000	1.00000	1.00000	2.00000
$E_{b,ij}$ (eV)	-0.89972	-0.80673	-0.72203	-0.15155	-0.14502	-0.14147	-1.07749
$r_{e,ij}$ (Å)	2.66680	2.74222	3.02522	4.63104	4.80648	4.47548	2.58562
$r_{c\phi,ij}$ (Å)	4.87400	5.16300	5.59600	7.05100	7.18800	6.64600	4.61400
α_{ij}	9.46539	8.11784	9.70187	9.15829	9.62763	10.56250	10.22510
β_{ij}	4.95034	3.34598	4.42598	4.78979	4.78210	6.22070	5.40188
$A_{\varphi_{ij}}$ (eV)	0.77787	0.40042	0.59680	0.30471	0.45441	0.57043	1.04099
ζ_{ij}	0.60000	0.60000	0.60000	0.60000	0.60000	0.60000	0.60000
$r_{s\varphi,ij}$ (Å)	2.00000	2.00000	2.00000	2.00000	2.00000	2.00000	2.00000
$r_{c\varphi,ij}$ (Å)	6.22200	6.38200	6.62500	7.87024	7.97224	7.73831	6.05300
$A_{\eta_{ij}}$	0.02178	0.02178	0.02178	0.02178	0.02178	0.02178	0.02178
$r_{s\eta,ij}$ (Å)	2.81400	2.98100	3.23100	2.00000	2.00000	2.00000	2.66400
$r_{c\eta,ij}$ (Å)	7.60600	8.05800	8.73300	0.00000	0.00000	0.00000	7.20100
ij	**KCl**	**KBr**	**KI**	**RbRb**	**RbCs**	**RbF**	**RbCl**
Pair type	2.00000	2.00000	2.00000	1.00000	1.00000	2.00000	2.00000
$E_{b,ij}$ (eV)	-0.81301	-0.67522	-0.60446	-0.13877	-0.13538	-1.08227	-0.78154
$r_{e,ij}$ (Å)	3.09098	3.28783	3.52691	4.98192	4.65093	2.75408	3.25411
$r_{c\phi,ij}$ (Å)	5.43700	5.70300	6.10700	7.32500	6.78400	4.87600	5.69000
α_{ij}	12.57250	17.29350	14.08930	10.09700	11.03190	13.74680	15.32750
β_{ij}	7.07103	10.99570	9.09123	4.77441	6.21300	7.62257	7.54027
$A_{\varphi_{ij}}$ (eV)	0.14487	0.11194	0.30858	0.67765	0.85066	1.68721	0.51848
ζ_{ij}	0.60000	0.60000	0.60000	0.60000	0.60000	0.60000	0.60000
$r_{s\varphi,ij}$ (Å)	2.00000	2.00000	2.00000	2.00000	2.00000	2.00000	2.00000
$r_{c\varphi,ij}$ (Å)	6.54400	6.70400	6.94700	8.07424	7.84031	6.19700	6.68800
$A_{\eta_{ij}}$	0.02178	0.02178	0.02178	0.02178	0.02178	0.02178	0.02178
$r_{s\eta,ij}$ (Å)	3.13900	3.29300	3.52600	2.00000	2.00000	2.81500	3.28500
$r_{c\eta,ij}$ (Å)	8.48500	8.90100	9.53100	0.00000	0.00000	7.60900	8.87900

ij	RbBr	RbI	CsCs	CsF	CsCl	CsBr	CsI
Pair type	2.00000	2.00000	1.00000	2.00000	2.00000	2.00000	2.00000
$E_{b,ij}$ (eV)	-0.64488	-0.53162	-0.13207	-0.98283	-0.58967	-0.55406	-0.53436
$r_{e,ij}$ (Å)	3.42871	3.67205	4.31993	3.00067	3.49584	3.63216	3.83332
$r_{c\phi,ij}$ (Å)	5.94800	6.34400	6.24200	5.20500	5.97500	6.23200	6.62100
α_{ij}	14.88040	15.07420	11.96680	13.85420	11.43370	12.53320	12.40740
β_{ij}	9.54926	9.76271	7.65160	7.78713	6.92530	8.04481	7.93021
$A_{\varphi_{ij}}$ (eV)	0.01377	0.07462	1.06785	0.23092	2.16292	2.19975	2.04456
ζ_{ij}	0.60000	0.60000	0.60000	0.60000	0.60000	0.60000	0.60000
$r_{s\varphi,ij}$ (Å)	2.00000	2.00000	2.00000	2.00000	2.00000	2.00000	2.00000
$r_{c\varphi,ij}$ (Å)	6.84800	7.09100	7.60638	6.36600	6.85700	7.01700	7.26000
$A_{\eta_{ij}}$	0.02178	0.02178	0.02178	0.02178	0.02178	0.02178	0.02178
$r_{s\eta,ij}$ (Å)	3.43400	3.66300	2.00000	3.00500	3.45000	3.59800	3.82300
$r_{c\eta,ij}$ (Å)	9.28200	9.90100	0.00000	8.12300	9.32500	9.72500	10.33400
ij	**FF**	**FCl**	**FBr**	**FI**	**ClCl**	**ClBr**	**ClI**
Pair type	1.00000	1.00000	1.00000	1.00000	1.00000	1.00000	1.00000
$E_{b,ij}$ (eV)	-0.13323	-0.16693	-0.16007	-0.15664	-0.20915	-0.20056	-0.19627
$r_{e,ij}$ (Å)	4.00256	4.37798	4.36421	4.60572	4.75339	4.73962	4.98114
$r_{c\phi,ij}$ (Å)	6.00900	6.28900	6.43800	6.66700	6.56900	6.71800	6.94700
α_{ij}	7.76977	8.04293	8.02241	8.39409	8.31608	8.29557	8.66725
β_{ij}	2.98983	3.29726	4.14812	4.16730	3.60469	4.45555	4.47472
$A_{\varphi_{ij}}$ (eV)	0.10029	0.40767	0.43519	0.38866	1.65712	1.76897	1.57985
ζ_{ij}	0.60000	0.60000	0.60000	0.60000	0.60000	0.60000	0.60000
$r_{s\varphi,ij}$ (Å)	2.00000	2.00000	2.00000	2.00000	2.00000	2.00000	2.00000
$r_{c\varphi,ij}$ (Å)	7.02733	7.28443	7.39415	7.56061	7.54153	7.65125	7.81771
$A_{\eta_{ij}}$	0.02178	0.02178	0.02178	0.02178	0.02178	0.02178	0.02178
$r_{s\eta,ij}$ (Å)	2.00000	2.00000	2.00000	2.00000	2.00000	2.00000	2.00000
$r_{c\eta,ij}$ (Å)	0.00000	0.00000	0.00000	0.00000	0.00000	0.00000	0.00000
ij	**BrBr**	**BrI**	**II**				
Pair type	1.00000	1.00000	1.00000				
$E_{b,ij}$ (eV)	-0.19232	-0.18820	-0.18417				
$r_{e,ij}$ (Å)	4.72585	4.96737	5.20889				
$r_{c\phi,ij}$ (Å)	6.86700	7.09600	7.32500				
α_{ij}	8.27505	8.64673	9.01841				
β_{ij}	5.30641	5.32559	5.34476				
$A_{\varphi_{ij}}$ (eV)	1.88838	1.68649	1.50618				

ζ_{ij}	0.60000	0.60000	0.60000				
$r_{s\varphi,ij}$ (Å)	2.00000	2.00000	2.00000				
$r_{c\varphi,ij}$ (Å)	7.76097	7.92744	8.09390				
$A_{\eta_{ij}}$	0.02178	0.02178	0.02178				
$r_{s\eta,ij}$ (Å)	2.00000	2.00000	2.00000				
$r_{c\eta,ij}$ (Å)	0.00000	0.00000	0.00000				

Table B3. Full list of pair parameters of the EIM database. Here pair type = 1 is defined by Eq. (8), and pair type = 2 is defined by Eq. (9)

ij	**LiLi**	**LiNa**	**LiK**	**LiRb**	**LiCs**	**LiF**	**LiCl**
Pair type	1.00000	1.00000	1.00000	1.00000	1.00000	2.00000	2.00000
$E_{b,ij}$ (eV)	-0.22568	-0.19424	-0.19070	-0.18197	-0.17067	-1.29909	-1.02865
$r_{e,ij}$ (Å)	3.33991	3.62224	4.01203	4.16022	3.79847	1.94355	2.46554
$r_{c\phi,ij}$ (Å)	5.00000	5.52642	6.20241	6.40040	5.88052	3.67917	4.46850
α_{ij}	7.65374	7.82698	8.40184	8.86381	9.86462	13.08814	13.26993
β_{ij}	2.71441	3.42908	3.80790	3.76969	5.35873	5.09341	4.39065
$A_{\varphi_{ij}}$ (eV)	0.60899	0.73755	0.48485	0.68193	0.85507	0.50682	0.88787
ζ_{ij}	0.60000	0.60000	0.60000	0.60000	0.60000	0.60000	0.60000
$r_{s\varphi,ij}$ (Å)	2.00000	2.00000	2.00000	2.00000	2.00000	2.00000	2.00000
$r_{c\varphi,ij}$ (Å)	7.06601	7.23713	7.47406	7.56620	7.66493	5.48034	5.95550
$A_{\eta_{ij}}$	0.00000	0.00000	0.00000	0.00000	0.00000	0.02178	0.02178
$r_{s\eta,ij}$ (Å)	0.00000	0.00000	0.00000	0.00000	0.00000	2.07429	2.54944
$r_{c\eta,ij}$ (Å)	0.00000	0.00000	0.00000	0.00000	0.00000	5.60623	6.89035
ij	**LiBr**	**LiI**	**LiLa**	**LiNd**	**LiEu**	**LiEr**	**LiCe**
Pair type	2.00000	2.00000	1.00000	1.00000	1.00000	1.00000	1.00000
$E_{b,ij}$ (eV)	-0.77459	-0.70061	-0.38189	-0.34761	-0.29013	-0.35583	-0.40230
$r_{e,ij}$ (Å)	2.73180	3.01137	3.57480	3.49717	3.67494	3.44485	3.55031
$r_{c\phi,ij}$ (Å)	4.71516	5.10982	5.50209	5.00000	5.67463	5.00000	5.41498
α_{ij}	14.13194	17.44074	8.83138	9.72503	9.89705	9.02769	8.43415
β_{ij}	6.66671	6.02029	3.67437	3.72083	3.83215	3.10410	2.97156
$A_{\varphi_{ij}}$ (eV)	1.82734	1.29799	0.99459	0.95451	0.46328	0.41731	2.30450
ζ_{ij}	0.60000	0.60000	0.60000	0.60000	0.60000	0.60000	0.60000
$r_{s\varphi,ij}$ (Å)	2.00000	2.00000	2.00000	2.00000	2.00000	2.00000	2.00000
$r_{c\varphi,ij}$ (Å)	6.10399	6.34156	7.24503	7.21278	7.18908	7.15157	7.23055

$A_{\eta_{ij}}$	0.02178	0.02178	0.00000	0.00000	0.00000	0.00000	0.00000
$r_{s\eta,ij}$ (Å)	2.69793	2.93550	0.00000	0.00000	0.00000	0.00000	0.00000
$r_{c\eta,ij}$ (Å)	7.29163	7.93369	0.00000	0.00000	0.00000	0.00000	0.00000
ij	**LiSc**	**LiY**	**LiGd**	**NaNa**	**NaK**	**NaRb**	**NaCs**
Pair type	1.00000	1.00000	1.00000	1.00000	1.00000	1.00000	1.00000
$E_{b,ij}$ (eV)	-0.36785	-0.41817	-0.39446	-0.16717	-0.16413	-0.15661	-0.14689
$r_{e,ij}$ (Å)	3.38998	3.48595	3.49714	3.90458	4.29437	4.44255	4.08080
$r_{c\phi,ij}$ (Å)	5.00000	5.00000	5.00000	6.05283	6.72883	6.92682	6.40694
α_{ij}	6.82519	7.58335	7.39643	8.00021	8.57508	9.03704	10.03786
β_{ij}	2.62893	2.62332	2.58337	4.14375	4.52257	4.48436	6.07340
$A_{\varphi_{ij}}$ (eV)	0.32299	0.37234	1.30450	0.86612	0.61341	0.81049	0.98363
ζ_{ij}	0.60000	0.60000	0.60000	0.60000	0.60000	0.60000	0.60000
$r_{s\varphi,ij}$ (Å)	2.00000	2.00000	2.00000	2.00000	2.00000	2.00000	2.00000
$r_{c\varphi,ij}$ (Å)	7.05614	7.15815	7.18316	7.40825	7.64518	7.73732	7.83605
$A_{\eta_{ij}}$	0.00000	0.00000	0.00000	0.00000	0.00000	0.00000	0.00000
$r_{s\eta,ij}$ (Å)	0.00000	0.00000	0.00000	0.00000	0.00000	0.00000	0.00000
$r_{c\eta,ij}$ (Å)	0.00000	0.00000	0.00000	0.00000	0.00000	0.00000	0.00000
ij	**NaF**	**NaCl**	**NaBr**	**NaI**	**NaLa**	**NaNd**	**NaEu**
Pair type	2.00000	2.00000	2.00000	2.00000	1.00000	1.00000	1.00000
$E_{b,ij}$ (eV)	-1.22615	-0.83062	-0.75755	-0.56633	-0.32868	-0.29917	-0.24970
$r_{e,ij}$ (Å)	2.16372	2.66639	2.84533	3.25102	3.85714	3.77951	3.95727
$r_{c\phi,ij}$ (Å)	4.10672	4.89605	5.14271	5.53737	6.02851	5.52642	6.20104
α_{ij}	10.96328	9.71565	8.23243	9.51851	9.00461	9.89827	10.07028
β_{ij}	3.97859	3.48756	3.04200	3.87627	4.38904	4.43550	4.54682
$A_{\varphi_{ij}}$ (eV)	0.54417	0.43742	0.01424	0.41558	1.12315	1.08307	0.59184
ζ_{ij}	0.60000	0.60000	0.60000	0.60000	0.60000	0.60000	0.60000
$r_{s\varphi,ij}$ (Å)	2.00000	2.00000	2.00000	2.00000	2.00000	2.00000	2.00000
$r_{c\varphi,ij}$ (Å)	5.73772	6.21288	6.36136	6.59894	7.41615	7.38390	7.36020
$A_{\eta_{ij}}$	0.02178	0.02178	0.02178	0.02178	0.00000	0.00000	0.00000
$r_{s\eta,ij}$ (Å)	2.33167	2.80682	2.95530	3.19288	0.00000	0.00000	0.00000
$r_{c\eta,ij}$ (Å)	6.30179	7.58591	7.98720	8.62925	0.00000	0.00000	0.00000
ij	**NaEr**	**NaCe**	**NaSc**	**NaY**	**NaGd**	**KK**	**KRb**
Pair type	1.00000	1.00000	1.00000	1.00000	1.00000	1.00000	1.00000
$E_{b,ij}$ (eV)	-0.30625	-0.34625	-0.31659	-0.35990	-0.33949	-0.16114	-0.15376
$r_{e,ij}$ (Å)	3.72718	3.83264	3.67232	3.76828	3.77947	4.68416	4.83234
$r_{c\phi,ij}$ (Å)	5.52642	5.94139	5.52642	5.52642	5.52642	7.40482	7.60281

α_{ij}	9.20092	8.60738	6.99842	7.75658	7.56966	9.14994	9.61191
β_{ij}	3.81877	3.68623	3.34360	3.33799	3.29804	4.90138	4.86317
$A_{\varphi_{ij}}$ (eV)	0.54587	2.43306	0.45156	0.50090	1.43306	0.36071	0.55779
ζ_{ij}	0.60000	0.60000	0.60000	0.60000	0.60000	0.60000	0.60000
$r_{s\varphi,ij}$ (Å)	2.00000	2.00000	2.00000	2.00000	2.00000	2.00000	2.00000
$r_{c\varphi,ij}$ (Å)	7.32269	7.40167	7.22726	7.32927	7.35428	7.88212	7.97426
$A_{\eta_{ij}}$	0.00000	0.00000	0.00000	0.00000	0.00000	0.00000	0.00000
$r_{s\eta,ij}$ (Å)	0.00000	0.00000	0.00000	0.00000	0.00000	0.00000	0.00000
$r_{c\eta,ij}$ (Å)	0.00000	0.00000	0.00000	0.00000	0.00000	0.00000	0.00000
ij	**KCs**	**KF**	**KCl**	**KBr**	**KI**	**KLa**	**KNd**
Pair type	1.00000	2.00000	2.00000	2.00000	2.00000	1.00000	1.00000
$E_{b,ij}$ (eV)	-0.14421	-1.18602	-0.79374	-0.67713	-0.55624	-0.32269	-0.29372
$r_{e,ij}$ (Å)	4.47059	2.52982	3.10617	3.28848	3.56701	4.24693	4.16930
$r_{c\phi,ij}$ (Å)	7.08293	4.69872	5.48804	5.73470	6.12937	6.70450	6.20241
α_{ij}	10.61272	10.23802	12.44912	17.29416	14.20623	9.57948	10.47313
β_{ij}	6.45221	5.31658	7.47901	10.73015	6.81739	4.76786	4.81431
$A_{\varphi_{ij}}$ (eV)	0.73093	1.01171	0.12779	0.03602	0.49396	0.87045	0.83037
ζ_{ij}	0.60000	0.60000	0.60000	0.60000	0.60000	0.60000	0.60000
$r_{s\varphi,ij}$ (Å)	2.00000	2.00000	2.00000	2.00000	2.00000	2.00000	2.00000
$r_{c\varphi,ij}$ (Å)	8.07298	6.09409	6.56924	6.71773	6.95531	7.65308	7.62083
$A_{\eta_{ij}}$	0.00000	0.02178	0.02178	0.02178	0.02178	0.00000	0.00000
$r_{s\eta,ij}$ (Å)	0.00000	2.68803	3.16318	3.31167	3.54924	0.00000	0.00000
$r_{c\eta,ij}$ (Å)	0.00000	7.26488	8.54900	8.95028	9.59234	0.00000	0.00000
ij	**KEu**	**KEr**	**KCe**	**KSc**	**KY**	**KGd**	**RbRb**
Pair type	1.00000	1.00000	1.00000	1.00000	1.00000	1.00000	1.00000
$E_{b,ij}$ (eV)	-0.24516	-0.30067	-0.33994	-0.31083	-0.35334	-0.33331	-0.14672
$r_{e,ij}$ (Å)	4.34706	4.11697	4.22243	4.06211	4.15807	4.16926	4.98052
$r_{c\phi,ij}$ (Å)	6.87704	6.20241	6.61739	6.20241	6.20241	6.20241	7.80080
α_{ij}	10.64515	9.77579	9.18225	7.57329	8.33145	8.14453	10.07387
β_{ij}	4.92563	4.19758	4.06504	3.72242	3.71680	3.67685	4.82496
$A_{\varphi_{ij}}$ (eV)	0.33914	0.29317	2.18036	0.19885	0.24820	1.18036	0.75486
ζ_{ij}	0.60000	0.60000	0.60000	0.60000	0.60000	0.60000	0.60000
$r_{s\varphi,ij}$ (Å)	2.00000	2.00000	2.00000	2.00000	2.00000	2.00000	2.00000
$r_{c\varphi,ij}$ (Å)	7.59714	7.55962	7.63860	7.46419	7.56620	7.59121	8.06640
$A_{\eta_{ij}}$	0.00000	0.00000	0.00000	0.00000	0.00000	0.00000	0.00000

$r_{sη,ij}$ (Å)	0.00000	0.00000	0.00000	0.00000	0.00000	0.00000	0.00000
$r_{cη,ij}$ (Å)	0.00000	0.00000	0.00000	0.00000	0.00000	0.00000	0.00000
ij	**RbCs**	**RbF**	**RbCl**	**RbBr**	**RbI**	**RbLa**	**RbNd**
Pair type	1.00000	2.00000	2.00000	2.00000	2.00000	1.00000	1.00000
$E_{b,ij}$ (eV)	-0.13761	-1.13027	-0.79910	-0.63953	-0.52070	-0.30792	-0.28027
$r_{e,ij}$ (Å)	4.61877	2.75127	3.26805	3.43444	3.68800	4.39511	4.31748
$r_{cϕ,ij}$ (Å)	7.28092	4.92894	5.71826	5.96492	6.35959	6.90249	6.40040
α_{ij}	11.07469	13.54158	15.23589	15.08755	15.25155	10.04144	10.93510
β_{ij}	6.41400	8.57137	9.03745	8.88035	9.25572	4.72965	4.77611
$A_{\varphi_{ij}}$ (eV)	0.92800	1.69416	0.49653	0.04784	0.12296	1.06752	1.02744
ζ_{ij}	0.60000	0.60000	0.60000	0.60000	0.60000	0.60000	0.60000
$r_{sφ,ij}$ (Å)	2.00000	2.00000	2.00000	2.00000	2.00000	2.00000	2.00000
$r_{cφ,ij}$ (Å)	8.16512	6.23267	6.70783	6.85632	7.09389	7.74522	7.71297
$A_{\eta_{ij}}$	0.00000	0.02178	0.02178	0.02178	0.02178	0.00000	0.00000
$r_{sη,ij}$ (Å)	0.00000	2.82661	3.30177	3.45025	3.68783	0.00000	0.00000
$r_{cη,ij}$ (Å)	0.00000	7.63941	8.92353	9.32482	9.96688	0.00000	0.00000
ij	**RbEu**	**RbEr**	**RbCe**	**RbSc**	**RbY**	**RbGd**	**CsCs**
Pair type	1.00000	1.00000	1.00000	1.00000	1.00000	1.00000	1.00000
$E_{b,ij}$ (eV)	-0.23393	-0.28691	-0.32438	-0.29659	-0.33716	-0.31805	-0.12906
$r_{e,ij}$ (Å)	4.49525	4.26515	4.37062	4.21029	4.30625	4.31744	4.25702
$r_{cϕ,ij}$ (Å)	7.07503	6.40040	6.81538	6.40040	6.40040	6.40040	6.76104
α_{ij}	11.10711	10.23775	9.64423	8.03527	8.79343	8.60651	12.07550
β_{ij}	4.88743	4.15937	4.02683	3.68421	3.67859	3.63864	8.00304
$A_{\varphi_{ij}}$ (eV)	0.53622	0.49025	2.37743	0.39593	0.44528	1.37743	1.10115
ζ_{ij}	0.60000	0.60000	0.60000	0.60000	0.60000	0.60000	0.60000
$r_{sφ,ij}$ (Å)	2.00000	2.00000	2.00000	2.00000	2.00000	2.00000	2.00000
$r_{cφ,ij}$ (Å)	7.68928	7.65176	7.73074	7.55633	7.65835	7.68335	8.26384
$A_{\eta_{ij}}$	0.00000	0.00000	0.00000	0.00000	0.00000	0.00000	0.00000
$r_{sη,ij}$ (Å)	0.00000	0.00000	0.00000	0.00000	0.00000	0.00000	0.00000
$r_{cη,ij}$ (Å)	0.00000	0.00000	0.00000	0.00000	0.00000	0.00000	0.00000
ij	**CsF**	**CsCl**	**CsBr**	**CsI**	**CsLa**	**CsNd**	**CsEu**
Pair type	2.00000	2.00000	2.00000	2.00000	1.00000	1.00000	1.00000
$E_{b,ij}$ (eV)	-1.05839	-0.57190	-0.55477	-0.49501	-0.28880	-0.26287	-0.21940
$r_{e,ij}$ (Å)	2.99795	3.50124	3.65497	3.88950	4.03336	3.95573	4.13349
$r_{cϕ,ij}$ (Å)	5.17560	5.96492	6.21159	6.60625	6.38261	5.88052	6.55515
α_{ij}	14.25017	11.48304	12.51291	12.36723	11.04226	11.93591	12.10793

β_{ij}	7.53482	6.67861	6.76394	7.17185	6.31869	6.36514	6.47646
$A_{\varphi_{ij}}$ (eV)	0.07802	2.10294	2.23552	2.24715	1.24066	1.20058	0.70936
ζ_{ij}	0.60000	0.60000	0.60000	0.60000	0.60000	0.60000	0.60000
$r_{s\varphi,ij}$ (Å)	2.00000	2.00000	2.00000	2.00000	2.00000	2.00000	2.00000
$r_{c\varphi,ij}$ (Å)	6.38116	6.85632	7.00480	7.24238	7.84394	7.81169	7.78800
$A_{\eta_{ij}}$	0.02178	0.02178	0.02178	0.02178	0.00000	0.00000	0.00000
$r_{s\eta,ij}$ (Å)	2.97510	3.45025	3.59874	3.83631	0.00000	0.00000	0.00000
$r_{c\eta,ij}$ (Å)	8.04070	9.32482	9.72610	10.36816	0.00000	0.00000	0.00000
ij	**CsEr**	**CsCe**	**CsSc**	**CsY**	**CsGd**	**FF**	**FCl**
Pair type	1.00000	1.00000	1.00000	1.00000	1.00000	1.00000	1.00000
$E_{b,ij}$ (eV)	-0.26909	-0.30423	-0.27817	-0.31623	-0.29830	-0.14440	-0.16652
$r_{e,ij}$ (Å)	3.90340	4.00887	3.84854	3.94450	3.95569	3.75912	4.16180
$r_{c\phi,ij}$ (Å)	5.88052	6.29550	5.88052	5.88052	5.88052	5.77417	6.42239
α_{ij}	11.23857	10.64503	9.03607	9.79423	9.60731	7.68291	7.94444
β_{ij}	5.74841	5.61587	5.27325	5.26763	5.22768	2.88331	3.13414
$A_{\varphi_{ij}}$ (eV)	0.66339	2.55058	0.56907	0.61842	1.55058	0.53589	1.24877
ζ_{ij}	0.60000	0.60000	0.60000	0.60000	0.60000	0.60000	0.60000
$r_{s\varphi,ij}$ (Å)	2.00000	2.00000	2.00000	2.00000	2.00000	2.00000	2.00000
$r_{c\varphi,ij}$ (Å)	7.75049	7.82946	7.65505	7.75707	7.78208	7.00412	7.29591
$A_{\eta_{ij}}$	0.00000	0.00000	0.00000	0.00000	0.00000	0.00000	0.00000
$r_{s\eta,ij}$ (Å)	0.00000	0.00000	0.00000	0.00000	0.00000	0.00000	0.00000
$r_{c\eta,ij}$ (Å)	0.00000	0.00000	0.00000	0.00000	0.00000	0.00000	0.00000
ij	**FBr**	**FI**	**FLa**	**FNd**	**FEu**	**FEr**	**FCe**
Pair type	1.00000	1.00000	2.00000	2.00000	2.00000	2.00000	2.00000
$E_{b,ij}$ (eV)	-0.16199	-0.14496	-2.21684	-2.04324	-1.82849	-2.18880	-2.23805
$r_{e,ij}$ (Å)	4.15023	4.30576	2.48880	2.46653	2.32799	2.33128	2.38356
$r_{c\phi,ij}$ (Å)	6.42323	6.72553	4.12646	4.04588	3.98668	3.89295	4.09028
α_{ij}	7.92274	8.36150	11.87585	11.45115	10.94877	11.30788	8.21292
β_{ij}	3.71302	3.90441	3.92613	3.79027	4.03202	3.74026	3.35348
$A_{\varphi_{ij}}$ (eV)	1.47934	1.09475	0.03669	1.15280	0.93682	0.31388	0.08753
ζ_{ij}	0.60000	0.60000	0.60000	0.60000	0.60000	0.60000	0.60000
$r_{s\varphi,ij}$ (Å)	2.00000	2.00000	2.00000	2.00000	2.00000	2.00000	2.00000
$r_{c\varphi,ij}$ (Å)	7.38709	7.53299	5.74960	5.70109	5.66546	5.60903	5.72782
$A_{\eta_{ij}}$	0.00000	0.00000	0.02178	0.02178	0.02178	0.02178	0.02178
$r_{s\eta,ij}$ (Å)	0.00000	0.00000	2.34354	2.29504	2.25940	2.20298	2.32177

$r_{c\eta,ij}$ (Å)	0.00000	0.00000	6.33390	6.20281	6.10650	5.95401	6.27504
ij	**FSc**	**FY**	**FGd**	**ClCl**	**ClBr**	**ClI**	**ClLa**
Pair type	2.00000	2.00000	2.00000	1.00000	1.00000	1.00000	2.00000
$E_{b,ij}$ (eV)	-2.60387	-3.20441	-2.21534	-0.19335	-0.18885	-0.16932	-2.17930
$r_{e,ij}$ (Å)	2.09584	2.24282	2.31540	4.56088	4.54724	4.71360	2.83295
$r_{c\phi,ij}$ (Å)	3.65451	3.90939	3.97188	7.07062	7.07146	7.37376	4.91578
α_{ij}	8.13162	8.89973	8.00000	8.21541	8.20174	8.62917	11.04560
β_{ij}	3.72333	4.14193	3.20000	3.42749	3.99738	4.19818	4.09655
$A_{\varphi_{ij}}$ (eV)	3.95415	3.57369	0.01000	1.94402	2.18847	1.79845	1.45423
ζ_{ij}	0.60000	0.60000	0.60000	0.60000	0.60000	0.60000	0.60000
$r_{s\varphi,ij}$ (Å)	2.00000	2.00000	2.00000	2.00000	2.00000	2.00000	2.00000
$r_{c\varphi,ij}$ (Å)	5.46550	5.61893	5.65655	7.58770	7.67888	7.82477	6.22475
$A_{\eta_{ij}}$	0.02178	0.02178	0.02178	0.00000	0.00000	0.00000	0.02178
$r_{s\eta,ij}$ (Å)	2.05944	2.21288	2.25049	0.00000	0.00000	0.00000	2.81870
$r_{c\eta,ij}$ (Å)	5.56610	5.98076	6.08242	0.00000	0.00000	0.00000	7.61801
ij	**ClNd**	**ClEu**	**ClEr**	**ClCe**	**ClSc**	**ClY**	**ClGd**
Pair type	2.00000	2.00000	2.00000	2.00000	2.00000	2.00000	2.00000
$E_{b,ij}$ (eV)	-2.19743	-1.87233	-2.30202	-2.25657	-2.66172	-2.61454	-2.12192
$r_{e,ij}$ (Å)	2.74611	2.70231	2.63391	2.74474	2.46351	2.54501	2.73626
$r_{c\phi,ij}$ (Å)	4.83520	4.77600	4.68227	4.87960	4.44383	4.69872	4.76121
α_{ij}	12.54440	12.78480	12.97720	9.34702	13.26486	8.59787	9.77758
β_{ij}	4.31551	5.52775	4.70280	3.42891	5.30594	3.55645	4.64053
$A_{\varphi_{ij}}$ (eV)	2.16651	1.95677	3.38116	0.02474	5.34024	4.91674	4.76557
ζ_{ij}	0.60000	0.60000	0.60000	0.60000	0.60000	0.60000	0.60000
$r_{s\varphi,ij}$ (Å)	2.00000	2.00000	2.00000	2.00000	2.00000	2.00000	2.00000
$r_{c\varphi,ij}$ (Å)	6.17625	6.14061	6.08419	6.20298	5.94065	6.09409	6.13170
$A_{\eta_{ij}}$	0.02178	0.02178	0.02178	0.02178	0.02178	0.02178	0.02178
$r_{s\eta,ij}$ (Å)	2.77019	2.73455	2.67813	2.79692	2.53459	2.68803	2.72565
$r_{c\eta,ij}$ (Å)	7.48693	7.39062	7.23813	7.55916	6.85022	7.26488	7.36654
ij	**BrBr**	**BrI**	**BrLa**	**BrNd**	**BrEu**	**BrEr**	**BrCe**
Pair type	1.00000	1.00000	2.00000	2.00000	2.00000	2.00000	2.00000
$E_{b,ij}$ (eV)	-0.18446	-0.16538	-2.08647	-1.96464	-1.62436	-2.08211	-1.94065
$r_{e,ij}$ (Å)	4.53360	4.69996	2.91134	2.87565	2.81725	2.76710	2.84094
$r_{c\phi,ij}$ (Å)	7.07230	7.37460	5.16244	5.08187	5.02267	4.92894	5.12627
α_{ij}	8.18807	8.61550	10.44890	11.50618	12.01921	12.74972	8.52091
β_{ij}	4.56727	4.76808	3.54378	5.27378	6.61730	6.60393	3.48076

$A_{\varphi_{ij}}$ (eV)	2.43293	2.04291	2.29208	3.89024	4.35277	3.98881	4.58273
ζ_{ij}	0.60000	0.60000	0.60000	0.60000	0.60000	0.60000	0.60000
$r_{s\varphi,ij}$ (Å)	2.00000	2.00000	2.00000	2.00000	2.00000	2.00000	2.00000
$r_{c\varphi,ij}$ (Å)	7.77006	7.91595	6.37324	6.32474	6.28910	6.23267	6.35146
$A_{\eta_{ij}}$	0.00000	0.00000	0.02178	0.02178	0.02178	0.02178	0.02178
$r_{s\eta,ij}$ (Å)	0.00000	0.00000	2.96718	2.91868	2.88304	2.82662	2.94540
$r_{c\eta,ij}$ (Å)	0.00000	0.00000	8.01930	7.88821	7.79190	7.63941	7.96044
ij	**BrSc**	**BrY**	**BrGd**	**II**	**ILa**	**INd**	**IEu**
Pair type	2.00000	2.00000	2.00000	1.00000	2.00000	2.00000	2.00000
$E_{b,ij}$ (eV)	-2.34252	-2.91820	-2.19374	-0.14828	-1.92645	-1.96509	-1.44843
$r_{e,ij}$ (Å)	2.50856	2.73906	2.78250	4.86632	3.11594	3.01490	2.95305
$r_{c\phi,ij}$ (Å)	4.69049	4.94538	5.00787	7.67689	5.55711	5.47653	5.41733
α_{ij}	13.31513	10.87897	11.81128	9.04293	12.73027	10.46500	12.80858
β_{ij}	5.88250	4.92211	4.28981	4.96888	4.69477	3.92326	7.45812
$A_{\varphi_{ij}}$ (eV)	5.60000	5.50000	4.27640	1.65289	5.03117	4.40543	5.11446
ζ_{ij}	0.60000	0.60000	0.60000	0.60000	0.60000	0.60000	0.60000
$r_{s\varphi,ij}$ (Å)	2.00000	2.00000	2.00000	2.00000	2.00000	2.00000	2.00000
$r_{c\varphi,ij}$ (Å)	6.08914	6.24257	6.28019	8.06185	6.61082	6.56231	6.52668
$A_{\eta_{ij}}$	0.02178	0.02178	0.02178	0.00000	0.02178	0.02178	0.02178
$r_{s\eta,ij}$ (Å)	2.68308	2.83651	2.87413	0.00000	3.20476	3.15625	3.12062
$r_{c\eta,ij}$ (Å)	7.25150	7.66617	7.76783	0.00000	8.66136	8.53027	8.43396
ij	**IEr**	**ICe**	**ISc**	**IY**	**IGd**	**LaLa**	**LaNd**
Pair type	2.00000	2.00000	2.00000	2.00000	2.00000	1.00000	1.00000
$E_{b,ij}$ (eV)	-2.43479	-1.86077	-2.14356	-1.96886	-1.78296	-0.64623	-0.58821
$r_{e,ij}$ (Å)	2.90794	3.13773	2.72848	2.98428	2.99455	3.80969	3.73206
$r_{c\phi,ij}$ (Å)	5.32360	5.52093	5.08516	5.34004	5.40253	6.00419	5.50209
α_{ij}	12.42147	12.87257	12.94894	7.18876	11.43193	10.00901	10.90267
β_{ij}	6.17047	6.33885	6.61313	6.66496	4.47275	4.63433	4.68079
$A_{\varphi_{ij}}$ (eV)	5.00081	1.61849	3.67926	5.44885	3.39806	1.38018	1.34010
ζ_{ij}	0.60000	0.60000	0.60000	0.60000	0.60000	0.60000	0.60000
$r_{s\varphi,ij}$ (Å)	2.00000	2.00000	2.00000	2.00000	2.00000	2.00000	2.00000
$r_{c\varphi,ij}$ (Å)	6.47025	6.58904	6.32672	6.48015	6.51777	7.42404	7.39179
$A_{\eta_{ij}}$	0.02178	0.02178	0.02178	0.02178	0.02178	0.00000	0.00000
$r_{s\eta,ij}$ (Å)	3.06419	3.18298	2.92066	3.07409	3.11171	0.00000	0.00000
$r_{c\eta,ij}$ (Å)	8.28147	8.60250	7.89356	8.30823	8.40988	0.00000	0.00000

ij	LaEu	LaEr	LaCe	LaSc	LaY	LaGd	NdNd
Pair type	1.00000	1.00000	1.00000	1.00000	1.00000	1.00000	1.00000
$E_{b,ij}$ (eV)	-0.49095	-0.60213	-0.68076	-0.62246	-0.70760	-0.66748	-0.53540
$r_{e,ij}$ (Å)	3.90983	3.67974	3.78520	3.62487	3.72084	3.73203	3.65443
$r_{c\phi,ij}$ (Å)	6.17672	5.50209	5.91707	5.50209	5.50209	5.50209	5.00000
α_{ij}	11.07468	10.20532	9.61178	8.00282	8.76098	8.57406	11.79632
β_{ij}	4.79211	4.06406	3.93152	3.58889	3.58328	3.54333	4.72725
$A_{\varphi_{ij}}$ (eV)	0.84888	0.80291	2.69009	0.70859	0.75794	1.69009	1.30002
ζ_{ij}	0.60000	0.60000	0.60000	0.60000	0.60000	0.60000	0.60000
$r_{s\varphi,ij}$ (Å)	2.00000	2.00000	2.00000	2.00000	2.00000	2.00000	2.00000
$r_{c\varphi,ij}$ (Å)	7.36810	7.33059	7.40956	7.23515	7.33717	7.36218	7.35954
$A_{\eta_{ij}}$	0.00000	0.00000	0.00000	0.00000	0.00000	0.00000	0.00000
$r_{s\eta,ij}$ (Å)	0.00000	0.00000	0.00000	0.00000	0.00000	0.00000	0.00000
$r_{c\eta,ij}$ (Å)	0.00000	0.00000	0.00000	0.00000	0.00000	0.00000	0.00000
ij	**NdEu**	**NdEr**	**NdCe**	**NdSc**	**NdY**	**NdGd**	**EuEu**
Pair type	1.00000	1.00000	1.00000	1.00000	1.00000	1.00000	1.00000
$E_{b,ij}$ (eV)	-0.44687	-0.54807	-0.61965	-0.56657	-0.64408	-0.60756	-0.37298
$r_{e,ij}$ (Å)	3.83220	3.60211	3.70757	3.54724	3.64321	3.65440	4.00997
$r_{c\phi,ij}$ (Å)	5.67463	5.00000	5.41498	5.00000	5.00000	5.00000	6.34925
α_{ij}	11.96834	11.09898	10.50543	8.89647	9.65463	9.46771	12.14035
β_{ij}	4.83857	4.11051	3.97798	3.63535	3.62974	3.58979	4.94989
$A_{\varphi_{ij}}$ (eV)	0.80880	0.76283	2.65001	0.66851	0.71786	1.65001	0.31757
ζ_{ij}	0.60000	0.60000	0.60000	0.60000	0.60000	0.60000	0.60000
$r_{s\varphi,ij}$ (Å)	2.00000	2.00000	2.00000	2.00000	2.00000	2.00000	2.00000
$r_{c\varphi,ij}$ (Å)	7.33585	7.29834	7.37731	7.20291	7.30492	7.32993	7.31216
$A_{\eta_{ij}}$	0.00000	0.00000	0.00000	0.00000	0.00000	0.00000	0.00000
$r_{s\eta,ij}$ (Å)	0.00000	0.00000	0.00000	0.00000	0.00000	0.00000	0.00000
$r_{c\eta,ij}$ (Å)	0.00000	0.00000	0.00000	0.00000	0.00000	0.00000	0.00000
ij	**EuEr**	**EuCe**	**EuSc**	**EuY**	**EuGd**	**ErEr**	**ErCe**
Pair type	1.00000	1.00000	1.00000	1.00000	1.00000	1.00000	1.00000
$E_{b,ij}$ (eV)	-0.45745	-0.51719	-0.47289	-0.53758	-0.50710	-0.56104	-0.63431
$r_{e,ij}$ (Å)	3.77988	3.88534	3.72501	3.82098	3.83217	3.54979	3.65525
$r_{c\phi,ij}$ (Å)	5.67463	6.08960	5.67463	5.67463	5.67463	5.00000	5.41498
α_{ij}	11.27099	10.67743	9.06847	9.82663	9.63971	10.40163	9.80808
β_{ij}	4.22183	4.08930	3.74667	3.74106	3.70111	3.49378	3.36124
$A_{\varphi_{ij}}$ (eV)	0.27160	2.15879	0.17728	0.22663	1.15879	0.22563	2.11281

ζ_{ij}	0.60000	0.60000	0.60000	0.60000	0.60000	0.60000	0.60000
$r_{s\varphi,ij}$ (Å)	2.00000	2.00000	2.00000	2.00000	2.00000	2.00000	2.00000
$r_{c\varphi,ij}$ (Å)	7.27464	7.35362	7.17921	7.28123	7.30623	7.23713	7.31611
$A_{\eta_{ij}}$	0.00000	0.00000	0.00000	0.00000	0.00000	0.00000	0.00000
$r_{s\eta,ij}$ (Å)	0.00000	0.00000	0.00000	0.00000	0.00000	0.00000	0.00000
$r_{c\eta,ij}$ (Å)	0.00000	0.00000	0.00000	0.00000	0.00000	0.00000	0.00000
ij	**ErSc**	**ErY**	**ErGd**	**CeCe**	**CeSc**	**CeY**	**CeGd**
Pair type	1.00000	1.00000	1.00000	1.00000	1.00000	1.00000	1.00000
$E_{b,ij}$ (eV)	-0.57998	-0.65932	-0.62194	-0.71715	-0.65573	-0.74542	-0.70316
$r_{e,ij}$ (Å)	3.49492	3.59089	3.60208	3.76071	3.60038	3.69635	3.70754
$r_{c\phi,ij}$ (Å)	5.00000	5.00000	5.00000	5.82995	5.41498	5.41498	5.41498
α_{ij}	8.19912	8.95728	8.77036	9.21455	7.60559	8.36375	8.17683
β_{ij}	3.01862	3.01300	2.97305	3.22870	2.88608	2.88046	2.84051
$A_{\varphi_{ij}}$ (eV)	0.13131	0.18066	1.11281	4.00000	2.01850	2.06785	3.00000
ζ_{ij}	0.60000	0.60000	0.60000	0.60000	0.60000	0.60000	0.60000
$r_{s\varphi,ij}$ (Å)	2.00000	2.00000	2.00000	2.00000	2.00000	2.00000	2.00000
$r_{c\varphi,ij}$ (Å)	7.14170	7.24371	7.26872	7.39509	7.22068	7.32269	7.34770
$A_{\eta_{ij}}$	0.00000	0.00000	0.00000	0.00000	0.00000	0.00000	0.00000
$r_{s\eta,ij}$ (Å)	0.00000	0.00000	0.00000	0.00000	0.00000	0.00000	0.00000
$r_{c\eta,ij}$ (Å)	0.00000	0.00000	0.00000	0.00000	0.00000	0.00000	0.00000
ij	**ScSc**	**ScY**	**ScGd**	**YY**	**YGd**	**GdGd**	
Pair type	1.00000	1.00000	1.00000	1.00000	1.00000	1.00000	
$E_{b,ij}$ (eV)	-0.59956	-0.68158	-0.64293	-0.77481	-0.73088	-0.68944	
$r_{e,ij}$ (Å)	3.44005	3.53602	3.54721	3.63198	3.64317	3.65437	
$r_{c\phi,ij}$ (Å)	5.00000	5.00000	5.00000	5.00000	5.00000	5.00000	
α_{ij}	5.99663	6.75479	6.56787	7.51296	7.32603	7.13911	
β_{ij}	2.54346	2.53784	2.49789	2.53222	2.49227	2.45233	
$A_{\varphi_{ij}}$ (eV)	0.03699	0.08634	1.01850	0.13569	1.06785	2.00000	
ζ_{ij}	0.60000	0.60000	0.60000	0.60000	0.60000	0.60000	
$r_{s\varphi,ij}$ (Å)	2.00000	2.00000	2.00000	2.00000	2.00000	2.00000	
$r_{c\varphi,ij}$ (Å)	7.04627	7.14828	7.17329	7.25029	7.27530	7.30031	
$A_{\eta_{ij}}$	0.00000	0.00000	0.00000	0.00000	0.00000	0.00000	
$r_{s\eta,ij}$ (Å)	0.00000	0.00000	0.00000	0.00000	0.00000	0.00000	
$r_{c\eta,ij}$ (Å)	0.00000	0.00000	0.00000	0.00000	0.00000	0.00000	

APPENDIX C: STRUCTURAL FACTORS FOR ALL 640 COMPOUNDS

The structural factors calculated for all 640 compounds are listed in Table C1 in decreasing order of relative energy difference.

Table C1. Relative energy difference ΔE_0, minimum energy structure S_{min}, maximum energy structure S_{max}, tolerance factors t'_B, $t'_{B'}$, t', average normal distortion ε, standard deviation of halogen atoms δ, total shear distortion γ, and atomic volume Ω for all 640 compounds.t'_B t'_B.

Compound	ΔE_0 (eV)	S_{min}	S_{max}	t'_B	$t'_{B'}$	t'	ε	δ (Å)	γ	Ω (Å^3)
Li_2RbYF_6	3.991	$a^-b^0c^-$	$a^0a^0a^0$	0.500	0.613	0.550	0.00000	0.23480	0.00000	23.32955
Li_2RbScF_6	3.663	$a^0b^+c^-$	$a^0a^0a^0$	0.500	0.656	0.567	0.00000	0.29585	0.00000	21.62573
Li_2KYF_6	3.482	$a^+b^-b^-$	$a^0a^0a^0$	0.543	0.613	0.576	0.00000	0.10637	0.00000	19.59743
Li_2NaYF_6	3.176	$a^-a^-c^-$	$a^0a^0a^0$	0.635	0.613	0.624	0.00001	0.04472	0.00000	15.37272
Li_2KScF_6	2.972	$a^-b^0c^-$	$a^0a^0a^0$	0.543	0.656	0.594	0.00000	0.17073	0.00000	17.94455
Li_2RbEuF_6	2.694	$a^-a^-a^-$	$a^0a^0a^0$	0.500	0.590	0.541	0.00000	0.20042	0.00000	24.88859
Li_2KErF_6	2.608	$a^-a^-c^-$	$a^0a^0a^0$	0.543	0.590	0.565	0.00000	0.07699	0.00000	21.08557
Li_2RbErF_6	2.602	$a^+a^+c^-$	$a^0a^0a^0$	0.500	0.590	0.541	0.00000	0.19671	0.00000	24.84432
Li_2RbLaF_6	2.587	$a^0b^+b^+$	$a^0a^0a^0$	0.500	0.552	0.525	0.00000	0.12667	0.00000	27.17940
Na_2RbScF_6	2.515	$a^-b^0c^-$	$a^0a^0a^0$	0.556	0.730	0.631	0.00002	0.29509	0.00000	21.04390
Na_2KYF_6	2.467	$a^-b^0c^-$	$a^0a^0a^0$	0.605	0.682	0.641	0.00000	0.10092	0.00000	18.93849
Li_2KGdF_6	2.460	$a^-a^-a^-$	$a^0a^0a^0$	0.543	0.594	0.567	0.00000	0.09007	0.00000	20.63405
Li_2NaScF_6	2.448	$a^-a^-c^-$	$a^0a^0a^0$	0.635	0.656	0.645	0.27271	5.24162	0.95234	25.03248
Li_2RbGdF_6	2.444	$a^0b^+b^+$	$a^0a^0a^0$	0.500	0.594	0.542	0.00001	0.21116	0.00003	24.29859
Na_2RbYF_6	2.434	$a^+a^+c^-$	$a^0a^0a^0$	0.556	0.682	0.613	0.00000	0.23339	0.00000	22.91073
Li_2KCeF_6	2.369	$a^-a^-a^-$	$a^0a^0a^0$	0.543	0.577	0.559	0.00000	0.06361	0.00000	21.84211
Li_2KEuF_6	2.344	$a^-b^+c^-$	$a^0a^0a^0$	0.543	0.590	0.566	0.00000	0.08139	0.00000	21.31915
Na_2LiYF_6	2.279	$a^-a^-c^-$	$BaNiO_3$	0.787	0.682	0.731	0.00001	0.12007	0.00000	12.89693
Li_2RbCeF_6	2.251	$a^+a^+c^-$	$a^0a^0a^0$	0.500	0.577	0.535	0.00000	0.18256	0.00000	25.38000
Li_2KNdF_6	2.234	$a^-a^-a^-$	$a^0a^0a^0$	0.543	0.557	0.550	0.00000	0.02063	0.00000	22.80706
Li_2NaNdF_6	2.218	$a^+b^-b^-$	$a^0a^0a^0$	0.635	0.557	0.594	0.00000	0.12820	0.00000	18.38542
Li_2NaLaF_6	2.218	$a^-a^-a^-$	$a^0a^0a^0$	0.635	0.552	0.591	0.00000	0.13894	0.00000	19.12265
Na_2RbNdF_6	2.203	$a^+b^-b^-$	$a^0a^0a^0$	0.556	0.620	0.586	0.00000	0.14044	0.00000	26.20992
K_2CsYF_6	2.200	$a^-b^0a^-$	$BaNiO_3$	0.597	0.798	0.683	0.28219	6.64429	0.98405	46.09629
Li_2CsEuF_6	2.173	$a^+a^+c^-$	$a^0a^0a^0$	0.458	0.590	0.516	0.00000	0.31348	0.00000	29.00693
Na_2CsCeF_6	2.070	$a^+b^-b^-$	$a^0a^0a^0$	0.510	0.642	0.569	0.01030	0.35946	0.02553	30.01950
Na_2KScF_6	2.068	$a^-a^-c^-$	$a^0a^0a^0$	0.605	0.730	0.662	0.00009	0.16666	0.00024	17.13635
Li_2KLaF_6	2.041	$a^-a^-a^-$	$a^0a^0a^0$	0.543	0.552	0.548	0.00000	0.00792	0.00000	23.40849
Li_2NaErF_6	1.998	$a^+b^-b^-$	$a^0a^0a^0$	0.635	0.590	0.611	0.00000	0.07201	0.00000	16.82693
Na_2KNdF_6	1.927	$a^-a^-a^-$	$a^0a^0a^0$	0.605	0.620	0.612	0.00000	0.01711	0.00000	21.99293
Na_2CsEuF_6	1.918	$a^+b^-b^-$	$a^0a^0a^0$	0.510	0.657	0.575	0.00000	0.31342	0.00000	28.58765

Compound	ΔE_0 (eV)	S_{min}	S_{max}	t'_B	$t'_{B'}$	t'	ε	δ (Å)	γ	Ω (Å^3)
Na_2CsLaF_6	1.907	$a^+b^-b^-$	$a^0a^0a^0$	0.510	0.615	0.558	0.46617	10.77518	1.58158	60.09678
Na_2RbLaF_6	1.898	$a^+b^-b^-$	$a^0a^0a^0$	0.556	0.615	0.584	0.00000	0.12538	0.00000	26.82111
Na_2RbErF_6	1.891	$a^+b^-b^-$	$a^0a^0a^0$	0.556	0.656	0.602	0.00000	0.19640	0.00000	24.27161
Na_2RbCeF_6	1.849	$a^+b^-b^-$	$a^0a^0a^0$	0.556	0.642	0.596	0.00000	0.18576	0.00000	24.92100
Li_2CsYCl_6	1.845	$a^0a^0c^-$	$a^0a^0a^0$	0.498	0.685	0.577	0.00000	0.36003	0.00000	43.92486
Na_2CsYF_6	1.844	$a^-b^0c^-$	$BaNiO_3$	0.510	0.682	0.584	0.44710	9.85405	1.52066	50.52362
Li_2NaCeF_6	1.812	$a^+a^+c^-$	$a^0a^0a^0$	0.635	0.577	0.604	0.00000	0.08124	0.00000	17.72303
Na_2KLaF_6	1.812	$a^-a^-a^-$	$a^0a^0a^0$	0.605	0.615	0.610	0.00000	0.00266	0.00000	22.68170
Na_2RbGdF_6	1.792	$a^+b^-b^-$	$a^0a^0a^0$	0.556	0.661	0.604	0.00000	0.21527	0.00000	23.73974
Na_2RbEuF_6	1.784	$a^+b^-b^-$	$a^0a^0a^0$	0.556	0.657	0.602	0.00000	0.20132	0.00000	24.35612
Li_2NaGdF_6	1.772	$a^+b^-b^-$	$a^0a^0a^0$	0.635	0.594	0.614	0.00000	0.05218	0.00000	16.52616
K_2RbYF_6	1.688	$a^-a^-c^-$	$a^0a^0a^0$	0.650	0.798	0.716	0.00001	0.23087	0.00000	22.29749
$Li_2CsScCl_6$	1.671	$a^0a^0c^+$	$a^0a^0a^0$	0.498	0.708	0.585	0.00000	0.40976	0.00000	41.28498
$Li_2CsGdCl_6$	1.654	$a^+a^+c^-$	$a^0a^0a^0$	0.498	0.637	0.559	0.00000	0.30429	0.00000	47.04012
Na_2KErF_6	1.625	$a^-a^-a^-$	$a^0a^0a^0$	0.605	0.656	0.629	0.00000	0.07345	0.00000	20.25856
Li_2KYCl_6	1.622	$a^-b^0c^-$	$a^0a^0a^0$	0.561	0.685	0.617	0.00000	0.20400	0.00000	35.81773
Li_2RbYCl_6	1.620	$a^+a^+c^-$	$a^0a^0a^0$	0.533	0.685	0.600	0.00000	0.28530	0.00000	39.90084
Li_2KGdCl_6	1.612	$a^-b^+c^-$	$a^0a^0a^0$	0.561	0.637	0.597	0.00000	0.14600	0.00000	39.06743
$Li_2CsErCl_6$	1.600	$a^+a^+c^-$	$a^0a^0a^0$	0.498	0.662	0.568	0.00000	0.34846	0.00000	44.84391
Li_2KLaCl_6	1.595	$a^0a^0c^-$	$a^0a^0a^0$	0.561	0.615	0.587	0.00000	0.10850	0.00000	40.67759
$Li_2RbGdCl_6$	1.592	$a^0a^0c^+$	$a^0a^0a^0$	0.533	0.637	0.581	0.00000	0.22582	0.00000	42.81681
$Li_2RbLaCl_6$	1.591	$a^0a^0c^-$	$a^0a^0a^0$	0.533	0.615	0.572	0.00000	0.19033	0.00000	44.54581
Li_2NaEuF_6	1.585	$a^+b^-b^-$	$a^0a^0a^0$	0.635	0.590	0.612	0.00000	0.06655	0.00000	16.99221
$Li_2CsCeCl_6$	1.585	$a^+a^+c^-$	$a^0a^0a^0$	0.498	0.635	0.558	0.00000	0.29553	0.00000	47.77707
K_2RbNdF_6	1.578	$a^+b^-b^-$	$BaNiO_3$	0.650	0.725	0.686	0.00000	0.14368	0.00000	25.30736
Na_2CsNdF_6	1.562	$a^+a^+c^-$	$a^0a^0a^0$	0.510	0.620	0.560	0.46267	10.64637	1.57044	58.96651
$Li_2CsLaCl_6$	1.549	$a^+a^+c^-$	$a^0a^0a^0$	0.498	0.615	0.550	0.00000	0.26907	0.00000	49.07158
$Li_2CsLaBr_6$	1.541	$a^+a^+c^-$	$a^0a^0a^0$	0.529	0.664	0.588	0.00000	0.30320	0.00000	54.82856
$Na_2RbLaCl_6$	1.521	$a^-b^0a^-$	$a^0a^0a^0$	0.577	0.666	0.618	0.00000	0.18989	0.00001	43.30188
Na_2KGdF_6	1.518	$a^-a^-a^-$	$a^0a^0a^0$	0.605	0.661	0.632	0.00000	0.09316	0.00000	19.83764
Li_2KNdCl_6	1.513	$a^-b^0c^-$	$a^0a^0a^0$	0.561	0.635	0.596	0.00000	0.14414	0.00000	39.39500
$Li_2CsNdCl_6$	1.512	$a^-b^-c^-$	$a^0a^0a^0$	0.498	0.635	0.558	0.00000	0.30525	0.00000	47.23885
$Li_2RbCeCl_6$	1.507	$a^0a^0c^-$	$a^0a^0a^0$	0.533	0.635	0.580	0.00000	0.21870	0.00000	43.17207
$Li_2CsEuCl_6$	1.502	$a^-a^-c^-$	$a^0a^0a^0$	0.498	0.645	0.562	0.00000	0.31961	0.00000	46.11649
$Li_2RbNdCl_6$	1.501	$a^0a^0c^+$	$a^0a^0a^0$	0.533	0.635	0.580	0.00000	0.22547	0.00000	43.06690
Li_2KCeCl_6	1.500	$a^0a^0c^-$	$a^0a^0a^0$	0.561	0.635	0.596	0.00000	0.13838	0.00000	39.26774
$Li_2CsCeBr_6$	1.493	$a^+a^+c^-$	$a^0a^0a^0$	0.529	0.680	0.595	0.00000	0.32155	0.00000	53.64296
Li_2KErCl_6	1.492	$a^-b^+c^-$	$a^0a^0a^0$	0.561	0.662	0.607	0.00000	0.18593	0.00000	37.11679
Na_2KCeF_6	1.490	$a^-a^-a^-$	$a^0a^0a^0$	0.605	0.642	0.623	0.00000	0.06320	0.00000	20.98715
$Li_2RbErCl_6$	1.484	$a^-b^-c^-$	$a^0a^0a^0$	0.533	0.662	0.591	0.00000	0.26671	0.00000	40.90325
K_2RbLaF_6	1.484	$a^+b^-b^-$	$a^0a^0a^0$	0.650	0.719	0.683	0.00004	0.12555	0.00000	25.97978
$Li_2CsScBr_6$	1.458	$a^0a^0c^-$	$a^0a^0a^0$	0.529	0.770	0.627	0.00000	0.45150	0.00000	46.36816

Compound	ΔE_0 (eV)	S_{min}	S_{max}	t'_B	$t'_{B'}$	t'	ε	δ (Å)	γ	Ω (Å^3)
Li_2CsYBr_6	1.452	$a^-a^-a^-$	$a^0a^0a^0$	0.529	0.705	0.604	0.00000	0.37499	0.00000	50.50157
K_2RbScF_6	1.452	$a^-a^-c^-$	$a^0a^0a^0$	0.650	0.854	0.738	0.00000	0.30010	0.00000	20.34505
$Li_2RbScCl_6$	1.441	$a^0a^0c^-$	$a^0a^0a^0$	0.533	0.708	0.608	0.00000	0.33520	0.00000	37.66388
Na_2LiScF_6	1.437	$a^-a^-c^-$	$BaNiO_3$	0.787	0.730	0.758	0.00000	0.04804	0.00000	11.37304
Na_2KEuF_6	1.432	$a^+b^-b^-$	$a^0a^0a^0$	0.605	0.657	0.630	0.00001	0.07677	0.00000	20.34625
$Na_2RbNdCl_6$	1.430	$a^0a^0c^-$	$a^0a^0a^0$	0.577	0.687	0.627	0.00000	0.22340	0.00000	41.96783
Na_2KLaCl_6	1.426	$a^-b^+c^-$	$a^0a^0a^0$	0.607	0.666	0.635	0.00000	0.10635	0.00000	38.95368
Li_2RbNdF_6	1.426	$a^-a^-a^-$	$a^0a^0a^0$	0.500	0.557	0.527	0.30286	5.52811	1.04332	28.28725
$Li_2CsGdBr_6$	1.398	$a^0a^0c^-$	$a^0a^0a^0$	0.529	0.694	0.600	0.00000	0.35544	0.00000	51.91195
$Li_2NaNdCl_6$	1.395	$a^0a^0c^-$	$a^0a^0a^0$	0.654	0.635	0.644	0.00000	0.01953	0.00000	31.85832
Li_2KEuCl_6	1.394	$a^0a^0c^+$	$a^0a^0a^0$	0.561	0.645	0.600	0.00000	0.15584	0.00000	38.01592
Li_2KScCl_6	1.394	$a^-a^-a^-$	$a^0a^0a^0$	0.561	0.708	0.626	0.00000	0.24765	0.00000	33.86544
$Li_2RbEuCl_6$	1.391	$a^0a^0c^+$	$a^0a^0a^0$	0.533	0.645	0.584	0.00000	0.24300	0.00000	41.93175
Li_2KCeBr_6	1.384	$a^0a^0c^+$	$a^0a^0a^0$	0.587	0.680	0.630	0.00000	0.18542	0.00000	45.94607
Li_2KLaBr_6	1.380	$a^0a^0c^+$	$a^0a^0a^0$	0.587	0.664	0.623	0.00000	0.16456	0.00000	47.16167
$Li_2CsErBr_6$	1.377	$a^-b^-c^-$	$a^0a^0a^0$	0.529	0.698	0.602	0.00000	0.36543	0.00000	51.14441
$Li_2CsEuBr_6$	1.375	$a^-a^-a^-$	$a^0a^0a^0$	0.529	0.686	0.597	0.00000	0.34185	0.00000	52.42057
$Li_2RbCeBr_6$	1.365	$a^0a^0c^+$	$a^0a^0a^0$	0.562	0.680	0.616	0.00000	0.24224	0.00000	48.97053
K_2RbErF_6	1.361	$a^+b^-b^-$	$a^0a^0a^0$	0.650	0.767	0.704	0.00000	0.19821	0.00000	23.50822
$Li_2RbLaBr_6$	1.351	$a^0a^0c^+$	$a^0a^0a^0$	0.562	0.664	0.609	0.00000	0.22205	0.00000	50.18098
$Li_2CsNdBr_6$	1.343	$a^-b^0a^-$	$a^0a^0a^0$	0.529	0.672	0.592	0.00000	0.32106	0.00000	53.74231
$Na_2RbErCl_6$	1.342	$a^-b^+c^-$	$a^0a^0a^0$	0.577	0.716	0.639	0.00000	0.26450	0.00000	39.73781
Na_2KNdCl_6	1.336	$a^-b^+c^-$	$a^0a^0a^0$	0.607	0.687	0.644	0.00000	0.13721	0.00000	37.66181
Na_2CsErF_6	1.334	$a^0a^0c^-$	$a^0a^0a^0$	0.510	0.656	0.574	0.42420	10.35000	1.44706	54.87324
Na_2LiNdF_6	1.319	$a^-a^-c^-$	$BaNiO_3$	0.787	0.620	0.694	0.00000	0.20144	0.00000	15.54828
Na_2LiLaF_6	1.315	$a^+b^-b^-$	$BaNiO_3$	0.787	0.615	0.690	0.00000	0.21623	0.00000	16.22425
$Li_2NaErCl_6$	1.294	$a^-a^-a^-$	$a^0a^0a^0$	0.654	0.662	0.658	0.00000	0.00093	0.00000	28.93187
K_2RbGdF_6	1.266	$a^+b^-b^-$	$a^0a^0a^0$	0.650	0.773	0.706	0.00000	0.21993	0.00000	22.93407
Li_2NaYBr_6	1.265	$a^-a^-a^-$	$a^0a^0a^0$	0.679	0.705	0.692	0.00000	0.02915	0.00000	34.17133
$Li_2NaCeBr_6$	1.260	$a^-b^-c^-$	$a^0a^0a^0$	0.679	0.680	0.679	0.00000	0.00004	0.00000	35.89133
Li_2RbYBr_6	1.252	$a^+b^-b^-$	$a^0a^0a^0$	0.562	0.705	0.626	0.00000	0.29390	0.00000	46.32146
$Li_2NaCeCl_6$	1.252	$a^-a^-a^-$	$a^0a^0a^0$	0.654	0.635	0.644	0.11393	3.12738	0.44540	46.38111
$Na_2RbEuCl_6$	1.249	$a^0a^0c^-$	$a^0a^0a^0$	0.577	0.698	0.632	0.00000	0.23641	0.00000	40.82007
$Li_2NaGdBr_6$	1.238	$a^-a^-a^-$	$a^0a^0a^0$	0.679	0.694	0.686	0.00000	0.02177	0.00000	35.57984
$Li_2RbGdBr_6$	1.224	$a^+b^-b^-$	$a^0a^0a^0$	0.562	0.694	0.621	0.00000	0.27307	0.00000	47.54949
Li_2KEuBr_6	1.222	$a^-a^-a^-$	$a^0a^0a^0$	0.587	0.686	0.633	0.00000	0.20118	0.00000	45.07561
$Li_2NaScCl_6$	1.220	$a^-a^-a^-$	$a^0a^0a^0$	0.654	0.708	0.680	0.00000	0.04108	0.00000	25.20808
$Li_2RbScBr_6$	1.220	$a^-b^0c^-$	$a^0a^0a^0$	0.562	0.770	0.650	0.00000	0.37374	0.00000	42.40635
$Li_2NaLaBr_6$	1.219	$a^-a^-a^-$	$a^0a^0a^0$	0.679	0.664	0.671	0.00000	0.01213	0.00000	38.14161
$Li_2RbNdBr_6$	1.205	$a^+b^-b^-$	$a^0a^0a^0$	0.562	0.672	0.612	0.00000	0.24022	0.00000	49.36068
Li_2KYBr_6	1.189	$a^-a^-a^-$	$a^0a^0a^0$	0.587	0.705	0.641	0.00000	0.23690	0.00000	43.55753
$Li_2NaErBr_6$	1.184	$a^-a^-a^-$	$a^0a^0a^0$	0.679	0.698	0.688	0.00000	0.02750	0.00000	35.24176

Compound	ΔE_0 (eV)	S_{min}	S_{max}	t'_B	$t'_{B'}$	t'	ε	δ (Å)	γ	Ω (Å^3)
$Li_2RbEuBr_6$	1.178	$a^-b^0a^-$	$a^0a^0a^0$	0.562	0.686	0.618	0.00000	0.26006	0.00000	47.95201
$Li_2NaEuCl_6$	1.172	$a^-a^-a^-$	$a^0a^0a^0$	0.654	0.645	0.649	0.00000	0.01741	0.00000	30.14433
$K_2RbLaBr_6$	1.168	$a^0a^0c^+$	$a^0a^0a^0$	0.677	0.799	0.733	0.00000	0.22324	0.00002	48.08022
$Li_2RbErBr_6$	1.164	$a^-b^0a^-$	$a^0a^0a^0$	0.562	0.698	0.623	0.00000	0.28415	0.00000	46.95890
$Li_2NaNdBr_6$	1.163	$a^-a^-a^-$	$a^0a^0a^0$	0.679	0.672	0.675	0.00000	0.00007	0.00000	37.86876
$Li_2NaEuBr_6$	1.163	$a^-a^-a^-$	$a^0a^0a^0$	0.679	0.686	0.682	0.00000	0.00005	0.00000	35.46243
$Na_2CsLaCl_6$	1.159	$a^0a^0c^-$	$a^0a^0a^0$	0.539	0.666	0.595	0.18053	5.74987	0.72732	81.08149
Li_2KGdBr_6	1.156	$a^-a^-a^-$	$a^0a^0a^0$	0.587	0.694	0.636	0.00000	0.21518	0.00000	44.68713
Li_2KScBr_6	1.153	$a^-a^-a^-$	$a^0a^0a^0$	0.587	0.770	0.666	0.00000	0.31600	0.00000	39.78276
Na_2CsYCl_6	1.153	$a^+b^-b^-$	$BaNiO_3$	0.539	0.741	0.624	0.20840	6.35763	0.84898	76.49168
Li_2KNdBr_6	1.152	$a^-a^-a^-$	$a^0a^0a^0$	0.587	0.672	0.627	0.00000	0.17951	0.00000	46.42730
$Li_2NaScBr_6$	1.147	$a^-a^-a^-$	$a^0a^0a^0$	0.679	0.770	0.722	0.00000	0.08325	0.00000	29.38442
Li_2CsEuI_6	1.143	$a^0a^0c^-$	$a^0a^0a^0$	0.547	0.721	0.622	0.00000	0.38041	0.00000	62.83283
Li_2CsYI_6	1.138	$a^-b^-c^-$	$a^0a^0a^0$	0.547	0.714	0.620	0.00000	0.36171	0.00000	63.87365
K_2CsNdF_6	1.135	$a^+a^+a^+$	$BaNiO_3$	0.597	0.725	0.655	0.39454	9.45211	1.35176	59.93155
Li_2CsScI_6	1.134	$a^-b^0c^-$	$a^0a^0a^0$	0.547	0.780	0.644	0.00002	0.45672	0.00000	57.88569
$Na_2CsGdCl_6$	1.131	$a^+b^-b^-$	$a^0a^0a^0$	0.539	0.689	0.605	0.22663	7.27656	0.92993	84.17752
Li_2CsErI_6	1.127	$a^-a^-c^-$	$a^0a^0a^0$	0.547	0.732	0.627	0.00000	0.40384	0.00000	61.20919
Li_2KErBr_6	1.126	$a^-a^-a^-$	$a^0a^0a^0$	0.587	0.698	0.638	0.00000	0.22546	0.00000	44.15797
$K_2RbCeBr_6$	1.126	$a^0a^0c^-$	$a^0a^0a^0$	0.677	0.819	0.741	0.00000	0.24811	0.00000	46.43055
Li_2CsLaI_6	1.122	$a^-a^-c^-$	$a^0a^0a^0$	0.547	0.683	0.608	0.00000	0.31868	0.00000	66.55468
$Na_2RbScCl_6$	1.119	$a^-a^-a^-$	$a^0a^0a^0$	0.577	0.765	0.658	0.00000	0.32868	0.00000	36.46332
Li_2CsGdI_6	1.108	$a^-b^-c^-$	$a^0a^0a^0$	0.547	0.711	0.619	0.00000	0.35743	0.00000	64.34493
Li_2CsNdI_6	1.098	$a^-b^-c^-$	$a^0a^0a^0$	0.547	0.706	0.617	0.00000	0.34740	0.00000	64.76447
$Na_2RbErBr_6$	1.095	$a^0a^0c^-$	$a^0a^0a^0$	0.586	0.727	0.649	0.00004	0.27433	0.00011	45.33267
Li_2KYI_6	1.093	$a^-a^-c^-$	$a^0a^0a^0$	0.597	0.714	0.650	0.00000	0.22375	0.00000	55.71387
Li_2KLaI_6	1.089	$a^-a^-a^-$	$a^0a^0a^0$	0.597	0.683	0.637	0.00000	0.17920	0.00000	58.35888
$K_2RbLaCl_6$	1.089	$a^-a^-c^-$	$a^0a^0a^0$	0.672	0.775	0.720	0.00000	0.19075	0.00000	42.21609
$Na_2CsNdCl_6$	1.086	$a^+b^-b^-$	$a^0a^0a^0$	0.539	0.687	0.604	0.20117	6.30273	0.81711	81.36948
Na_2KCeCl_6	1.086	$a^+b^-b^-$	$a^0a^0a^0$	0.607	0.687	0.644	0.00000	0.13980	0.00000	37.17728
$Na_2RbGdCl_6$	1.082	$a^-b^0a^-$	$BaNiO_3$	0.577	0.689	0.628	0.01239	0.45295	0.04862	44.86042
Li_2RbYI_6	1.082	$a^-a^-c^-$	$a^0a^0a^0$	0.577	0.714	0.638	0.00000	0.28654	0.00000	59.38824
Na_2CsScF_6	1.078	$a^+b^-b^-$	$BaNiO_3$	0.510	0.730	0.601	0.32147	7.23044	1.11374	43.24461
Li_2CsCeI_6	1.076	$a^-a^-c^-$	$a^0a^0a^0$	0.547	0.679	0.606	0.00000	0.31429	0.00000	67.13467
Li_2RbErI_6	1.075	$a^-a^-a^-$	$a^0a^0a^0$	0.577	0.732	0.646	0.00000	0.32824	0.00000	56.91384
Li_2RbLaI_6	1.073	$a^-a^-a^-$	$a^0a^0a^0$	0.577	0.683	0.626	0.00000	0.24500	0.00000	62.03286
$Na_2CsErCl_6$	1.070	$a^+b^-b^-$	$a^0a^0a^0$	0.539	0.716	0.615	0.20673	6.36690	0.84178	78.30346
Li_2KGdI_6	1.070	$a^-a^-a^-$	$a^0a^0a^0$	0.597	0.711	0.649	0.00000	0.21848	0.00000	56.13721
Li_2KNdI_6	1.067	$a^-a^-a^-$	$a^0a^0a^0$	0.597	0.706	0.647	0.00000	0.21130	0.00000	56.54870
$Na_2CsCeCl_6$	1.065	$a^+b^-b^-$	$a^0a^0a^0$	0.539	0.687	0.604	0.18551	5.84822	0.74853	79.86004
Li_2KEuI_6	1.059	$a^-a^-c^-$	$a^0a^0a^0$	0.597	0.721	0.653	0.00000	0.23845	0.00000	54.65164
Li_2RbGdI_6	1.058	$a^-a^-c^-$	$a^0a^0a^0$	0.577	0.711	0.637	0.00001	0.28323	0.00000	59.81832

Compound	ΔE_0 (eV)	S_{min}	S_{max}	t'_B	$t'_{B'}$	t'	ε	δ (Å)	γ	Ω (Å^3)
K_2RbCeF_6	1.058	$a^+a^+c^-$	$a^0a^0a^0$	0.650	0.750	0.697	0.00000	0.19056	0.00000	23.99174
Na_2CsYBr_6	1.056	$a^+b^-b^-$	$BaNiO_3$	0.550	0.735	0.629	0.22140	7.07411	0.90677	90.70860
Li_2NaEuI_6	1.055	$a^-a^-a^-$	$a^0a^0a^0$	0.655	0.721	0.686	0.00000	0.08776	0.00000	46.55123
Li_2RbNdI_6	1.053	$a^-a^-c^-$	$a^0a^0a^0$	0.577	0.706	0.635	0.00000	0.27492	0.00000	60.24058
Li_2KCeI_6	1.052	$a^-a^-a^-$	$a^0a^0a^0$	0.597	0.679	0.635	0.00000	0.17306	0.00000	58.99248
Li_2NaLaI_6	1.050	$a^-a^-a^-$	$a^0a^0a^0$	0.655	0.683	0.669	0.00001	0.04062	0.00000	50.64929
Li_2RbCeI_6	1.040	$a^-a^-c^-$	$a^0a^0a^0$	0.577	0.679	0.624	0.00000	0.23615	0.00000	62.57227
Li_2KErI_6	1.038	$a^-a^-a^-$	$a^0a^0a^0$	0.597	0.732	0.658	0.00000	0.26250	0.00000	53.33112
Li_2NaYI_6	1.035	$a^-a^-a^-$	$a^0a^0a^0$	0.655	0.714	0.683	0.00000	0.07944	0.00000	47.74787
$Na_2CsLaBr_6$	1.034	$a^-a^-a^-$	$a^0a^0a^0$	0.550	0.691	0.613	0.20177	6.65631	0.81968	95.21409
Na_2KYBr_6	1.031	$a^-a^-a^-$	$a^0a^0a^0$	0.612	0.735	0.668	0.00156	0.23462	0.00554	42.16297
Li_2NaNdI_6	1.024	$a^-a^-a^-$	$a^0a^0a^0$	0.655	0.706	0.680	0.00000	0.07317	0.00000	48.67450
$Na_2CsCeBr_6$	1.023	$a^+b^-b^-$	$a^0a^0a^0$	0.550	0.708	0.619	0.22065	7.17790	0.90390	95.36594
Li_2RbScI_6	1.022	$a^-a^-a^-$	$a^0a^0a^0$	0.577	0.780	0.664	0.00000	0.38480	0.00000	53.69798
Na_2KEuCl_6	1.021	$a^-a^-a^-$	$a^0a^0a^0$	0.607	0.698	0.649	0.00000	0.15068	0.00000	36.61915
K_2CsLaF_6	1.019	$a^+a^+c^-$	$BaNiO_3$	0.597	0.719	0.652	0.39986	9.63238	1.36891	61.48115
Li_2NaGdI_6	1.015	$a^-a^-a^-$	$a^0a^0a^0$	0.655	0.711	0.682	0.00000	0.07665	0.00000	48.26147
Li_2NaCeI_6	1.013	$a^-a^-a^-$	$a^0a^0a^0$	0.655	0.679	0.667	0.00000	0.03840	0.00000	51.63397
$K_2RbGdCl_6$	1.013	$a^+b^-b^-$	$a^0a^0a^0$	0.672	0.803	0.732	0.00000	0.22850	0.00000	40.19326
Li_2RbEuI_6	1.011	$a^-b^0c^-$	$a^0a^0a^0$	0.577	0.721	0.641	0.00000	0.30262	0.00000	58.31868
Li_2KScI_6	1.009	$a^-a^-a^-$	$a^0a^0a^0$	0.597	0.780	0.676	0.00000	0.31695	0.00000	50.08712
Li_2NaErI_6	1.003	$a^-a^-a^-$	$a^0a^0a^0$	0.655	0.732	0.691	0.00002	0.11082	0.00000	45.50839
$Na_2CsNdBr_6$	1.001	$a^+b^-b^-$	$a^0a^0a^0$	0.550	0.700	0.616	0.22139	7.31177	0.90635	96.57262
Na_2LiCeF_6	0.998	$a^-a^-c^-$	$BaNiO_3$	0.787	0.642	0.707	0.00000	0.14929	0.00000	14.86945
K_2RbYBr_6	0.992	$a^+b^-b^-$	$a^0a^0a^0$	0.677	0.849	0.753	0.00038	0.28506	0.00096	44.53920
$Na_2CsGdBr_6$	0.991	$a^+b^-b^-$	$BaNiO_3$	0.550	0.723	0.625	0.22457	7.22324	0.92043	93.47881
Na_2KErBr_6	0.988	$a^-a^-a^-$	$a^0a^0a^0$	0.612	0.727	0.664	0.00000	0.22111	0.00000	42.64586
$Na_2CsEuBr_6$	0.980	$a^+b^-b^-$	$a^0a^0a^0$	0.550	0.714	0.622	0.20941	6.79145	0.85276	92.14577
K_2RbEuF_6	0.978	$a^-a^-a^-$	$a^0a^0a^0$	0.650	0.768	0.704	0.00000	0.20086	0.00000	23.56871
Na_2KScCl_6	0.975	$a^-a^-a^-$	$a^0a^0a^0$	0.607	0.765	0.677	0.00000	0.23680	0.00000	32.40667
Li_2NaScI_6	0.974	$a^-a^-a^-$	$a^0a^0a^0$	0.655	0.780	0.712	0.00001	0.15548	0.00000	41.94109
$K_2RbEuBr_6$	0.970	$a^-a^-c^-$	$a^0a^0a^0$	0.677	0.825	0.744	0.00000	0.25355	0.00000	46.32758
$Na_2RbScBr_6$	0.969	$a^-a^-a^-$	$a^0a^0a^0$	0.586	0.802	0.677	0.00000	0.36310	0.00000	40.51654
Na_2LiErF_6	0.959	$a^-b^+c^-$	$BaNiO_3$	0.787	0.656	0.716	0.00000	0.14829	0.00000	14.19188
$Na_2CsEuCl_6$	0.959	$a^0a^0c^+$	$a^0a^0a^0$	0.539	0.698	0.608	0.18347	5.72442	0.73970	76.99911
$K_2RbErBr_6$	0.957	$a^+b^-b^-$	$a^0a^0a^0$	0.677	0.840	0.750	0.00000	0.27481	0.00000	45.40505
$K_2RbErCl_6$	0.952	$a^+b^-b^-$	$a^0a^0a^0$	0.672	0.834	0.744	0.00000	0.26186	0.00000	38.74910
K_2RbYCl_6	0.945	$a^+b^-b^-$	$a^0a^0a^0$	0.672	0.863	0.756	0.00000	0.29352	0.00000	36.99979
$Na_2CsErBr_6$	0.940	$a^+b^-b^-$	$BaNiO_3$	0.550	0.727	0.627	0.21892	7.03568	0.89563	91.78791
$K_2RbCeCl_6$	0.938	$a^-a^-c^-$	$a^0a^0a^0$	0.672	0.800	0.731	0.00000	0.22425	0.00000	40.56355
$Na_2LiLaCl_6$	0.938	$a^-b^-c^-$	$a^0a^0a^0$	0.765	0.666	0.712	0.00000	0.11740	0.00000	28.65102
$K_2RbEuCl_6$	0.934	$a^-b^+c^-$	$a^0a^0a^0$	0.672	0.813	0.736	0.00000	0.23709	0.00000	40.06020

Compound	ΔE_0 (eV)	S_{min}	S_{max}	t'_B	$t'_{B'}$	t'	ε	δ (Å)	γ	Ω (Å^3)
Na_2CsYI_6	0.932	$a^-a^-c^-$	$a^0a^0a^0$	0.591	0.770	0.669	0.00000	0.34390	0.00000	61.09373
Na_2CsNdI_6	0.913	$a^+b^-b^-$	$a^0a^0a^0$	0.591	0.762	0.666	0.00002	0.33258	0.00005	61.96133
$K_2RbScBr_6$	0.913	$a^-a^-c^-$	$a^0a^0a^0$	0.677	0.927	0.783	0.00000	0.36522	0.00000	40.58352
Na_2CsGdI_6	0.908	$a^-a^-c^-$	$a^0a^0a^0$	0.591	0.768	0.668	0.00000	0.34215	0.00000	61.54871
Na_2CsErI_6	0.907	$a^-a^-c^-$	$a^0a^0a^0$	0.591	0.791	0.676	0.00000	0.37824	0.00000	58.66565
$Li_2NaGdCl_6$	0.896	$a^0a^0c^-$	$a^0a^0a^0$	0.654	0.637	0.645	0.05590	1.47567	0.20480	39.52217
Na_2KScBr_6	0.887	$a^-a^-a^-$	$a^0a^0a^0$	0.612	0.802	0.694	0.00000	0.31139	0.00000	38.12790
$Li_2NaLaCl_6$	0.881	$a^0a^0c^-$	$a^0a^0a^0$	0.654	0.615	0.634	0.06744	1.81207	0.24609	43.00363
Rb_2CsNdF_6	0.881	$a^+b^-b^-$	$BaNiO_3$	0.649	0.789	0.712	0.36123	8.80032	1.24382	59.62349
Na_2CsScI_6	0.878	$a^-a^-c^-$	$a^0a^0a^0$	0.591	0.843	0.695	0.00000	0.42951	0.00000	54.94460
$K_2RbScCl_6$	0.870	$a^+b^-b^-$	$BaNiO_3$	0.672	0.892	0.766	0.00000	0.32567	0.00000	35.74282
Rb_2KLaCl_6	0.851	$a^-b^+c^-$	$BaNiO_3$	0.744	0.816	0.778	0.00000	0.10249	0.00000	37.52992
Na_2RbYI_6	0.850	$a^-a^-a^-$	$a^0a^0a^0$	0.623	0.770	0.689	0.00001	0.28060	0.00001	56.87769
Na_2KCeI_6	0.845	$a^-a^-a^-$	$a^0a^0a^0$	0.644	0.733	0.686	0.00005	0.15457	0.00017	56.32913
$Na_2CsScBr_6$	0.843	$a^0a^0c^+$	$BaNiO_3$	0.550	0.802	0.653	0.21568	6.63181	0.87487	82.00665
$Na_2CsScCl_6$	0.841	$a^-b^-c^-$	$BaNiO_3$	0.539	0.765	0.632	0.20364	6.11846	0.82803	72.13879
Na_2KYI_6	0.839	$a^-a^-a^-$	$a^0a^0a^0$	0.644	0.770	0.702	0.00000	0.21100	0.00000	52.63377
Na_2LiEuF_6	0.836	$a^-b^0c^-$	$BaNiO_3$	0.787	0.657	0.716	0.00000	0.14189	0.00000	14.28570
Na_2RbGdI_6	0.836	$a^-a^-a^-$	$a^0a^0a^0$	0.623	0.768	0.688	0.00002	0.27803	0.00008	57.24279
Na_2KNdI_6	0.832	$a^-a^-a^-$	$a^0a^0a^0$	0.644	0.762	0.699	0.00000	0.20195	0.00000	53.30377
Na_2LiGdF_6	0.828	$a^-a^-a^-$	$BaNiO_3$	0.787	0.661	0.718	0.00000	0.11854	0.00000	13.79363
Na_2KGdI_6	0.827	$a^-a^-a^-$	$a^0a^0a^0$	0.644	0.768	0.701	0.00000	0.20688	0.00000	53.00034
Na_2RbNdI_6	0.823	$a^-a^-a^-$	$a^0a^0a^0$	0.623	0.762	0.686	0.00094	0.27080	0.00394	57.83987
Na_2KEuI_6	0.804	$a^-a^-a^-$	$a^0a^0a^0$	0.644	0.778	0.705	0.00000	0.21980	0.00000	51.65274
Rb_2KGdCl_6	0.798	$a^-b^+c^-$	$BaNiO_3$	0.744	0.845	0.791	0.00000	0.13984	0.00000	35.54620
Rb_2KNdCl_6	0.797	$a^-b^-c^-$	$a^0a^0a^0$	0.744	0.842	0.790	0.00000	0.13161	0.00000	36.16248
Na_2RbErI_6	0.793	$a^-a^-a^-$	$a^0a^0a^0$	0.623	0.791	0.697	0.00000	0.31340	0.00000	54.84729
K_2CsLaI_6	0.791	$a^0a^0c^+$	$BaNiO_3$	0.648	0.809	0.720	0.17492	6.15891	0.70314	109.44842
Na_2KErI_6	0.788	$a^-a^-a^-$	$a^0a^0a^0$	0.644	0.791	0.710	0.00000	0.24035	0.00000	50.80884
Rb_2CsLaF_6	0.786	$a^+a^+c^-$	$BaNiO_3$	0.649	0.782	0.709	0.36979	9.05222	1.27165	61.40759
Na_2CsLaI_6	0.784	$a^+b^-b^-$	$a^0a^0c^+$	0.591	0.738	0.656	0.24664	8.56954	1.01992	124.94394
Rb_2KLaF_6	0.778	$a^-b^+c^-$	$BaNiO_3$	0.769	0.782	0.775	0.00000	0.00005	0.00000	21.51747
K_2CsEuF_6	0.771	$a^-b^0c^-$	$BaNiO_3$	0.597	0.768	0.672	0.19033	4.70971	0.67445	43.68217
Li_2NaYCl_6	0.769	$a^-a^-a^-$	$BaNiO_3$	0.654	0.685	0.669	0.02769	0.66425	0.07585	31.14376
K_2RbEuI_6	0.769	$a^-b^+c^-$	$a^0a^0a^0$	0.684	0.854	0.760	0.00003	0.28870	0.00007	54.92282
Rb_2KNdF_6	0.764	$a^-a^-c^-$	$BaNiO_3$	0.769	0.789	0.779	0.00001	0.01205	0.00000	20.70560
Rb_2KCeCl_6	0.763	$a^-b^+c^-$	$BaNiO_3$	0.744	0.842	0.790	0.00000	0.13735	0.00000	35.94111
K_2RbErI_6	0.760	$a^+b^-b^-$	$a^0a^0a^0$	0.684	0.867	0.765	0.00000	0.31000	0.00000	54.07164
Rb_2KLaBr_6	0.753	$a^+b^-b^-$	$BaNiO_3$	0.738	0.834	0.783	0.00000	0.17671	0.00000	44.06308
Rb_2KEuCl_6	0.745	$a^-b^+c^-$	$BaNiO_3$	0.744	0.855	0.796	0.00000	0.14550	0.00000	35.58179
Na_2RbScI_6	0.739	$a^-a^-a^-$	$a^0a^0a^0$	0.623	0.843	0.717	0.00000	0.37003	0.00000	51.43333
K_2CsCeI_6	0.729	$a^0a^0c^+$	$BaNiO_3$	0.648	0.804	0.718	0.16923	5.98747	0.67819	109.60593

Compound	ΔE_0 (eV)	S_{min}	S_{max}	t'_B	$t'_{B'}$	t'	ε	δ (Å)	γ	Ω (Å^3)
$K_2NaNdBr_6$	0.727	$a^-b^+c^-$	$BaNiO_3$	0.817	0.809	0.813	0.00000	0.05320	0.00000	33.18972
$K_2NaLaBr_6$	0.727	$a^-b^+c^-$	$BaNiO_3$	0.817	0.799	0.808	0.00000	0.04990	0.00000	33.53028
$K_2CsNdBr_6$	0.724	$a^-a^-c^-$	$a^0a^0a^0$	0.636	0.809	0.712	0.13040	4.26219	0.50487	79.42989
Rb_2KCeBr_6	0.723	$a^+b^-b^-$	$BaNiO_3$	0.738	0.855	0.792	0.00000	0.20716	0.00000	42.41795
$Na_2LiNdCl_6$	0.720	$a^-a^-a^-$	$BaNiO_3$	0.765	0.687	0.724	0.00000	0.09237	0.00000	27.39576
K_2CsNdI_6	0.719	$a^-a^-c^-$	$BaNiO_3$	0.648	0.837	0.731	0.17495	6.09747	0.70265	105.94444
Rb_2KCeI_6	0.719	$a^-b^+c^-$	$BaNiO_3$	0.731	0.831	0.778	0.00027	0.14679	0.00113	55.02617
Rb_2KErCl_6	0.717	$a^-b^+c^-$	$BaNiO_3$	0.744	0.877	0.805	0.00000	0.17045	0.00000	34.23878
Na_2KScI_6	0.711	$a^-a^-a^-$	$a^0a^0a^0$	0.644	0.843	0.730	0.00000	0.29675	0.00000	47.47282
$Na_2LiLaBr_6$	0.708	$a^-a^-a^-$	$a^0a^0a^0$	0.736	0.691	0.713	0.00000	0.05511	0.00000	33.35492
Rb_2KEuBr_6	0.705	$a^+b^-b^-$	$BaNiO_3$	0.738	0.862	0.795	0.00000	0.20283	0.00000	42.76812
$Na_2LiNdBr_6$	0.705	$a^-b^+c^-$	$BaNiO_3$	0.736	0.700	0.718	0.00000	0.05640	0.00000	33.27629
$Na_2LiGdCl_6$	0.702	$a^-a^-a^-$	$a^0a^0a^0$	0.765	0.689	0.725	0.00000	0.08455	0.00000	26.65727
$K_2LiNdBr_6$	0.701	$a^+b^-b^-$	$BaNiO_3$	0.851	0.809	0.829	0.00000	0.05762	0.00000	32.74368
$K_2CsCeCl_6$	0.697	$a^0a^0c^-$	$BaNiO_3$	0.627	0.800	0.703	0.19061	5.55460	0.67548	72.72704
$K_2CsGdCl_6$	0.697	$a^0a^0c^+$	$BaNiO_3$	0.627	0.803	0.704	0.20957	6.04702	0.73968	73.71571
Rb_2KGdBr_6	0.695	$a^+b^-b^-$	$a^0a^0a^0$	0.738	0.873	0.800	0.00000	0.21769	0.00000	41.92118
$K_2LiLaBr_6$	0.694	$a^+b^-b^-$	$BaNiO_3$	0.851	0.799	0.824	0.00000	0.05714	0.00000	32.95903
$Na_2LiCeCl_6$	0.694	$a^-a^-c^-$	$a^0a^0a^0$	0.765	0.687	0.724	0.00005	0.07804	0.00000	27.19261
Rb_2KErBr_6	0.691	$a^+b^-b^-$	$a^0a^0a^0$	0.738	0.878	0.802	0.00000	0.21814	0.00000	41.92603
K_2RbScI_6	0.691	$a^-b^+c^-$	$a^0a^0a^0$	0.684	0.924	0.786	0.00000	0.36750	0.00000	50.60631
Rb_2KNdI_6	0.689	$a^-b^+c^-$	$BaNiO_3$	0.731	0.865	0.792	0.00000	0.19858	0.00000	51.79470
Rb_2KYI_6	0.684	$a^-b^+c^-$	$BaNiO_3$	0.731	0.874	0.796	0.00360	0.22361	0.00869	51.37946
K_2CsYI_6	0.678	$a^-a^-c^-$	$BaNiO_3$	0.648	0.845	0.734	0.17276	5.99718	0.69362	103.99389
Li_2CsNdF_6	0.677	$a^+a^+c^-$	$a^0a^0a^0$	0.458	0.557	0.503	0.28449	5.72680	0.96505	33.14818
Rb_2KGdI_6	0.676	$a^-b^-c^-$	$BaNiO_3$	0.731	0.871	0.795	0.00185	0.20816	0.00538	51.61295
Rb_2KYBr_6	0.675	$a^-b^+c^-$	$BaNiO_3$	0.738	0.887	0.806	0.00000	0.23001	0.00000	41.15662
K_2CsGdI_6	0.671	$a^-a^-c^-$	$BaNiO_3$	0.648	0.842	0.733	0.16793	5.84419	0.67298	103.74222
$Rb_2CsLaCl_6$	0.668	$a^-a^-c^-$	$BaNiO_3$	0.660	0.816	0.730	0.21062	6.14935	0.74346	76.57867
$K_2NaEuBr_6$	0.664	$a^+b^-b^-$	$BaNiO_3$	0.817	0.825	0.821	0.00000	0.03305	0.00000	32.27707
K_2CsCeF_6	0.662	$a^+a^+c^-$	$BaNiO_3$	0.597	0.750	0.665	0.20153	5.00554	0.71270	45.49398
$K_2NaCeBr_6$	0.660	$a^+b^-b^-$	$BaNiO_3$	0.817	0.819	0.818	0.00001	0.02204	0.00000	31.48070
Rb_2KYCl_6	0.650	$a^-b^+c^-$	$a^0a^0a^0$	0.744	0.908	0.818	0.00000	0.20434	0.00000	32.43625
$K_2CsNdCl_6$	0.649	$a^0a^0c^-$	$BaNiO_3$	0.627	0.800	0.703	0.20314	5.89443	0.71704	73.98769
$Na_2LiCeBr_6$	0.646	$a^-b^+c^-$	$a^0a^0a^0$	0.736	0.708	0.722	0.00000	0.02250	0.00000	31.72017
$Na_2LiEuBr_6$	0.642	$a^-b^+c^-$	$BaNiO_3$	0.736	0.714	0.725	0.00000	0.03515	0.00000	32.36744
K_2CsEuI_6	0.642	$a^+b^-b^-$	$BaNiO_3$	0.648	0.854	0.737	0.16862	5.78885	0.66668	100.42585
$Na_2LiGdBr_6$	0.640	$a^-b^+c^-$	$BaNiO_3$	0.736	0.723	0.730	0.00000	0.02042	0.00000	31.55357
$K_2NaErBr_6$	0.639	$a^+b^-b^-$	$BaNiO_3$	0.817	0.840	0.829	0.00000	0.02250	0.00000	31.49817
$Na_2LiErBr_6$	0.637	$a^-b^+c^-$	$BaNiO_3$	0.736	0.727	0.732	0.00000	0.02195	0.00000	31.74546
Na_2LiYBr_6	0.635	$a^-b^+c^-$	$BaNiO_3$	0.736	0.735	0.736	0.00000	0.00990	0.00000	30.95292
$Na_2LiEuCl_6$	0.635	$a^-b^+c^-$	$a^0a^0a^0$	0.765	0.698	0.730	0.00000	0.08095	0.00000	26.88391

Compound	ΔE_0 (eV)	S_{min}	S_{max}	t'_B	$t'_{B'}$	t'	ε	δ (Å)	γ	Ω (Å^3)
Rb_2CsYI_6	0.635	$a^-b^+c^-$	$BaNiO_3$	0.670	0.874	0.759	0.14078	4.86503	0.55708	96.09943
$K_2LiEuBr_6$	0.635	$a^+b^-b^-$	$BaNiO_3$	0.851	0.825	0.838	0.00000	0.03810	0.00000	31.93627
Cs_2RbNdF_6	0.634	$a^-b^-c^-$	$BaNiO_3$	0.770	0.859	0.813	0.00000	0.14405	0.00001	24.53927
Rb_2KEuI_6	0.633	$a^+b^-b^-$	$a^0a^0a^0$	0.731	0.883	0.800	0.00000	0.21485	0.00000	50.58071
$K_2NaGdBr_6$	0.632	$a^+b^-b^-$	$BaNiO_3$	0.817	0.836	0.826	0.00000	0.02090	0.00000	31.36626
Rb_2KErI_6	0.628	$a^+b^-b^-$	BaNiO3	0.731	0.897	0.806	0.00000	0.23254	0.00000	49.67219
$K_2LiCeBr_6$	0.625	$a^+b^-b^-$	$BaNiO_3$	0.851	0.819	0.835	0.00000	0.02233	0.00000	31.18649
Rb_2CsNdI_6	0.623	$a^-b^+c^-$	$BaNiO_3$	0.670	0.865	0.755	0.14203	4.93841	0.56294	97.90546
Na_2CsEuI_6	0.623	$a^-b^+c^-$	$BaNiO_3$	0.591	0.778	0.672	0.22984	7.93788	0.94554	115.30038
Rb_2CsGdI_6	0.623	$a^-b^+c^-$	$BaNiO_3$	0.670	0.871	0.758	0.13936	4.82869	0.54850	96.40862
Na_2LiLaI_6	0.622	$a^-b^+c^-$	$BaNiO_3$	0.763	0.738	0.750	0.00000	0.04031	0.00000	44.06558
Na_2KEuBr_6	0.618	$a^-a^-a^-$	$BaNiO_3$	0.612	0.714	0.659	0.13816	4.03885	0.49652	64.96396
K_2CsErI_6	0.615	$a^+b^-b^-$	$BaNiO_3$	0.648	0.867	0.742	0.16356	5.59895	0.65315	97.82075
Rb_2KErF_6	0.614	$a^+a^+a^+$	$a^0a^0a^0$	0.769	0.834	0.800	0.00000	0.06562	0.00000	18.98698
$Na_2LiErCl_6$	0.613	$a^+b^-b^-$	$BaNiO_3$	0.765	0.716	0.739	0.00000	0.05759	0.00000	25.67499
$K_2LiErBr_6$	0.612	$a^+b^-b^-$	$BaNiO_3$	0.851	0.840	0.846	0.00000	0.02397	0.00000	31.23917
Na_2LiCeI_6	0.610	$a^-a^-a^-$	$a^0a^0a^0$	0.763	0.733	0.748	0.00000	0.05070	0.00000	45.03614
Na_2CsCeI_6	0.608	$a^-b^-c^-$	$a^0a^0c^-$	0.591	0.733	0.654	0.24332	8.51204	1.00494	126.49504
$K_2NaLaCl_6$	0.607	$a^+b^-b^-$	$BaNiO_3$	0.824	0.775	0.799	0.00000	0.07790	0.00000	29.89741
$K_2LiGdBr_6$	0.601	$a^+b^-b^-$	$BaNiO_3$	0.851	0.836	0.843	0.00000	0.02056	0.00000	31.09568
Li_2CsScF_6	0.598	$a^-b^0a^-$	$a^0a^0a^0$	0.458	0.656	0.540	0.38356	8.06876	1.15801	32.12776
Li_2CsLaF_6	0.598	$a^+a^+c^-$	$a^0a^0a^0$	0.458	0.552	0.501	0.34886	7.00779	1.12847	38.84685
K_2NaYBr_6	0.597	$a^+b^-b^-$	$BaNiO_3$	0.817	0.849	0.833	0.00000	0.01525	0.00000	30.52929
Rb_2CsErI_6	0.597	$a^-b^+c^-$	$BaNiO_3$	0.670	0.897	0.767	0.13284	4.58479	0.52829	90.96677
K_2NaCeI_6	0.596	$a^+b^-b^-$	$BaNiO_3$	0.776	0.804	0.790	0.00000	0.02515	0.00000	45.56699
K_2NaLaI_6	0.595	$a^+b^-b^-$	$BaNiO_3$	0.776	0.809	0.792	0.00000	0.01345	0.00000	44.33288
K_2CsErF_6	0.594	$a^+a^+c^-$	$BaNiO_3$	0.597	0.767	0.671	0.23695	5.78104	0.83267	46.73072
Na_2LiYI_6	0.583	$a^-b^+c^-$	$BaNiO_3$	0.763	0.770	0.767	0.00000	0.00931	0.00000	41.60495
Rb_2CsYF_6	0.581	$a^+b^-b^-$	$BaNiO_3$	0.649	0.867	0.742	0.28114	6.63373	0.98064	46.31719
Rb_2KCeF_6	0.580	$a^-b^+c^-$	$BaNiO_3$	0.769	0.816	0.792	0.00000	0.06235	0.00000	19.62378
Rb_2KYF_6	0.575	$a^-b^0a^-$	$BaNiO_3$	0.769	0.867	0.815	0.00000	0.09230	0.00000	17.65800
K_2LiYBr_6	0.575	$a^+b^-b^-$	$BaNiO_3$	0.851	0.849	0.850	0.00000	0.01190	0.00000	30.46785
Na_2LiNdI_6	0.571	$a^-b^+c^-$	$BaNiO_3$	0.763	0.762	0.763	0.00000	0.00005	0.00000	42.19843
Na_2LiGdI_6	0.570	$a^-b^-c^-$	$BaNiO_3$	0.763	0.768	0.766	0.00000	0.00605	0.00000	41.92875
Rb_2KScCl_6	0.565	$a^-b^+c^-$	$a^0a^0a^0$	0.744	0.938	0.830	0.00000	0.22851	0.00000	31.49342
Rb_2CsCeF_6	0.557	$a^-a^-c^-$	$BaNiO_3$	0.649	0.816	0.723	0.23984	5.86483	0.84247	47.39240
K_2CsGdF_6	0.556	$a^+a^+c^-$	$BaNiO_3$	0.597	0.773	0.673	0.24426	5.90721	0.85730	46.23769
K_2CsYCl_6	0.555	$a^+b^-b^-$	$BaNiO_3$	0.627	0.863	0.727	0.23209	6.48819	0.81630	70.14835
$K_2CsEuCl_6$	0.551	$a^+b^-b^-$	$BaNiO_3$	0.627	0.813	0.708	0.19497	5.65600	0.69374	72.10621
Na_2RbCeI_6	0.550	$a^-a^-a^-$	$a^0a^0c^-$	0.623	0.733	0.674	0.00882	0.38697	0.03610	64.35393
Na_2LiYCl_6	0.543	$a^+b^-b^-$	$a^0a^0a^0$	0.765	0.741	0.753	0.00000	0.02115	0.00000	23.81854
$K_2NaNdCl_6$	0.541	$a^+b^-b^-$	$BaNiO_3$	0.824	0.800	0.812	0.00000	0.05355	0.00000	28.68023

Compound	ΔE_0 (eV)	S_{min}	S_{max}	t'_B	$t'_{B'}$	t'	ε	δ (Å)	γ	Ω (Å^3)
Rb_2KGdF_6	0.535	$a^+a^+a^+$	$BaNiO_3$	0.769	0.840	0.803	0.00000	0.09399	0.00000	18.34324
K_2NaNdI_6	0.535	$a^+b^-b^-$	$BaNiO_3$	0.776	0.837	0.805	0.00000	0.02465	0.00000	41.99830
K_2LiCeI_6	0.535	$a^+b^-b^-$	$BaNiO_3$	0.838	0.804	0.820	0.00000	0.05796	0.00000	43.89474
Na_2LiEuI_6	0.535	$a^-b^+c^-$	$BaNiO_3$	0.763	0.778	0.771	0.00000	0.01581	0.00000	41.11208
Rb_2KEuF_6	0.534	$a^-b^+c^-$	$BaNiO_3$	0.769	0.836	0.801	0.00000	0.07277	0.00000	19.26101
K_2LiLaI_6	0.533	$a^+b^-b^-$	$BaNiO_3$	0.838	0.809	0.823	0.00000	0.04185	0.00000	42.82589
Na_2LiErI_6	0.527	$a^-b^-c^-$	$BaNiO_3$	0.763	0.791	0.777	0.00000	0.03075	0.00000	40.50396
$K_2NaGdCl_6$	0.526	$a^+b^-b^-$	$BaNiO_3$	0.824	0.803	0.813	0.00000	0.04722	0.00000	27.91872
Rb_2KScBr_6	0.525	$a^+b^-b^-$	$BaNiO_3$	0.738	0.968	0.838	0.00000	0.31194	0.00000	37.59960
Rb_2NaCeI_6	0.525	$a^+b^-b^-$	$BaNiO_3$	0.802	0.831	0.816	0.00000	0.02440	0.00000	45.42207
$Rb_2CsLaBr_6$	0.523	$a^-b^0a^-$	$BaNiO_3$	0.664	0.834	0.740	0.21469	6.54408	0.75744	87.85545
Rb_2KScI_6	0.522	$a^-b^+c^-$	$BaNiO_3$	0.731	0.956	0.828	0.00000	0.29035	0.00000	46.28546
K_2NaYI_6	0.517	$a^+b^-b^-$	$BaNiO_3$	0.776	0.845	0.809	0.00000	0.03120	0.00000	41.26398
Rb_2NaLaI_6	0.516	$a^+b^-b^-$	$BaNiO_3$	0.802	0.837	0.819	0.00000	0.01314	0.00000	44.12014
K_2NaGdI_6	0.515	$a^+b^-b^-$	$BaNiO_3$	0.776	0.842	0.808	0.00000	0.02948	0.00000	41.74838
Cs_2KLaI_6	0.514	$a^+b^-b^-$	$BaNiO_3$	0.771	0.883	0.823	0.00000	0.15691	0.00000	53.31276
$K_2RbNdCl_6$	0.512	$a^-a^-c^-$	$BaNiO_3$	0.672	0.800	0.730	0.17203	4.89427	0.61149	65.20454
Cs_2KCeI_6	0.507	$a^+b^-b^-$	$BaNiO_3$	0.771	0.877	0.820	0.00000	0.14515	0.00000	54.40289
$K_2LiLaCl_6$	0.506	$a^+b^-b^-$	$a^0a^0a^0$	0.891	0.775	0.829	0.00000	0.11982	0.00000	28.16590
$K_2NaCeCl_6$	0.506	$a^+b^-b^-$	$BaNiO_3$	0.824	0.800	0.812	0.00003	0.03609	0.00000	28.63698
$Cs_2RbLaCl_6$	0.505	$a^-b^0a^-$	$a^0a^0a^0$	0.758	0.874	0.812	0.00001	0.19356	0.00000	41.17856
$K_2CsErCl_6$	0.503	$a^-b^+c^-$	$BaNiO_3$	0.627	0.834	0.716	0.22131	6.28863	0.77938	72.13692
Cs_2RbErF_6	0.500	$a^0a^0a^0$	$BaNiO_3$	0.770	0.909	0.834	0.00000	0.19675	0.00000	22.91253
Rb_2CsEuF_6	0.499	$a^-a^-c^-$	$BaNiO_3$	0.649	0.836	0.731	0.21884	5.35582	0.77147	45.29036
Cs_2RbLaI_6	0.497	$a^+a^+c^-$	$BaNiO_3$	0.746	0.883	0.808	0.00158	0.23135	0.00340	57.80067
$K_2CsErBr_6$	0.495	$a^+b^-b^-$	$BaNiO_3$	0.636	0.840	0.724	0.10940	2.91799	0.31791	63.82692
$Rb_2NaLaCl_6$	0.492	$a^+b^-b^-$	$BaNiO_3$	0.867	0.816	0.840	0.00000	0.08515	0.00000	29.17374
$K_2NaEuCl_6$	0.491	$a^+b^-b^-$	$BaNiO_3$	0.824	0.813	0.818	0.00000	0.04112	0.00000	28.16700
Li_2CsGdF_6	0.491	$a^+b^-b^-$	$a^0a^0a^0$	0.458	0.594	0.517	0.32532	8.71840	1.38440	45.30339
Cs_2RbCeI_6	0.490	$a^+a^+c^-$	$BaNiO_3$	0.746	0.877	0.806	0.00001	0.21599	0.00002	58.59888
$Cs_2RbGdCl_6$	0.484	$a^-b^0a^-$	$BaNiO_3$	0.758	0.905	0.825	0.00000	0.22842	0.00000	39.30386
$Rb_2CsEuCl_6$	0.483	$a^-b^+c^-$	$BaNiO_3$	0.660	0.855	0.745	0.21848	6.26471	0.77031	73.65973
$Cs_2RbLaBr_6$	0.476	$a^-b^0c^-$	$BaNiO_3$	0.753	0.888	0.815	0.00308	0.24090	0.01219	46.38318
$Na_2LiScCl_6$	0.475	$a^-b^+c^-$	$BaNiO_3$	0.765	0.765	0.765	0.00000	0.00364	0.00000	23.32017
K_2NaEuI_6	0.472	$a^+b^-b^-$	$BaNiO_3$	0.776	0.854	0.813	0.00000	0.03680	0.00000	41.37188
K_2LiNdI_6	0.468	$a^-b^+c^-$	$BaNiO_3$	0.838	0.837	0.837	0.00000	0.00007	0.00000	40.61788
K_2NaLaF_6	0.463	$a^-b^+c^-$	$BaNiO_3$	0.827	0.719	0.769	0.00000	0.14631	0.00000	17.77478
$Cs_2RbNdBr_6$	0.463	$a^-b^0a^-$	$BaNiO_3$	0.753	0.899	0.819	0.00001	0.22919	0.00000	45.73071
K_2NaErI_6	0.460	$a^+b^-b^-$	$BaNiO_3$	0.776	0.867	0.819	0.00000	0.04870	0.00000	40.52301
$Cs_2RbNdCl_6$	0.460	$a^-b^0a^-$	$a^0a^0a^0$	0.758	0.902	0.823	0.00000	0.21985	0.00000	39.94875
$Na_2LiScBr_6$	0.454	$a^-b^-c^-$	$BaNiO_3$	0.736	0.802	0.768	0.00000	0.06705	0.00000	27.94086
K_2NaNdF_6	0.454	$a^-b^+c^-$	$BaNiO_3$	0.827	0.725	0.773	0.00000	0.13283	0.00000	17.04722

Compound	ΔE_0 (eV)	S_{min}	S_{max}	t'_B	$t'_{B'}$	t'	ε	δ (Å)	γ	Ω (Å^3)
Rb_2LiCeI_6	0.453	$a^+b^-b^-$	$BaNiO_3$	0.866	0.831	0.848	0.00000	0.06030	0.00000	43.67897
$Cs_2RbCeBr_6$	0.452	$a^-b^0c^-$	$BaNiO_3$	0.753	0.910	0.824	0.00000	0.25579	0.00001	44.02640
K_2LiYI_6	0.450	$a^-b^+c^-$	$BaNiO_3$	0.838	0.845	0.841	0.00000	0.00859	0.00000	40.02927
Rb_2NaNdI_6	0.450	$a^+b^-b^-$	$BaNiO_3$	0.802	0.865	0.832	0.00000	0.02270	0.00000	41.64964
K_2LiGdI_6	0.447	$a^+b^-b^-$	$BaNiO_3$	0.838	0.842	0.840	0.00000	0.00481	0.00000	40.41066
Rb_2LiLaI_6	0.443	$a^+b^-b^-$	$BaNiO_3$	0.866	0.837	0.851	0.00000	0.04383	0.00000	42.59587
$K_2NaErCl_6$	0.442	$a^+b^-b^-$	$BaNiO_3$	0.824	0.834	0.829	0.00000	0.01898	0.00000	26.89909
Na_2LiScI_6	0.441	$a^-b^+c^-$	$BaNiO_3$	0.763	0.843	0.801	0.00000	0.09065	0.00000	37.65448
Cs_2RbCeF_6	0.441	$a^0a^0a^0$	$BaNiO_3$	0.770	0.889	0.826	0.00000	0.19217	0.00000	23.27850
$Rb_2CsCeCl_6$	0.438	$a^-b^0a^-$	$BaNiO_3$	0.660	0.842	0.740	0.21771	6.26914	0.76767	74.51343
$K_2LiNdCl_6$	0.438	$a^+b^-b^-$	$BaNiO_3$	0.891	0.800	0.843	0.00000	0.09407	0.00000	27.02911
Cs_2KNdI_6	0.437	$a^+b^-b^-$	$BaNiO_3$	0.771	0.912	0.836	0.00000	0.19647	0.00000	51.15709
$Cs_2RbEuBr_6$	0.433	$a^-b^0a^-$	$BaNiO_3$	0.753	0.917	0.827	0.00000	0.24831	0.00000	44.42822
Cs_2KYI_6	0.433	$a^+b^-b^-$	$BaNiO_3$	0.771	0.922	0.840	0.00000	0.20717	0.00000	50.58723
Cs_2KGdI_6	0.430	$a^+b^-b^-$	$BaNiO_3$	0.771	0.918	0.838	0.00000	0.20300	0.00000	50.94461
$Cs_2RbCeCl_6$	0.429	$a^-b^0a^-$	$BaNiO_3$	0.758	0.902	0.823	0.00000	0.22950	0.00000	39.47837
$Cs_2RbGdBr_6$	0.427	$a^-b^0c^-$	$BaNiO_3$	0.753	0.929	0.831	0.00000	0.26305	0.00000	43.78003
Rb_2NaGdI_6	0.427	$a^+b^-b^-$	$BaNiO_3$	0.802	0.871	0.835	0.00000	0.02671	0.00000	41.48740
Rb_2NaYI_6	0.422	$a^-a^-a^-$	$BaNiO_3$	0.802	0.874	0.836	0.00000	0.02733	0.00000	40.97480
Rb_2KLaI_6	0.422	$a^-b^+c^-$	$BaNiO_3$	0.731	0.837	0.780	0.14982	4.71790	0.53250	85.01847
$Rb_2CsGdCl_6$	0.420	$a^-b^0a^-$	$BaNiO_3$	0.660	0.845	0.741	0.23560	6.72281	0.82821	75.30108
$K_2LiGdCl_6$	0.419	$a^+b^-b^-$	$a^0a^0a^0$	0.891	0.803	0.844	0.00000	0.08820	0.00000	26.34192
$Cs_2RbEuCl_6$	0.419	$a^-b^0a^-$	$BaNiO_3$	0.758	0.916	0.829	0.00000	0.23619	0.00000	39.13745
Cs_2RbYBr_6	0.418	$a^-b^0a^-$	$BaNiO_3$	0.753	0.944	0.837	0.00000	0.27790	0.00000	43.00106
$Rb_2NaNdCl_6$	0.417	$a^+b^-b^-$	$BaNiO_3$	0.867	0.842	0.854	0.00000	0.06004	0.00000	28.02103
$Rb_2CsNdCl_6$	0.413	$a^-b^0a^-$	$BaNiO_3$	0.660	0.842	0.740	0.22690	6.52188	0.79879	75.59686
$Rb_2CsCeBr_6$	0.409	$a^+b^-b^-$	$BaNiO_3$	0.664	0.855	0.748	0.22089	6.64832	0.77849	85.61440
$Rb_2CsNdBr_6$	0.408	$a^-b^0a^-$	$BaNiO_3$	0.664	0.844	0.744	0.22140	6.71772	0.78025	87.88837
K_2LiEuI_6	0.406	$a^+b^-b^-$	$BaNiO_3$	0.838	0.854	0.846	0.00000	0.01065	0.00000	40.12104
$Cs_2RbErCl_6$	0.406	$a^-b^0a^-$	$a^0a^0a^0$	0.758	0.940	0.839	0.00000	0.26156	0.00000	37.95978
Cs_2RbGdF_6	0.405	$a^0a^0a^0$	$BaNiO_3$	0.770	0.916	0.837	0.00000	0.22372	0.00000	22.30882
Cs_2KEuI_6	0.405	$a^+b^-b^-$	$BaNiO_3$	0.771	0.931	0.844	0.00000	0.21324	0.00000	49.99603
$Cs_2RbErBr_6$	0.405	$a^-b^0a^-$	$BaNiO_3$	0.753	0.934	0.834	0.00000	0.26617	0.00000	43.81543
Cs_2RbYI_6	0.402	$a^-b^0c^-$	$BaNiO_3$	0.746	0.922	0.824	0.00000	0.27838	0.00000	54.78842
Rb_2CsCeI_6	0.401	$a^-b^+c^-$	$BaNiO_3$	0.670	0.831	0.742	0.20384	6.70597	0.71648	108.84536
$K_2LiCeCl_6$	0.400	$a^+b^-b^-$	$a^0a^0a^0$	0.891	0.800	0.843	0.00000	0.07725	0.00000	26.96845
Cs_2RbNdI_6	0.395	$a^-b^0a^-$	$BaNiO_3$	0.746	0.912	0.821	0.00000	0.26991	0.00000	55.37933
K_2LiErI_6	0.393	$a^+b^-b^-$	$BaNiO_3$	0.838	0.867	0.852	0.00000	0.02415	0.00000	39.34563
Cs_2RbGdI_6	0.393	$a^-b^0a^-$	$BaNiO_3$	0.746	0.918	0.823	0.00000	0.27528	0.00000	55.12275
$Rb_2NaGdCl_6$	0.393	$a^+b^-b^-$	$BaNiO_3$	0.867	0.845	0.855	0.00000	0.05334	0.00000	27.21431
Cs_2RbEuF_6	0.393	$a^0a^0a^0$	$BaNiO_3$	0.770	0.911	0.835	0.00000	0.20420	0.00000	22.87375
$Rb_2NaLaBr_6$	0.392	$a^+b^-b^-$	$BaNiO_3$	0.854	0.834	0.844	0.00000	0.05249	0.00000	33.15909

Compound	ΔE_0 (eV)	S_{min}	S_{max}	t'_B	$t'_{B'}$	t'	ε	δ (Å)	γ	Ω (Å^3)
Rb_2KNdBr_6	0.392	$a^-b^-c^-$	$BaNiO_3$	0.738	0.844	0.788	0.15889	4.64993	0.56603	69.13809
Cs_2KLaBr_6	0.391	$a^-b^-c^-$	$BaNiO_3$	0.786	0.888	0.834	0.00000	0.17732	0.00000	43.37383
$Rb_2CsEuBr_6$	0.390	$a^+b^-b^-$	$BaNiO_3$	0.664	0.862	0.750	0.21674	6.53979	0.76437	85.51002
$Rb_2NaCeCl_6$	0.388	$a^+b^-b^-$	$BaNiO_3$	0.867	0.842	0.854	0.00000	0.04169	0.00000	27.91782
Cs_2RbYCl_6	0.388	$a^-b^0a^-$	$a^0a^0a^0$	0.758	0.973	0.852	0.00000	0.29368	0.00000	36.16391
$Rb_2NaNdBr_6$	0.387	$a^+b^-b^-$	$BaNiO_3$	0.854	0.844	0.849	0.00000	0.05589	0.00000	32.89833
Rb_2NaEuI_6	0.387	$a^+b^-b^-$	$BaNiO_3$	0.802	0.883	0.841	0.00000	0.03647	0.00000	41.19635
Cs_2RbEuI_6	0.386	$a^-b^0c^-$	$BaNiO_3$	0.746	0.931	0.828	0.00000	0.28721	0.00000	54.10285
$K_2CsScCl_6$	0.386	$a^+b^-b^-$	$BaNiO_3$	0.627	0.892	0.736	0.23901	6.60218	0.84032	68.50148
$K_2LiEuCl_6$	0.386	$a^+b^-b^-$	$BaNiO_3$	0.891	0.813	0.850	0.00000	0.08207	0.00000	26.57337
Rb_2CsGdF_6	0.385	$a^+b^-b^-$	$BaNiO_3$	0.649	0.840	0.732	0.27000	6.46245	0.94348	47.33205
Cs_2KNdBr_6	0.381	$a^-b^-c^-$	$BaNiO_3$	0.786	0.899	0.839	0.00000	0.18160	0.00000	43.30719
$Rb_2LiLaCl_6$	0.380	$a^+b^-b^-$	$a^0a^0a^0$	0.937	0.816	0.872	0.00000	0.12236	0.00000	27.58479
$K_2NaScBr_6$	0.376	$a^+b^-b^-$	$BaNiO_3$	0.817	0.927	0.869	0.00002	0.05137	0.00000	27.06859
K_2RbLaI_6	0.374	$a^0a^0c^+$	$BaNiO_3$	0.684	0.809	0.741	0.08353	2.94859	0.30730	73.54964
Rb_2LiNdI_6	0.372	$a^+b^-b^-$	$BaNiO_3$	0.866	0.865	0.865	0.00000	0.00005	0.00000	40.32775
Rb_2NaErI_6	0.366	$a^+b^-b^-$	$BaNiO_3$	0.802	0.897	0.847	0.00000	0.04670	0.00000	40.28796
Cs_2KErI_6	0.364	$a^+b^-b^-$	$BaNiO_3$	0.771	0.946	0.850	0.00000	0.23057	0.00000	49.33392
$K_2CsScBr_6$	0.363	$a^-b^+c^-$	$BaNiO_3$	0.636	0.927	0.755	0.25004	7.20068	0.88063	78.81384
Rb_2CsErF_6	0.363	$a^+b^-b^-$	$BaNiO_3$	0.649	0.834	0.730	0.26414	6.37439	0.92388	47.94369
$K_2CsCeBr_6$	0.363	$a^0a^0c^+$	$BaNiO_3$	0.636	0.819	0.716	0.11242	4.73398	0.51738	68.35730
Cs_2RbYF_6	0.362	$a^-b^0a^-$	$BaNiO_3$	0.770	0.945	0.849	0.00000	0.23109	0.00000	21.81101
Cs_2KCeCl_6	0.362	$a^+b^-b^-$	$BaNiO_3$	0.797	0.902	0.846	0.00000	0.14175	0.00000	35.40046
$Rb_2NaEuCl_6$	0.358	$a^+b^-b^-$	$BaNiO_3$	0.867	0.855	0.861	0.00000	0.04756	0.00000	27.55719
Rb_2KScF_6	0.356	$a^-b^0a^-$	$BaNiO_3$	0.769	0.928	0.841	0.00000	0.16227	0.00000	15.76268
Cs_2KCeBr_6	0.356	$a^-b^0c^-$	$BaNiO_3$	0.786	0.910	0.843	0.00000	0.21033	0.00000	41.67878
$K_2LiScBr_6$	0.356	$a^+b^-b^-$	$BaNiO_3$	0.851	0.927	0.887	0.00000	0.06428	0.00000	27.27990
Cs_2RbErI_6	0.351	$a^-b^0a^-$	$BaNiO_3$	0.746	0.946	0.834	0.00000	0.30334	0.00000	53.30203
Rb_2LiGdI_6	0.348	$a^+b^-b^-$	$BaNiO_3$	0.866	0.871	0.868	0.00007	0.00440	0.00000	40.19848
$Rb_2LiLaBr_6$	0.347	$a^+b^-b^-$	$BaNiO_3$	0.889	0.834	0.861	0.00000	0.05699	0.00000	32.74126
$Rb_2LiNdBr_6$	0.347	$a^+b^-b^-$	$BaNiO_3$	0.889	0.844	0.866	0.00000	0.05812	0.00000	32.56491
Rb_2CsEuI_6	0.347	$a^-b^+c^-$	$BaNiO_3$	0.670	0.883	0.762	0.20977	6.75024	0.74135	102.10716
$Rb_2CsErBr_6$	0.345	$a^-b^+c^-$	$BaNiO_3$	0.664	0.878	0.756	0.22663	6.78103	0.79788	85.13103
Cs_2KEuBr_6	0.344	$a^-b^-c^-$	$BaNiO_3$	0.786	0.917	0.847	0.00000	0.20355	0.00000	42.12062
Rb_2LiYI_6	0.344	$a^-b^+c^-$	$BaNiO_3$	0.866	0.874	0.870	0.00000	0.00740	0.00000	39.81904
Cs_2KLaCl_6	0.344	$a^-b^0a^-$	$BaNiO_3$	0.797	0.874	0.834	0.00000	0.10213	0.00000	36.96963
$Rb_2CsGdBr_6$	0.343	$a^+b^-b^-$	$BaNiO_3$	0.664	0.873	0.754	0.22403	6.71119	0.78885	85.00771
K_2NaYCl_6	0.342	$a^+b^-b^-$	$BaNiO_3$	0.824	0.863	0.843	0.00000	0.01393	0.00000	25.04233
Cs_2KEuCl_6	0.341	$a^+b^-b^-$	$BaNiO_3$	0.797	0.916	0.852	0.00000	0.14323	0.00000	35.12254
Cs_2KGdBr_6	0.336	$a^-b^0c^-$	$BaNiO_3$	0.786	0.929	0.851	0.00000	0.21602	0.00000	41.48172
$K_2LiErCl_6$	0.335	$a^+b^-b^-$	$BaNiO_3$	0.891	0.834	0.861	0.00000	0.06105	0.00000	25.39719
Rb_2CsYCl_6	0.332	$a^+a^+c^-$	$BaNiO_3$	0.660	0.908	0.764	0.24038	6.69543	0.84430	70.60497

Compound	ΔE_0 (eV)	S_{min}	S_{max}	t'_B	$t'_{B'}$	t'	ε	δ (Å)	γ	Ω (Å^3)
K_2NaScI_6	0.326	$a^+b^-b^-$	$BaNiO_3$	0.776	0.924	0.844	0.00000	0.11080	0.00000	37.67590
Rb_2NaLaF_6	0.324	$a^-b^0a^-$	$BaNiO_3$	0.899	0.782	0.836	0.00000	0.14890	0.00000	17.17932
Cs_2KYBr_6	0.324	$a^-b^0a^-$	$BaNiO_3$	0.786	0.944	0.858	0.00000	0.22985	0.00000	40.77581
$Rb_2NaEuBr_6$	0.322	$a^+b^-b^-$	$BaNiO_3$	0.854	0.862	0.858	0.00000	0.03455	0.00000	32.14951
Cs_2KErBr_6	0.318	$a^-b^-c^-$	$BaNiO_3$	0.786	0.934	0.854	0.00000	0.21850	0.00000	41.53474
$Rb_2NaCeBr_6$	0.316	$a^+b^-b^-$	$BaNiO_3$	0.854	0.855	0.854	0.00001	0.01997	0.00000	31.58253
Rb_2LiEuI_6	0.312	$a^-b^+c^-$	$BaNiO_3$	0.866	0.883	0.874	0.00000	0.01025	0.00000	39.94318
Rb_2CsYBr_6	0.312	$a^+b^-b^-$	$BaNiO_3$	0.664	0.887	0.760	0.22806	6.78852	0.80279	84.02364
Rb_2CsLaI_6	0.311	$a^+a^+c^-$	$BaNiO_3$	0.670	0.837	0.745	0.20910	6.84653	0.73737	107.98839
$Cs_2RbScCl_6$	0.304	$a^-b^0a^-$	$a^0a^0a^0$	0.758	1.005	0.864	0.00000	0.32380	0.00000	35.14347
K_2LiNdF_6	0.302	$a^0a^0c^-$	$BaNiO_3$	0.920	0.725	0.811	0.00000	0.19901	0.00000	15.30971
Cs_2KGdCl_6	0.301	$a^-b^0a^-$	$BaNiO_3$	0.797	0.905	0.847	0.00000	0.13765	0.00000	35.09420
K_2LiLaF_6	0.301	$a^-b^0c^-$	$BaNiO_3$	0.920	0.719	0.807	0.00000	0.21453	0.00000	15.99661
Cs_2KNdCl_6	0.297	$a^-b^0a^-$	$BaNiO_3$	0.797	0.902	0.846	0.00000	0.12905	0.00000	35.82321
$Rb_2LiNdCl_6$	0.294	$a^+b^-b^-$	$BaNiO_3$	0.937	0.842	0.887	0.00001	0.09802	0.00000	26.51657
$Rb_2NaErCl_6$	0.294	$a^+b^-b^-$	$BaNiO_3$	0.867	0.877	0.872	0.00005	0.02546	0.00000	26.32495
K_2NaErF_6	0.294	$a^0a^0c^-$	$BaNiO_3$	0.827	0.767	0.796	0.00000	0.07994	0.00000	15.66510
Rb_2LiErI_6	0.290	$a^+b^-b^-$	$BaNiO_3$	0.866	0.897	0.881	0.00000	0.02426	0.00000	39.17586
$Rb_2NaErBr_6$	0.290	$a^+b^-b^-$	$BaNiO_3$	0.854	0.878	0.865	0.00000	0.02094	0.00000	31.55180
K_2NaYF_6	0.288	$a^0a^0c^-$	$BaNiO_3$	0.827	0.798	0.812	0.00000	0.05261	0.00000	14.31913
$Rb_2NaGdBr_6$	0.286	$a^+b^-b^-$	$BaNiO_3$	0.854	0.873	0.863	0.00000	0.01894	0.00000	31.49105
Cs_2RbScI_6	0.285	$a^-b^0a^-$	$BaNiO_3$	0.746	1.008	0.857	0.00000	0.36441	0.00000	50.04210
$Rb_2LiEuBr_6$	0.283	$a^+b^-b^-$	$BaNiO_3$	0.889	0.862	0.875	0.00000	0.03818	0.00000	31.86648
$Rb_2CsErCl_6$	0.278	$a^-b^0a^-$	$BaNiO_3$	0.660	0.877	0.753	0.23928	6.75055	0.84047	73.29809
$Cs_2RbScBr_6$	0.274	$a^-b^0a^-$	$a^0a^0a^0$	0.753	1.030	0.870	0.00000	0.35631	0.00000	39.31297
$Rb_2CsScCl_6$	0.274	$a^+a^+c^-$	$BaNiO_3$	0.660	0.938	0.775	0.24074	6.64501	0.84557	68.69689
$K_2NaScCl_6$	0.272	$a^+b^-b^-$	$BaNiO_3$	0.824	0.892	0.856	0.00001	0.03179	0.00000	24.46170
$Rb_2LiCeBr_6$	0.272	$a^+b^-b^-$	$BaNiO_3$	0.889	0.855	0.872	0.00000	0.02207	0.00000	31.26304
Cs_2NaCeI_6	0.272	$a^+b^-b^-$	$BaNiO_3$	0.846	0.877	0.861	0.00000	0.02518	0.00000	45.52477
K_2NaCeF_6	0.271	$a^-b^+c^-$	$BaNiO_3$	0.827	0.750	0.787	0.00000	0.07833	0.00000	16.46317
Rb_2NaNdF_6	0.270	$a^-b^0a^-$	$BaNiO_3$	0.899	0.789	0.840	0.00000	0.13245	0.00000	16.44022
$Rb_2LiCeCl_6$	0.270	$a^+b^-b^-$	$a^0a^0a^0$	0.937	0.842	0.887	0.00000	0.07905	0.00000	26.41479
Li_2CsCeF_6	0.266	$a^+a^+c^-$	$a^0a^0a^0$	0.458	0.577	0.511	0.33916	7.61415	1.06685	34.20320
$Rb_2LiGdCl_6$	0.262	$a^+b^-b^-$	$BaNiO_3$	0.937	0.845	0.888	0.00000	0.08933	0.00000	25.83267
Cs_2KScI_6	0.259	$a^+b^-b^-$	$BaNiO_3$	0.771	1.008	0.874	0.00000	0.28927	0.00000	46.18451
K_2LiScI_6	0.257	$a^-b^+c^-$	$BaNiO_3$	0.838	0.924	0.879	0.00000	0.08550	0.00000	36.59924
K_2NaEuF_6	0.254	$a^0a^0c^-$	$BaNiO_3$	0.827	0.768	0.797	0.00000	0.06999	0.00000	16.03490
Cs_2NaLaI_6	0.254	$a^+b^-b^-$	$BaNiO_3$	0.846	0.883	0.864	0.00000	0.01324	0.00000	44.27713
$Rb_2LiErBr_6$	0.251	$a^+b^-b^-$	$BaNiO_3$	0.889	0.878	0.883	0.00000	0.02314	0.00000	31.27040
$Rb_2LiGdBr_6$	0.245	$a^+b^-b^-$	$BaNiO_3$	0.889	0.873	0.881	0.00000	0.02095	0.00000	31.17826
$K_2RbGdBr_6$	0.244	$a^+b^-b^-$	$BaNiO_3$	0.677	0.836	0.748	0.12516	3.25316	0.38313	60.13700
K_2CsScF_6	0.243	$a^+a^+c^-$	$BaNiO_3$	0.597	0.854	0.702	0.31256	7.10454	1.08448	43.94040

Compound	ΔE_0 (eV)	S_{min}	S_{max}	t'_B	$t'_{B'}$	t'	ε	δ (Å)	γ	Ω (Å^3)
Rb_2NaYBr_6	0.243	$a^+b^-b^-$	$BaNiO_3$	0.854	0.887	0.870	0.00001	0.01079	0.00000	30.81457
$K_2CsEuBr_6$	0.242	$a^+b^-b^-$	$BaNiO_3$	0.636	0.825	0.719	0.11039	4.49102	0.49693	67.04607
$Rb_2LiEuCl_6$	0.235	$a^+b^-b^-$	$BaNiO_3$	0.937	0.855	0.894	0.00000	0.08703	0.00000	26.10945
K_2LiYCl_6	0.228	$a^+b^-b^-$	$a^0a^0a^0$	0.891	0.863	0.877	0.00000	0.02102	0.00000	23.71864
K_2NaGdF_6	0.228	$a^0a^0c^-$	$BaNiO_3$	0.827	0.773	0.799	0.00000	0.05149	0.00000	15.28054
Cs_2KErCl_6	0.226	$a^-b^0a^-$	$BaNiO_3$	0.797	0.940	0.863	0.00000	0.16995	0.00000	34.00143
Rb_2NaScI_6	0.226	$a^-b^+c^-$	$BaNiO_3$	0.802	0.956	0.872	0.00000	0.10610	0.00000	37.52089
Rb_2CsScI_6	0.223	$a^+b^-b^-$	$BaNiO_3$	0.670	0.956	0.788	0.21813	6.71433	0.75100	94.68004
Rb_2LiYBr_6	0.209	$a^+b^-b^-$	$BaNiO_3$	0.889	0.887	0.888	0.00000	0.01216	0.00000	30.61406
Cs_2KLaF_6	0.206	$a^-b^0a^-$	$BaNiO_3$	0.838	0.852	0.845	0.00000	0.00273	0.00000	21.34153
Li_2CsErF_6	0.194	$a^-a^-c^-$	$a^0a^0a^0$	0.458	0.590	0.516	0.30189	6.12792	1.14781	36.91825
$Rb_2CsScBr_6$	0.191	$a^+a^+c^-$	$BaNiO_3$	0.664	0.968	0.788	0.22831	6.62666	0.80347	77.74744
Cs_2KNdF_6	0.186	$a^-b^0a^-$	$BaNiO_3$	0.838	0.859	0.849	0.00000	0.01075	0.00000	20.71948
Cs_2LiCeI_6	0.178	$a^+b^-b^-$	$BaNiO_3$	0.913	0.877	0.895	0.00000	0.05691	0.00000	44.03272
Cs_2KYCl_6	0.177	$a^-b^0a^-$	$a^0a^0a^0$	0.797	0.973	0.876	0.00000	0.20355	0.00000	32.16463
Cs_2KScBr_6	0.177	$a^-b^0a^-$	$BaNiO_3$	0.786	1.030	0.892	0.00000	0.31150	0.00000	37.27880
Cs_2NaNdI_6	0.174	$a^-b^+c^-$	$BaNiO_3$	0.846	0.912	0.878	0.00000	0.02821	0.00000	42.35226
K_2LiErF_6	0.168	$a^0a^0c^-$	$BaNiO_3$	0.920	0.767	0.837	0.00000	0.14775	0.00000	13.99908
Cs_2NaGdI_6	0.168	$a^+b^-b^-$	$BaNiO_3$	0.846	0.918	0.881	0.00000	0.03052	0.00000	42.16782
$K_2LiScCl_6$	0.165	$a^+b^-b^-$	$BaNiO_3$	0.891	0.892	0.891	0.00000	0.00453	0.00000	23.22433
Cs_2RbScF_6	0.163	$a^-b^0a^-$	$BaNiO_3$	0.770	1.011	0.875	0.00000	0.29505	0.00000	20.16207
Cs_2NaYI_6	0.161	$a^+b^-b^-$	$BaNiO_3$	0.846	0.922	0.882	0.00001	0.03250	0.00000	41.72121
Rb_2NaYCl_6	0.160	$a^+b^-b^-$	$BaNiO_3$	0.867	0.908	0.887	0.00000	0.00924	0.00000	24.57532
$Rb_2LiErCl_6$	0.160	$a^+b^-b^-$	$BaNiO_3$	0.937	0.877	0.906	0.00002	0.06250	0.00000	25.02533
Cs_2LiLaI_6	0.159	$a^+b^-b^-$	$BaNiO_3$	0.913	0.883	0.898	0.00000	0.04016	0.00000	42.97359
Rb_2LiScI_6	0.147	$a^-b^+c^-$	$BaNiO_3$	0.866	0.956	0.909	0.00000	0.08520	0.00000	36.54052
K_2LiCeF_6	0.143	$a^-b^0c^-$	$BaNiO_3$	0.920	0.750	0.827	0.00000	0.14774	0.00000	14.77614
K_2LiYF_6	0.140	$a^0a^0c^-$	$BaNiO_3$	0.920	0.798	0.855	0.00000	0.11977	0.00000	12.65811
K_2LiEuF_6	0.138	$a^0a^0c^-$	$BaNiO_3$	0.920	0.768	0.838	0.00001	0.14199	0.00000	14.41122
Rb_2LiLaF_6	0.137	$a^-b^0a^-$	$BaNiO_3$	1.001	0.782	0.878	0.00000	0.21781	0.00000	15.48678
Rb_2NaCeF_6	0.122	$a^-b^0a^-$	$BaNiO_3$	0.899	0.816	0.856	0.00002	0.07684	0.00000	15.75897
Cs_2NaEuI_6	0.122	$a^+b^-b^-$	$BaNiO_3$	0.846	0.931	0.887	0.00000	0.03800	0.00000	41.48387
K_2NaScF_6	0.118	$a^0a^0c^-$	$BaNiO_3$	0.827	0.854	0.840	0.00000	0.01369	0.00000	12.75551
Cs_2KScCl_6	0.114	$a^-b^0a^-$	$BaNiO_3$	0.797	1.005	0.889	0.00000	0.23072	0.00000	31.43853
K_2CsScI_6	0.110	$a^+b^-b^-$	$BaNiO_3$	0.648	0.924	0.762	0.09282	3.33442	0.35284	67.82777
K_2LiGdF_6	0.104	$a^0a^0c^-$	$BaNiO_3$	0.920	0.773	0.840	0.00001	0.11670	0.00000	13.57459
Na_2RbLaI_6	0.100	$a^+b^-b^-$	$a^0a^0c^-$	0.623	0.738	0.676	0.16436	6.07452	0.71185	80.11823
K_2RbCeI_6	0.093	$a^0a^0c^+$	$BaNiO_3$	0.684	0.804	0.739	0.08542	3.24444	0.32889	66.94036
Cs_2NaErI_6	0.092	$a^+b^-b^-$	$BaNiO_3$	0.846	0.946	0.893	0.00000	0.05326	0.00000	40.95554
$K_2RbNdBr_6$	0.091	$a^0a^0c^-$	$BaNiO_3$	0.677	0.809	0.737	0.11853	3.78497	0.43925	62.09203
Rb_2NaEuF_6	0.087	$a^0a^0c^-$	$BaNiO_3$	0.899	0.836	0.866	0.00000	0.07278	0.00000	15.52648
$Rb_2NaScCl_6$	0.086	$a^+b^-b^-$	$BaNiO_3$	0.867	0.938	0.901	0.00000	0.02655	0.00000	24.15239

Compound	ΔE_0 (eV)	S_{min}	S_{max}	t'_B	$t'_{B'}$	t'	ε	δ (Å)	γ	Ω (Å^3)
Rb_2NaErF_6	0.085	$a^-b^0a^-$	$BaNiO_3$	0.899	0.834	0.866	0.00000	0.08404	0.00000	15.07452
Cs_2LiNdI_6	0.083	$a^+b^-b^-$	$BaNiO_3$	0.913	0.912	0.913	0.00000	0.00005	0.00000	41.11563
Na_2RbEuI_6	0.081	$a^-a^-a^-$	$BaNiO_3$	0.623	0.778	0.692	0.25581	5.77039	0.74708	69.70949
Cs_2LiGdI_6	0.077	$a^+b^-b^-$	$BaNiO_3$	0.913	0.918	0.916	0.00000	0.00500	0.00000	40.95208
Rb_2LiNdF_6	0.072	$a^-b^0a^-$	$BaNiO_3$	1.001	0.789	0.882	0.00000	0.19798	0.00000	14.86174
Cs_2LiYI_6	0.072	$a^+b^-b^-$	$BaNiO_3$	0.913	0.922	0.917	0.00001	0.00825	0.00000	40.59410
K_2RbYI_6	0.060	$a^-b^+c^-$	$BaNiO_3$	0.684	0.845	0.756	0.08607	3.20294	0.32962	64.67418
Cs_2KCeF_6	0.058	$a^-b^0a^-$	$BaNiO_3$	0.838	0.889	0.863	0.00000	0.06066	0.00000	20.05292
$Na_2RbEuBr_6$	0.053	$a^-b^+c^-$	$BaNiO_3$	0.586	0.714	0.644	0.15639	4.64966	0.53673	57.17162
$Rb_2NaScBr_6$	0.052	$a^+b^-b^-$	$BaNiO_3$	0.854	0.968	0.907	0.00000	0.06735	0.00000	28.14736
K_2RbNdI_6	0.050	$a^-b^+c^-$	$BaNiO_3$	0.684	0.837	0.753	0.09553	3.32388	0.33084	65.13663
$K_2CsLaCl_6$	0.049	$a^+b^-b^-$	$a^0a^0a^0$	0.627	0.775	0.694	0.23976	6.08326	0.63801	49.37295
K_2RbGdI_6	0.046	$a^-a^-c^-$	$BaNiO_3$	0.684	0.842	0.755	0.09263	3.27545	0.32685	64.92262
Na_2CsGdF_6	0.046	$a^-b^0a^-$	$a^0a^0a^0$	0.510	0.661	0.576	0.26596	5.89362	0.82108	33.80193
Cs_2KErF_6	0.045	$a^-b^0a^-$	$BaNiO_3$	0.838	0.909	0.872	0.00000	0.06453	0.00000	19.51332
Li_2CsYF_6	0.040	$a^-b^0a^-$	$a^0a^0a^0$	0.458	0.613	0.524	0.89996	16.72201	2.52642	29.28864
Cs_2RbLaF_6	0.034	$a^-b^0a^-$	$BaNiO_3$	0.770	0.852	0.809	0.19790	4.84779	0.70028	44.21104
$K_2CsGdBr_6$	0.032	$a^+a^+c^-$	$BaNiO_3$	0.636	0.836	0.722	0.27851	5.98395	0.72396	61.72514
K_2CsYBr_6	0.030	$a^+a^+c^-$	$BaNiO_3$	0.636	0.849	0.727	0.12005	3.79580	0.44142	61.96597
$Cs_2NaLaCl_6$	0.027	$a^+b^-b^-$	$BaNiO_3$	0.928	0.874	0.900	0.00000	0.08170	0.00000	29.55949
Cs_2KEuF_6	0.025	$a^-b^0a^-$	$BaNiO_3$	0.838	0.911	0.873	0.00000	0.07301	0.00000	19.60765
Rb_2NaGdF_6	0.023	$a^-b^0a^-$	$BaNiO_3$	0.899	0.840	0.869	0.00000	0.05028	0.00000	14.60834
$Rb_2LiScBr_6$	0.022	$a^+b^-b^-$	$BaNiO_3$	0.889	0.968	0.927	0.00000	0.06834	0.00000	27.93866
Cs_2LiEuI_6	0.019	$a^+b^-b^-$	$BaNiO_3$	0.913	0.931	0.922	0.00000	0.01185	0.00000	40.40998
Rb_2LiCeF_6	0.016	$a^+a^+a^+$	$BaNiO_3$	1.001	0.816	0.899	0.00000	0.11394	0.00000	14.37131
$Cs_2NaLaBr_6$	0.014	$a^+b^-b^-$	$BaNiO_3$	0.908	0.888	0.898	0.00001	0.05430	0.00000	33.04247
Rb_2LiYCl_6	0.014	$a^+b^-b^-$	$BaNiO_3$	0.937	0.908	0.922	0.00001	0.01925	0.00000	23.54561
$Cs_2NaNdBr_6$	0.013	$a^+b^-b^-$	$BaNiO_3$	0.908	0.899	0.904	0.00003	0.05284	0.00000	32.98388
Cs_2KGdF_6	0.010	$a^-b^0a^-$	$BaNiO_3$	0.838	0.916	0.875	0.00000	0.08811	0.00000	19.27153
$Cs_2LiLaBr_6$	0.009	$a^+b^-b^-$	$BaNiO_3$	0.946	0.888	0.916	0.00000	0.05595	0.00000	32.84501
Cs_2LiErI_6	0.008	$a^+b^-b^-$	$BaNiO_3$	0.913	0.946	0.929	0.00000	0.02780	0.00000	39.85580
$Cs_2LiNdBr_6$	0.008	$a^+b^-b^-$	$BaNiO_3$	0.946	0.899	0.922	0.00000	0.05510	0.00000	32.75861
K_2LiScF_6	0.006	$a^-b^-c^-$	$BaNiO_3$	0.920	0.854	0.886	0.00000	0.04812	0.00000	11.20302
$Cs_2NaNdCl_6$	0.005	$a^-b^+c^-$	$BaNiO_3$	0.928	0.902	0.915	0.00001	0.05335	0.00000	28.62757
Na_2KNdBr_6	0.002	$a^-a^-a^-$	$BaNiO_3$	0.612	0.700	0.653	0.13802	4.28488	0.51033	54.55596
$Na_2RbCeBr_6$	0.001	$a^0a^0c^-$	$BaNiO_3$	0.586	0.708	0.641	0.25632	5.75073	0.69735	49.98628
Na_2RbYCl_6	0.001	$a^0a^0c^-$	$BaNiO_3$	0.577	0.741	0.649	0.24080	5.72246	0.75232	43.20218
Na_2KLaBr_6	0.001	$a^-a^-a^-$	$BaNiO_3$	0.612	0.691	0.649	0.13365	4.14722	0.49070	54.35603
Na_2KGdBr_6	0.001	$a^-a^-a^-$	$BaNiO_3$	0.612	0.723	0.663	0.14068	4.14300	0.49760	52.54847
Na_2KCeBr_6	0.001	$a^-a^-a^-$	$BaNiO_3$	0.612	0.708	0.656	0.14167	4.15554	0.48188	52.68034
Cs_2LiScF_6	0.001	$a^0a^0a^0$	$BaNiO_3$	1.091	1.011	1.050	0.00002	0.02693	0.00000	15.20622
Na_2KGdCl_6	0.001	$a^0a^0c^-$	$BaNiO_3$	0.607	0.689	0.645	0.22673	4.70339	0.65253	39.28928

Compound	ΔE_0 (eV)	S_{min}	S_{max}	t'_B	$t'_{B'}$	t'	ε	δ (Å)	γ	Ω (Å^3)
$Na_2RbCeCl_6$	0.000	$a^0a^0c^-$	$BaNiO_3$	0.577	0.687	0.627	0.23551	5.44181	0.65943	44.82570
Rb_2NaYF_6	0.000	$a^-a^-a^-$	$BaNiO_3$	0.899	0.867	0.883	0.00000	0.05397	0.00000	13.89377
$K_2CsLaBr_6$	0.000	$a^0a^0c^-$	$BaNiO_3$	0.636	0.799	0.708	0.23538	5.50504	0.67432	58.18382
$Na_2RbNdBr_6$	0.000	$a^-b^+c^-$	$a^0a^0c^-$	0.586	0.700	0.638	0.26067	5.82567	0.70685	49.42069
Cs_2LiCeF_6	0.000	$a^0a^0a^0$	$BaNiO_3$	1.091	0.889	0.980	0.00000	0.14578	0.00001	16.66538
Cs_2NaLaF_6	0.000	$a^0a^0a^0$	$BaNiO_3$	0.980	0.852	0.911	0.00001	0.14014	0.00000	18.21032
Cs_2LiYF_6	0.000	$a^0a^0a^0$	$BaNiO_3$	1.091	0.945	1.013	0.00001	0.09585	0.00003	15.46698
Cs_2NaYBr_6	0.000	$a^0a^0a^0$	$BaNiO_3$	0.908	0.944	0.926	0.00002	0.00767	0.00000	31.00911
Cs_2NaEuF_6	0.000	$a^0a^0a^0$	$BaNiO_3$	0.980	0.911	0.944	0.00003	0.06351	0.00000	17.18687
$Cs_2NaEuBr_6$	0.000	$a^0a^0a^0$	$BaNiO_3$	0.908	0.917	0.913	0.00001	0.03363	0.00000	32.16742
Cs_2LiYBr_6	0.000	$a^0a^0a^0$	$BaNiO_3$	0.946	0.944	0.945	0.00003	0.00844	0.00000	30.87289
$Rb_2LiScCl_6$	0.000	$a^0a^0a^0$	$BaNiO_3$	0.937	0.938	0.938	0.00000	0.00338	0.00000	23.16263
Cs_2LiNdF_6	0.000	$a^0a^0a^0$	$BaNiO_3$	1.091	0.859	0.961	0.00004	0.19424	0.00012	16.64566
$Cs_2LiNdCl_6$	0.000	$a^0a^0a^0$	$BaNiO_3$	1.004	0.902	0.950	0.00000	0.09170	0.00000	27.31379
$Cs_2LiGdCl_6$	0.000	$a^0a^0a^0$	$BaNiO_3$	1.004	0.905	0.952	0.00000	0.08285	0.00000	26.71957
$Cs_2NaCeBr_6$	0.000	$a^0a^0a^0$	$BaNiO_3$	0.908	0.910	0.909	0.00005	0.01969	0.00000	31.67904
$Cs_2NaEuCl_6$	0.000	$a^0a^0a^0$	$BaNiO_3$	0.928	0.916	0.922	0.00000	0.03913	0.00000	28.16648
$Cs_2NaScBr_6$	0.000	$a^0a^0a^0$	$BaNiO_3$	0.908	1.030	0.965	0.00002	0.07510	0.00000	28.84040
$Cs_2NaGdBr_6$	0.000	$a^0a^0a^0$	$BaNiO_3$	0.908	0.929	0.918	0.00001	0.01697	0.00000	31.61369
Cs_2KYF_6	0.000	$a^0a^0a^0$	$BaNiO_3$	0.838	0.945	0.888	0.00003	0.09645	0.00000	18.58820
$Cs_2LiScCl_6$	0.000	$a^0a^0a^0$	$BaNiO_3$	1.004	1.005	1.005	0.00000	0.00400	0.00000	24.22514
$Cs_2LiErCl_6$	0.000	$a^0a^0a^0$	$BaNiO_3$	1.004	0.940	0.971	0.00004	0.05324	0.00000	26.00236
$Cs_2LiEuBr_6$	0.000	$a^0a^0a^0$	$BaNiO_3$	0.946	0.917	0.931	0.00006	0.03772	0.00000	32.00219
$Cs_2LiErBr_6$	0.000	$a^0a^0a^0$	$BaNiO_3$	0.946	0.934	0.940	0.00000	0.02331	0.00000	31.53123
$Cs_2LiCeCl_6$	0.000	$a^0a^0a^0$	$BaNiO_3$	1.004	0.902	0.950	0.00001	0.07592	0.00000	27.36015
Rb_2NaScF_6	0.000	$a^0a^0a^0$	$BaNiO_3$	0.899	0.928	0.913	0.00004	0.01300	0.00000	12.64321
$Na_2RbGdBr_6$	0.000	$a^0a^0a^0$	$BaNiO_3$	0.586	0.723	0.647	0.24218	5.34902	0.73087	50.11821
$Cs_2LiScBr_6$	0.000	$a^0a^0a^0$	$BaNiO_3$	0.946	1.030	0.986	0.00001	0.07159	0.00000	28.56991
$Cs_2LiCeBr_6$	0.000	$a^0a^0a^0$	$BaNiO_3$	0.946	0.910	0.928	0.00001	0.02130	0.00000	31.50233
$Cs_2LiEuCl_6$	0.000	$a^0a^0a^0$	$BaNiO_3$	1.004	0.916	0.958	0.00000	0.07954	0.00000	26.89858
Cs_2LiEuF_6	0.000	$a^0a^0a^0$	$BaNiO_3$	1.091	0.911	0.993	0.00000	0.13122	0.00000	16.30466
Rb_2CsScF_6	0.000	$a^0a^0a^0$	$BaNiO_3$	0.649	0.928	0.764	0.28092	6.51053	0.97982	43.84388
Rb_2LiEuF_6	0.000	$a^0a^0a^0$	$BaNiO_3$	1.001	0.836	0.911	0.00001	0.13824	0.00000	14.17640
Na_2KYCl_6	0.000	$a^0a^0a^0$	$BaNiO_3$	0.607	0.741	0.667	0.24432	5.06674	0.65965	37.72213
$Na_2RbLaBr_6$	0.000	$a^0a^0a^0$	$BaNiO_3$	0.586	0.691	0.634	0.25520	5.74060	0.69182	50.33551
Na_2KErCl_6	0.000	$a^0a^0a^0$	$BaNiO_3$	0.607	0.716	0.657	0.23121	4.73468	0.66547	38.52468
Cs_2LiLaF_6	0.000	$a^0a^0a^0$	$BaNiO_3$	1.091	0.852	0.957	0.00000	0.20807	0.00000	17.03651
Rb_2LiErF_6	0.000	$a^0a^0a^0$	$BaNiO_3$	1.001	0.834	0.910	0.00000	0.14641	0.00000	13.68679
Na_2KLaI_6	0.000	$a^0a^0a^0$	$BaNiO_3$	0.644	0.738	0.688	0.13033	4.42290	0.48778	67.11906
$Cs_2LiLaCl_6$	0.000	$a^0a^0a^0$	$BaNiO_3$	1.004	0.874	0.935	0.00000	0.11955	0.00000	28.23302
Cs_2LiScI_6	0.000	$a^0a^0a^0$	$BaNiO_3$	0.913	1.008	0.958	0.00001	0.08881	0.00000	37.44776
Cs_2LiYCl_6	0.000	$a^0a^0a^0$	$BaNiO_3$	1.004	0.973	0.988	0.00000	0.01661	0.00000	24.67344

Compound	ΔE_0 (eV)	S_{min}	S_{max}	t'_B	$t'_{B'}$	t'	ε	δ (Å)	γ	Ω (Å^3)
Cs_2NaScI_6	0.000	$a^0a^0a^0$	$BaNiO_3$	0.846	1.008	0.920	0.00000	0.11644	0.00000	38.49199
$Cs_2NaScCl_6$	0.000	$a^0a^0a^0$	$BaNiO_3$	0.928	1.005	0.965	0.00000	0.04587	0.00000	25.31979
Cs_2NaScF_6	0.000	$a^0a^0a^0$	$BaNiO_3$	0.980	1.011	0.995	0.00003	0.02323	0.00000	15.80421
Cs_2NaYF_6	0.000	$a^0a^0a^0$	$BaNiO_3$	0.980	0.945	0.962	0.00002	0.03325	0.00000	16.26897
Cs_2KScF_6	0.000	$a^0a^0a^0$	$BaNiO_3$	0.838	1.011	0.917	0.00001	0.16255	0.00000	17.55474
Cs_2NaYCl_6	0.000	$a^0a^0a^0$	$BaNiO_3$	0.928	0.973	0.950	0.00000	0.01706	0.00000	25.68549
$Cs_2NaGdCl_6$	0.000	$a^0a^0a^0$	$BaNiO_3$	0.928	0.905	0.916	0.00000	0.04537	0.00000	27.90752
Rb_2LiYF_6	0.000	$a^0a^0a^0$	$BaNiO_3$	1.001	0.867	0.929	0.00000	0.12050	0.00000	12.59136
Cs_2NaGdF_6	0.000	$a^0a^0a^0$	$BaNiO_3$	0.980	0.916	0.947	0.00002	0.05218	0.00000	16.99833
$Cs_2NaCeCl_6$	0.000	$a^0a^0a^0$	$BaNiO_3$	0.928	0.902	0.915	0.00002	0.03675	0.00000	28.59747
Rb_2LiScF_6	0.000	$a^0a^0a^0$	$BaNiO_3$	1.001	0.928	0.963	0.00000	0.04760	0.00000	11.76410
$Cs_2LiGdBr_6$	0.000	$a^0a^0a^0$	$BaNiO_3$	0.946	0.929	0.937	0.00001	0.02037	0.00000	31.39680
Rb_2LiGdF_6	0.000	$a^0a^0a^0$	$BaNiO_3$	1.001	0.840	0.914	0.00012	0.11407	0.00000	13.26093
Cs_2LiGdF_6	0.000	$a^0a^0a^0$	$BaNiO_3$	1.091	0.916	0.995	0.00002	0.12143	0.00000	16.17906
Cs_2NaNdF_6	0.000	$a^0a^0a^0$	$BaNiO_3$	0.980	0.859	0.916	0.00000	0.12691	0.00000	17.71133
Cs_2NaErF_6	0.000	$a^0a^0a^0$	$BaNiO_3$	0.980	0.909	0.943	0.00001	0.06915	0.00000	16.97532
Na_2RbYBr_6	0.000	$a^0a^0a^0$	$BaNiO_3$	0.586	0.735	0.652	0.25675	5.99825	0.71829	49.00338
Cs_2NaCeF_6	0.000	$a^0a^0a^0$	$BaNiO_3$	0.980	0.889	0.932	0.00001	0.07597	0.00000	17.60122
$Cs_2NaErBr_6$	0.000	$a^0a^0a^0$	$BaNiO_3$	0.908	0.934	0.921	0.00000	0.01791	0.00000	31.77822
$Cs_2NaErCl_6$	0.000	$a^0a^0a^0$	$BaNiO_3$	0.928	0.940	0.934	0.00000	0.01515	0.00000	27.17287
Cs_2LiErF_6	0.000	$a^0a^0a^0$	$BaNiO_3$	1.091	0.909	0.992	0.00000	0.13480	0.00000	16.09534

REFERENCES

1 V. M. Goldschmidt, Geochemisce Verterlungsgesetze der Elemente. Norske Videnskap, Oslo, 1927.

2 A. S. Bhalla, R. Guo, and R. Roy, *Mat. Res. Innovat.*, **4**, 3 (2000).

3 C. Z. Ye, J. Yang, L. X. Yao, and N. Y. Chen, *Chinese Sci. Bull.*, **47**, 458 (2002).

4 R. D. Shannon, *Acta Cryst. Sec. A*, **32**, 751(1976).

5 I. D. Brown, *"the chemical bond in inorganic chemistry: the bond valence model,"* Oxford University Press, Oxford (2002).

6 I. D. Brown, *Chem. Rev.*, **109**, 6858 (2009).

7 M. W. Lufaso, and P. M. Woodward, *Acta Cryst. B*, **57**, 725 (2001).

8 M. W. Lufaso, P. W. Barnes, and P. M. Woodward, *Acta Cryst. B*, **62**, 397 (2006).

9 M. W. Lufaso, *Chem. Mater.*, **16**, 2148 (2004).

10 L. Pauling, *"the nature of the chemical bond,"* 2nd edition, p. 164, Cornell University Press (1945).

11 L. Pauling, *J. Amer. Chem. Soc.*, **54**, 3570 (1932).

12 R. T. Sanderson, *J. Chem. Phys.*, **23**, 2467 (1955).

13 R. P. Iczkowski, and J. L. Margrave, *J. Amer. Chem. Society*, **83**, 3547 (1961).

14 E. Mooser, and W. B. Pearson, *Acta Cryst.*, **12**, 1015 (1959).

15 X. W. Zhou, and F. P. Doty, *Phys. Rev. B*, **78**, 224307 (2008).

16 S. R. Phillpot, S. B. Sinnott, and A. Asthagiri, *Annu. Rev. Mater. Res.*, **37**, 239 (2007).

17 M. Baudin, and K. Hermansson, *Surf. Sci.*, **474**, 107 (2001).

18 B. G. Dick, and A. W. Overhauser, *Phys. Rev. B*, **112**, 90 (1958).

19 A. Dwivedi, and A. N. Cormack, *Philos. Mag. A*, **61**, 1 (1990).

20 P. J. D. Lindan, and M. J. Gillan, *J. Phys.: Condens. Matter*, **5**, 1019 (1993).

21 G. V. Lewis, and C. R. A. Catlow, *J. Phys. C*, **18**, 1149 (1985).

22 M. S. Khan, M. S. Islam, and D. R. Bates, *J. Mater. Chem.*, **8**, 2299 (1998).

23 C. R. A. Catlow, *J. Chem. Soc. Faraday Trans.*, **86**, 1167 (1990).

24 M. R. Levy, A. Patel, C. R. Stanek, K. McClellan, and R. W. Grimes, *Phys. Stat. Sol. C*, **4**, 1226 (2007).

25 X. W. Zhou, H. N. G. Wadley, J. –S. Filhol, and M. N. Neurock, *Phys. Rev. B*, **69**, 035402 (2004).

26 T. Campbell, R. K. Kalia, A. Nakano, P. Vashishta, S. Ogata, and S. Rodgers, *Phys. Rev. Lett.*, **82**, 4866 (1999).

27 S. Ogata, and T. J. Campbell, *J. Phys.: Condens. Matter*, **10**, 11449 (1998).

28 Y. Ma, and S. H. Garofalini, *J. Chem. Phys.*, **128**, 084505 (2008).

29 F. H. Streitz, and J. W. Mintmire, *Phys. Rev. B*, **50**, 11996 (1984).

30 A. K. Rappe, and W. A. Goddard, *J. Phys. Chem.*, **95**, 3358 (1991).

31 S. W. Rick, S. J. Stuart, and B. J. Berne, *J. Chem. Phys.*, **101**, 6141 (1994).

32 A. J. Rowley, P. J̈emmer, M. Wilson, and P. A. Madden, *J. Chem. Phys.*, **108**, 10209 (1998).

33 M. Wilson, and P. A. Madden, N. C. Pyper, and J. H. Harding, *J. Chem. Phys.*, **104**, 8068 (1996).

34 P. A. Madden, and M. Wilson, *Chem. Soc. Rev.*, **25**, 339 (1996).

35 B. Rotenberg, M. Salanne, C. Simon, and R. Vuilleumier, *Phys. Rev. Lett.*, **104**, 138301 (2010).

36 P. Tangney, and S. Scandolo, *J. Chem. Phys.*, **117**, 8898 (2002).

37 J. P. M. Lommerse, A. J. Stone, R. Taylor, and F. H. Allen, *J. Am. Chem. Soc.*, **118**, 3108 (1996).

38 K. Albe, J. Nord, and K. Nordlund, *Phil. Mag.*, **8**, 3477 (2009).

39 M. S. Daw, and M. I. Baskes, *Phys. Rev. B*, **29**, 6443 (1984).

40 S. M. Foiles, M. I. Baskes, and M. S. Daw, and F. P. Doty, *Phys. Rev. B*, **33**, 7983 (1986).

41 S. J. Plimpton, *J. Comp. Phys.*, **117**, 1 (1995).

42 Code downloadable at lammps.sandia.gov.

43 J. Tersoff, *Phys. Rev. B*, **37**, 6991 (1988).

44 J. Tersoff, *Phys. Rev. B*, **39**, 5566 (1989).

45 X. W. Zhou, H. N. G. Wadley, R. A. Johnson, D. J. Larson, N. Tabat, A. Cerezo, A. K. Petford-Long, G. D. W. Smith, P. H. Clifton, R. L. Martens, and T. F. Kelly, *Acta Mater.*, **49**, 4005 (2001).

46 X. W. Zhou, R. A. Johnson, and H. N. G. Wadley, *Phys. Rev. B*, **69**, 144113 (2004).

47 A. L. Allred, *J. Inorg. Nucl. Chem.*, **17**, 215 (1961).

48 R. S. Mulliken, *J. Chem. Phys.*, **2**, 782 (1934).

49 J. D. H. Donnay, and H. M. Ondik, *"crystal data, determinative tables,"* 3rd ed., Vol. 2 (inorganic compounds), U. S. Department of Commerce, National Bureau of Standards, and Joint Committee on Power Diffraction Standards, U. S. A., 1973.

50 X. W. Zhou, J. A. Zimmerman, B. M. Wong, and J. J. Hoyt, *J. Mater. Res.*, **23**, 704 (2008).

51 I. Barin, *"thermochemical data of pure substances,"* VCH, Weinheim, 1993.

52 Wolfram Research Inc., 2007, available online at: http://www.wolfram.com/products/mathematica/index.html.

53 http://www.chemicool.com

54 S. V. Karpenko, A. K. Kyarov, and A. I. Temrokov, *High Temp.*, **38**, 722 (2000).

55 A. M. Hofmeister, *Phys. Rev. B*, **56**, 5835 (1997).

56 S. Froyen, and M. L. Cohen, *J. Phys. C*, **19**, 2623 (1986).

57 C. O. Rodriguez, and M. Methfessel, *Phys. Rev. B*, **45**, 90 (1992).

58 P. A. G. O'hare, G. K. Johnson, I. R. Tasker, H. E. Flotow, and C. W. Struck, J. Chem. Thermodynamics, 19, 77 (1987).

59 G. Meyer, *Prog. Solid St. Chem.*, **14**, 141 (1982).

60 A. M. Glazer, *Acta Cryst. B*, **28**, 3384 (1972).

61 A. M. Glazer, *Acta Cryst. A*, **31**, 756 (1975).

62 K. S. Aleksandrov, and J. Bartolome, *Phase Transitions*, **74**, 255 (2001).

63 L. Liang, L. Wencong, and C. Nianyi, *J. Phys. Chem. Sol.*, **65**, 855 (2004).

64 M. Parrinello, and A. Rahman, *J. Appl. Phys.*, **52**, 7182 (1981).

65 G. Knoll, "*Radiation Detection and Measurement*," 3rd ed., New York: Wiley, 1999.

66 O. Guillot-Noël, J. T. M. de Hass, P. Dorenbos, C.W.E. van Eijk, K. Krämer, and H. U. Gűdel, *J. Lumin.*, **85** 21-35 (1999).

67 E.V.D. van Loef, P. Dorenbos, C. W. E. van Eijk, K. Krämer, and H. U. Gűdel, *Appl. Phys. Lett.*, **79** [10] 1573-1575 (2001).

68 K. S. Shah, J. Glodo, W. H. Higgins, E. V. D. van Loef, W. W. Moses, S. E. Derenzo and M. J. Weber, *IEEE Trans. Nucl. Sci*., 52 [6] 3157-3159 (2005).

69 M. D. Birowosuto, P. Dorenbos, and C. W. E. van Eijk, K.W. Krämer, and H. U. Gűdel, *J. Appl. Phys*., **99** 123520 (2006).

70 J. Glodo, W. M. Higgins, E. V. D. van Loef, and K. S. Shah, *IEEE Nucl. Sci. Symposium Conference Record*, 1574-1577 (2006).

71 J. C. van't Spijker, P. Dorenbos, C. W. E. van Eijk, M. S. Wickleder, H. U. Gudel, and P. A. Rodnyi, *J. Lumin.* **72-74** 786-788. (1997).

72 Jarek Glodo, Edgar V. D. van Loef, William M. Higgins, and Kanai S. Shah, *IEEE Nucl. Sci. Symposium Conference Record*, 1208-1211 (2006).

73 Edgar V. D. van Loef, William M. Higgins, Michael R. Squillante, and Kanai S. Shah, *IEEE Nucl. Sci. Symposium Conference Record*, 1183-1186 (2006).

74 Urmila shirwadlkar, J. Glodo, Edgar V. D. van Loef, Rastgo Hawrami, Sharmishtha Mukhopadhyay, Alexei Churilov, William M. Higgins, Kanai S. Shah, *Nucl. Instr. and Meth.* **A** (2010), doi:10.16/j.nima2010.08.050.

75 Jong k. Cheon, Sunghwan Kim, Gul Rooh, J. H. So. H.J. Kim and H. Park, *Nucl. Instr. and Meth.* **A** (2011), doi:10.1016/j.nima2011.02.038.

76 Sunghwan Kim, Gul Rooh, H. J. Kim, Do S. Kim, S. J. Kang, *J. Crystal Growth*, **317** 84-86 (2011).

77 P. Doty, D. McGregor, M. Harrison, K. Findley and R Polichar, SPIE **6707,** 670705 (2007).

78 G. Meyer, *Prog. Solid St. Chem.*, **14**, 141-219 (1982).

79 A. Bessiere, P. Dorenbos, C. W. E. van Eijk, K. W. Kramer, and H. U. Gudel, *Nucl. Instr. and Meth.* **A 537** 242-246 (2005).

80 M. D. Birowosuto, P. Dorenbos, J. T. M. de Hass, Carel W. E. Van Eijk, Karl W. Kramer and Hans U. Gudel, *IEEE Nucl. Sci. Symposium Conference Record*, **55** 1152-1155 (2008).

81 D. W. Lee, L. C. Stonehill, A. Klimenko, J. R. Terry, S. R. Tornga, *Nucl. Instr. and Meth.* **A 664** 1-5 (2012).

82 M. E. Villafuerte-Catrejon, M. R. Estrada, J. Gomez-Lara, J. Duque, and R. Pomes, *J. Solid State Chem*., **132** 1-5 (1997).

83 T. J. Boyle, P. Yang, L. A. M. Ottley, M. A. Rodriguez, T. M. Alam and S. Hoppe, in preparation (2012), and P. Yang, T. J. Boyle, N. S. Bell, M. R. Sanchez, L. A. M. Ottley, and C. F. Chen, Sandia Report, Sandia National Laboratories, SAND2008-6978 and SAND2007-0719.

84 M. A. Rodriguez, T. J. Boyle, P. Yang, D. L. Harris, *Powder Diffraction*, **23**, 121-124 (2008).

85 B. H. Toby, J. Appl. Cryst., 34, 210-221 (2001)

86 A. C. Larson, R. B. VonDreele, "General Structure Analysis System (GSAS)," Los Alamos National Laboratories, LAUR 86-748 (2000).

87 P. Yang, C. B. DiAntonio, T. J. Boyle, M. A. Rodriguez, and M. R. Sanchez, *SPIE* 670709, (2007).

88 J. Kutscher and A. Schneide, *Z. Anorg. Allg. Chem.*, **386** [1] 38-46 (1971).

89 J. Sangster and A. D. Pelton, *J. Phys. Chem*., **16** [3] 509-561 (1987).

90 L. Liu, W. Lu, and N. Chen, *J. Phys. Chem. Solids*, **65** 855-860 (2004).

91 R. D. Shannon, *Acta Cryst.*, **A32** 751-766 (1976).

92 V. Poblete, G. Navarro, V. Martin, and M. Alvarez, *Powder Diffraction*, **17**, 10-13 (2002).

93 G. Schilling, C. Kunert, T. Schleid, and G. Meyer, *Z. Anorg. Allg. Chem.* **618**, 12-14 (1992).

94 G. Blasse, B. C. Grabmaier, "*Luminescence Materials*," Springer Verlag, pp. 45-47 (1994).

95 C. Reber, H. Gűdel, G. Meyer, T. Schleid, and C. A. Dual, *Inorganic Chem.*, **28** [16] 3249-3581 (1989).

96 W. M. Higgins, J. Glodo, E. Van Loef, M. Klugerman, T. Gupta, L. Cirignano, P. Wong, and K. S. Shah, *J. Crystal. Growth*, **287** 239 (2006).

97 K. S. Shah, J. Glodo, M. Klugerman, L. Cirigenano, W. W. Moses, S. E. Derenzo, and M. J. Weber, *Nucl. Instr. and Meth.* **A. 505** 76 (2003).

DISTRIBUTION

MS0887	Carol Adkins	1800
MS0866	James H. Aubert	1819
MS0885	Terrence Aselage	1810
MS9154	William P. Ballard	8100
MS0970	Michael Cieslak	5700
MS9153	Russell G. Miller	8200
MS1411	Paul Clem	1816
MS9042	Mary E. Gonzales	8250
MS9402	Alfredo Morales	8131
MS9402	Christopher Moen	8256
MS0971	Robert Huelskamp	5730
MS9004	James Lund	8130
MS1411	Mark A. Rodriguiz	1819
MS0971	Robert Tachau	5767
MS0958	Pin Yang	1816
MS9404	Xiaowang Zhou	8256
MS9154	Technical Library	9536 (electronic copy)


Sandia National Laboratories